3-10-2010

Relative Orbit Elements for Satellites in Elliptical Orbits

Kirk W. Johnson

RELATIVE ORBIT ELEMENTS FOR SATELLITES IN ELLIPTICAL ORBITS

THESIS

Kirk W. Johnson, Captain, USAF

AFIT/GA/ENY/10-M04

DEPARTMENT OF THE AIR FORCE
AIR UNIVERSITY

AIR FORCE INSTITUTE OF TECHNOLOGY

Wright-Patterson Air Force Base, Ohio

AFIT/GA/ENY/10-M04

RELATIVE ORBIT ELEMENTS FOR SATELLITES IN ELLIPTICAL ORBITS

THESIS

Presented to the Faculty

Department of Aeronautics and Astronautics

Graduate School of Engineering and Management

Air Force Institute of Technology

Air University

Air Education and Training Command

In Partial Fulfillment of the Requirements for the

Degree of Master of Science in Astronautical Engineering

Kirk W. Johnson, BS

Captain, USAF

March 2010

AFIT/GA/ENY/10-M04

RELATIVE ORBIT ELEMENTS FOR SATELLITES IN ELLIPTICAL ORBITS

Kirk W. Johnson, BS
Captain, USAF

Approved:

_____//signed//_____	_____
Lt Col Douglas D. Decker (Chairman)	Date
_____//signed//_____	_____
William E. Wiesel, PhD (Member)	Date
_____//signed//_____	_____
Lt Col (R) Kerry D. Hicks, PhD (Member)	Date
_____//signed//_____	_____
T. Alan Lovell, PhD (Member)	Date

Abstract

The purpose of this research was to describe the unperturbed relative motion of Earth satellites in elliptical orbits using a simple dynamics model whose parameters allow significant geometrical insight and operational efficacy. The goal was to retain the advantages of the Relative Orbit Elements (ROE) realization of the Hill-Clohessy-Wiltshire (HCW) equations, a linearized dynamics model for circular reference orbits. Specifically, this thesis analyzed the geometry of satellite rendezvous and proximity operations using the ROE parameters to characterize the model's utility. Next, through a comprehensive literature review, this thesis sought possible approaches for developing a similarly useful parameterization for chief orbits with nonzero eccentricity. The approach selected was a novel linear time-varying system which requires both chief and deputy satellites to remain close to a virtual chief on a known circular orbit. The research derived and solved the equations of motion, expressing the solution in terms of simple geometric parameters. Numerical simulations compared the new model against both HCW and Keplerian two-body motion, revealing less accurate performance than HCW for some cases. Error analysis explained this behavior and found restricted regions where the new model performed accurately. Finally, this study identified new approaches for researching relative satellite motion on elliptical orbits.

Acknowledgments

On my own, I could not have completed an undertaking as large as this project. I would like to thank all those who have helped me along the way.

First, "I thank Christ Jesus our Lord, who has given me strength" (1 Timothy 1:12).

To my best friend, my wife: thanks for everything you've done over the last eighteen months. Without your unbelievable support, encouragement, and help, I don't know where I would be. I love you with all my heart!

To my son and daughter: thanks for being good kids, even when Daddy had homework to do *again*.

To Mom and Dad: thanks for everything you taught me about life, especially trigonometry.

Thanks also to my advisor, Lt Col Doug Decker. Your patient advice and suggestions nudged me in the right direction when I needed it.

Special thanks go to my sponsor, Dr. Alan Lovell, whose work constitutes the starting point of this study, and who invested a great deal of time into helping me understand the relevant issues and vetting my ideas.

Kirk W. Johnson

Table of Contents

Page

ABSTRACT ..... **IV**

ACKNOWLEDGMENTS ..... **V**

I. INTRODUCTION **1**

BACKGROUND: RELATIVE SATELLITE MOTION MODELS 1
PROBLEM STATEMENT 6
NOTATION AND REFERENCE FRAMES 7

II. LITERATURE REVIEW **11**

CIRCULAR CHIEF PROBLEM 11
Hill-Clohessy-Wiltshire Model. *11*
Quadratic Models. *13*
ELLIPTICAL CHIEF PROBLEM 14
Lawden's Equations: the First Generation. *14*
Lawden's Equations: Later Developments. *18*
Equivalent Forms. *20*
Bounded-motion Analysis of Lawden's Equations. *22*
Low-eccentricity Approximations. *25*
Quadratic Models. *28*
APPLICATIONS OF RELATIVE MOTION 30
HIGHER-FIDELITY MODELS 31
MODEL COMPARISONS 32
SUMMARY 33

III. RELATIVE ORBIT ELEMENTS FOR THE CIRCULAR CHIEF PROBLEM **34**

THE HCW MODEL 34
A GEOMETRIC PARAMETERIZATION OF THE SOLUTION 36
THE THREE-DIMENSIONAL GEOMETRY OF THE RELATIVE TRAJECTORY 41
Projection into the Orbit Plane. *41*
Instantaneous Plane of the Trajectory *42*
The True Ellipse. *44*
BRIEF EXAMPLE. 53

IV. PARAMETERIZED MODELS OF THE ELLIPTICAL CHIEF PROBLEM **54**

OBJECTIVES 54
POSSIBLE APPROACHES 56
Neglect Chief Eccentricity. *56*
Lawden's Equations. *56*
First- and Second-order Eccentricity Approximations. *59*
Change of Reference Frames. *59*
The Virtual Chief Method. *59*
THE VIRTUAL CHIEF EQUATIONS 60
Reference Frames for the Actual and Virtual Chief. *61*
Vector Equations. *64*

Scalar Equations. ... *65*
THE VIRTUAL CHIEF SOLUTION ... 71
Vector Solution. ... *72*
Scalar Solution. ... *75*
State Transition Matrix. ... *80*
Parameterization. ... *81*
Bounded Motion. ... *88*

V. NUMERICAL RESULTS AND CONCLUSIONS ... 90

EXAMPLES ... 90
ERROR ANALYSIS: PHASE 1 ... 97
ERROR ANALYSIS: PHASE 2 ... 102
CONCLUSIONS AND RECOMMENDATIONS ... 109

APPENDIX A: IDENTITIES ... 112

COMMON TRIGONOMETRIC IDENTITIES ... 112
IDENTITIES FOR THE ATAN2 FUNCTION ... 113

APPENDIX B: HARMONIC ADDITION THEOREM ... 115

APPENDIX C: AN ELLIPSE ORIENTED ARBITRARILY IN THREE DIMENSIONS ... 120

APPENDIX D: TWO-BODY ORBIT PROPERTIES ... 123

APPENDIX E: ELEMENTS OF THE VIRTUAL CHIEF STATE TRANSITION MATRIX ... 126

APPENDIX F: MATLAB CODE ... 135

RELATIVE SATELLITE MOTION PLOTS AND COMPARISONS ... 135
The Algorithm. ... *135*
The Code. ... *139*
THE TWO-BODY KEPLERIAN TRUTH MODEL ... 145
The Algorithm. ... *145*
The Rotation Matrices. ... *147*
The Code. ... *151*
Examples Compared against Satellite Toolkit. ... *154*
THE VIRTUAL CHIEF METHOD ... 158
The Algorithm. ... *158*
The Code. ... *159*
HILL-CLOHESSY-WILTSHIRE EQUATIONS ... 160
The Algorithm. ... *160*
The Code. ... *160*
TRANSFORMING VIRTUAL CHIEF PARAMETERS TO CARTESIAN INITIAL CONDITIONS ... 162
The Algorithm. ... *162*
The Code. ... *162*

APPENDIX G: A DECREASING FUNCTION OF TIME ... 167

BIBLIOGRAPHY ... 169

VITA ... 181

List of Figures

Figure Page

Figure 1. Chief's LVLH frame 8

Figure 2. Direction of theta 45

Figure 3. Direction of beta 46

Figure 4. Reference Frames 62

Figure 5. Example I Trajectory 92

Figure 6. Example I Error 92

Figure 7. Example I Error Magnitude 93

Figure 8. Example II Trajectory 94

Figure 9. Example II Error 95

Figure 10. Example II Error Magnitude 95

Figure 11. Example III Trajectory 96

Figure 12. Example III Error 97

Figure 13. Example III Error Magnitude 97

Figure 14. Phase 2 Geometry 104

Figure 15. Index = 0 106

Figure 16. Index = 1 106

Figure 17. Index = 3 (x0 = 16 km) 107

Figure 18. Index = 3 (x0 = -32 km) 107

Figure 19. Phase 2 Error versus x0 108

Figure 20. Phase 2 VC Error versus Index 109

Figure 21. Eq. (A.16) 114

Figure 22. Coordinates vs. Time 137

Figure 23. Coordinates vs. Chief True Anomaly 137

Figure 24. Relative Trajectory 138

Figure 25. Error vs. Time 138

Figure 26. Rotation from i to q 148

Figure 27. Rotation from q to n 149

Figure 28. First Example Results 155

Figure 29. Second Example Results 156

Figure 30. Third Example Results 158

List of Tables

Table Page

Table 1. Example I Conditions 91

Table 2. Example II Conditions 93

Table 3. Example III Conditions 96

Table 4. Model Accuracy, Series 1 98

Table 5. Model Accuracy, Series 2 99

Table 6. Phase 2 Results 105

Table 7. Input for the First Example 154

Table 8. Input for the Second Example 156

Table 9. Input for Third Example 157

RELATIVE ORBIT ELEMENTS FOR SATELLITES IN ELLIPTICAL ORBITS

I. Introduction

Background: Relative Satellite Motion Models

Dynamics models are mathematical representations of how an object or system of objects behaves in accordance with the physics of forces and motion. A relative satellite motion model is a type of dynamics model describing the motion of one orbiting spacecraft as seen from another. Modeling the relative motion of Earth satellites is a tremendously important subject with a great diversity of applications, as we shall see. It is also a well-studied subject; many important contributions to the study were made before and during the dawn of the Space Age.

In fact, the most celebrated accomplishments of the Space Age would not have been possible without a good understanding of relative satellite motion. The Apollo astronauts could not have traveled safely to the Moon and back without the capability to rendezvous and dock in their spacecraft; this is a key application of relative satellite motion. Likewise, the history of international cooperation in space, dating back to the Apollo-Soyuz missions, has depended to some extent on merging two very different technologies for achieving spacecraft rendezvous and docking: the astronaut-dependent approach favored by the United States and the more automated approach favored by Russia (and, formerly, the Soviet Union).

Today's space technology involves many other practical uses of relative satellite motion. These include formation flying, in which multiple spacecraft orbit together with their relative motion precisely controlled in order to obtain and correlate certain data from the environment. They also include proximity operations, in which one satellite maneuvers near another, possibly for purposes other than docking, such as photographing or inspecting for damage from various perspectives. Proximity operations are often grouped together with techniques for terminal rendezvous in a category of operations called RPO (rendezvous and proximity operations). Although RPO of various types have been performed for decades, it has only been recently, and with considerable difficulty, that RPO have been attempted *autonomously*, meaning that the maneuvers are planned by computers on-board one or more of the spacecraft, rather than by humans or higher-powered computers on the ground. As we shall see, autonomy adds special requirements to the type of relative satellite motion model which must be employed.

At this point, it may be helpful to emphasize the subtle but important distinction between the terms automated and autonomous, as used in this study. Autonomy (sometimes called full autonomy or autonomous planning) implies that guidance, navigation, and control are accomplished with neither astronauts nor ground stations in the loop, and that maneuvers are planned by the on-board computer [38, 44, 104]. Automated (or automatic) RPO has been used since 1967, when early unmanned Soyuz vehicles docked during the Kosmos 186/188 mission [104]. Automated rendezvous as still practiced by Progress cargo vehicles involves a pre-determined flight profile, with

some maneuvers initiated by ground controllers, and other maneuvers calculated from the relative navigation sensor data [31].

Selecting the best dynamics model to use for a particular application often depends on a trade-off between simplicity and accuracy. Every dynamics model is an approximation; that is, mathematically representing every force and the motion of every object in the universe is neither possible nor helpful. Rather, an engineer need only model those forces which make a noticeable difference for the given application. Likewise, an engineer can represent those forces, as well as the resulting motion, with a mathematical approximation. This approximation may be simpler and less accurate than the most accurate description offered by physics, so long as the resulting error is not too great for the given application.

As an example, consider a spacecraft attempting autonomous RPO. Autonomy in space systems depends on the computer software, including navigation filters, guidance algorithms, and control systems, operating without direction from control stations on Earth. On the one hand, the dynamics model at the core of each of these software functions must be accurate enough for any given operation to succeed within the mission's error tolerance. On the other hand, if the model is not simple enough to implement with the available computing power, the spacecraft cannot perform the function. In particular, spacecraft trajectory design is usually the subject of extensive pre-mission planning using high-speed computers and high-fidelity physics models. This practice is good and useful, but for truly autonomous RPO, the trajectory planning function must be replicated on-board.

The field of relative satellite motion includes models that consider a variety of forces. In the present study, though, we will focus on models which include only a simplified representation of the Earth's gravity. Each satellite will be considered a point mass, and the Earth will be considered a uniform sphere, so that its gravity field decreases with the distance squared from the Earth's center. We call this approximation the two-body assumption, because it is the basis for the classical two-body problem of astrodynamics. The trajectory of a spacecraft moving in such an inverse-square gravity field is a simple Keplerian orbit, which can be described in terms of the classical parameters known as orbit elements. Commonly known properties of two-body orbits can be found in any astrodynamics text; for convenience, several are listed in Appendix D.

Of course, in reality, satellites experience many forces other than inverse-square gravity. In general, the accuracy of the two-body assumption tends to decrease over time as these forces perturb the orbit. However, relative satellite motion models which do not consider such perturbing forces are accurate enough for some applications over limited time scales.

Other approximations can be used to simplify relative satellite motion models. Many models assume that the dynamics are governed by a set of linear differential equations; this linearization usually requires assuming small differences in the variables. For example, if the distance between two satellites is small enough compared to their distance from the Earth's center, or if the differences in their classical orbit elements are small enough, then any terms in the equations of motion which contain one small variable

multiplied by another may be neglected. Such linearized models are the main emphasis of the present study. If a given application cannot accept the error that results from neglecting all nonlinear terms, it may require a model which retains the quadratic terms, but neglects terms which are third-order or higher in the variables; these quadratic models are more accurate but also more complex than linearized ones.

Another approximation commonly used for relative satellite motion models involves the eccentricity of the satellite orbits. Several properties of two-body orbits can be approximated by power series expansions in terms of orbital eccentricity. If a given application can be restricted to satellites in low-eccentricity orbits, then truncating these power series expansions after the first-order or second-order terms will introduce only a small amount of error. If the application is restricted to orbits with negligible eccentricity, then only the zeroth-order terms need to be retained.

The simplest and most commonly-applied relative satellite motion models address the circular chief problem; that is, they describe the motion of one satellite, a deputy, with respect to a chief satellite whose orbit has zero eccentricity. Modeling the circular chief problem is discussed in more detail in Chapters II and III. For now, it suffices to say that the most common model is the Hill-Clohessy-Wiltshire (HCW) model, a two-body linearized model [40, 16]. One particularly useful realization of the HCW model is the Relative Orbit Elements (ROEs) developed at the Air Force Research Laboratory and AFIT [60]. As we shall see, ROEs provide unique insight into the geometry of the relative trajectory and are simple enough to serve as the foundation for maneuver schemes and guidance algorithms suitable for autonomous RPO. Lovell and Tragesser

described this advantage of ROEs as "operational efficacy", because they "lend themselves well to the development of on-board guidance and/or mission planning software" [60].

Another group of relative satellite motion models address the elliptical chief problem, in which the chief's orbit is permitted to be noncircular; that is, the chief eccentricity may take on values between zero and one. Modeling the elliptical chief problem is discussed in more detail in Chapters II and IV. In this problem, even after making the two-body assumption, a satellite's angular velocity, angular acceleration, and distance from the Earth's center are no longer constants, as they are in the circular chief problem. For this reason, elliptical chief models tend to be more complex.

Problem Statement

Although many relative satellite motion models exist for the elliptical chief problem, none have been stated in a way that lends itself to the same high degree of operational efficacy as have ROEs for the circular chief problem. In other words, there is a need for realizations of relative satellite motion which do not restrict the eccentricity of the chief satellite's orbit to zero, but which are still practical enough to facilitate autonomous guidance and maneuver schemes.

This need is the basis for the current research. This thesis attempts to answer the following two questions: What characteristics of the ROE realization provide operational efficacy? How can we retain those advantageous characteristics while relaxing the eccentricity restriction?

The thesis is organized in five chapters. The remainder of Chapter I introduces the reference frames and some of the mathematical notation used throughout the later chapters. Chapter II is a comprehensive (although not exhaustive) survey of the vast literature on relative satellite motion models. Chapter III includes a brief overview of the HCW model and a detailed derivation and geometric analysis of the ROE parameters for the circular chief problem. Chapter IV lays out five possible approaches for handling eccentricity in the chief's orbit; it then follows through with the approach selected, called the Virtual Chief method, by deriving and solving the equations of motion for a new relative satellite motion model. The chapter continues by deriving a parameterized version of the Virtual Chief model's solution, analyzing the new parameters for their geometric significance. Chapter V examines numerical simulation results and evaluates the accuracy of the Virtual Chief model; finding its accuracy significantly less than would be desired, the chapter concludes with a theoretical analysis of the approximation errors and recommendations for future development.

Notation and Reference Frames

The reference frame most commonly used to describe relative satellite motion is a local-vertical local-horizontal (LVLH) frame, sometimes called an orbital or Hill frame. The center of an LVLH frame is fixed to a satellite, and its coordinate axes rotate at the same rate as the satellite moves through its orbit. When considering a relative satellite motion model, we can say that the chief satellite exists at point C, and its LVLH frame is frame **c**, as in Figure 1. The frame's orthogonal unit basis vectors are defined in this

thesis as follows: $\hat{c}_1$ is parallel to the position vector from the Earth's center to the chief, in the outward sense. $\hat{c}_2$ is orthogonal to $\hat{c}_1$, within the plane of the chief's orbit, and in the same sense as the chief's inertial velocity vector. $\hat{c}_3$ completes the right-handed set.

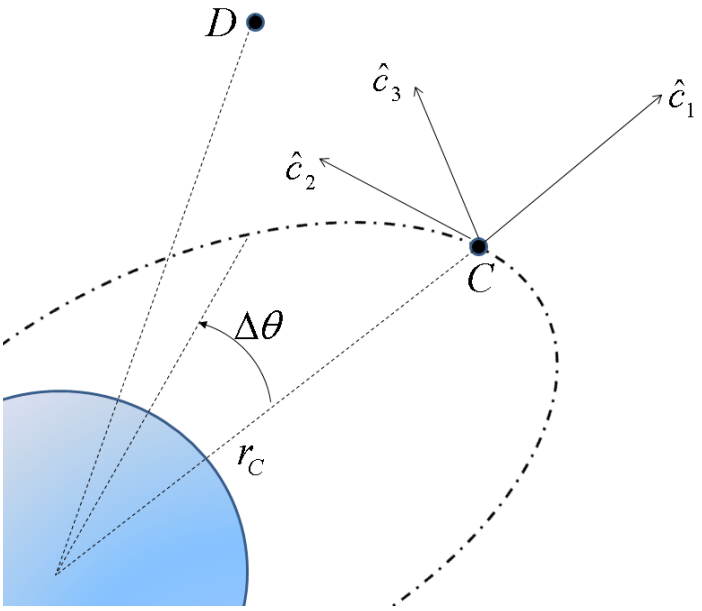

Figure 1. Chief's LVLH frame

Of course, dynamics cannot be performed without an inertial reference. In studying relative satellite motion, the most commonly used inertial frames are Earth-centered inertial (ECI) frames. Some of these are perifocal frames, oriented to a satellite's orbit plane. If **i** is an ECI frame, then we can say that the angular velocity of frame **c** with respect to **i** is $\vec{\omega}_{c/i}$.

Also, if the deputy satellite is located at point D, we can say that its position relative to the chief is $\vec{r}_{D/C}$. A relative satellite motion model must be able to describe not

only position, but also the deputy's relative velocity, or the time derivative of the relative position vector with respect to the **c**-frame, denoted $^{c}\frac{d}{dt}\vec{r}_{D/C}$. This description is usually (although not always) accomplished via equations of motion which define the relative acceleration, the **c**-frame second time derivative, $^{c}\frac{d^2}{dt^2}\vec{r}_{D/C}$.

If we assign variables x, y, and z as the **c**-frame relative position components, then we can write the relative position in either of the following ways:

$$\begin{aligned}\vec{r}_{D/C} &= x\hat{c}_1 + y\hat{c}_2 + z\hat{c}_3 \\ &= \begin{bmatrix} x \\ y \\ z \end{bmatrix}_c\end{aligned}$$

The solution of a relative satellite motion model, then, must give values for all three components of relative position and all three components of relative velocity for any time t. In other words, using a dot to represent a scalar time derivative, we must know $x(t), y(t)$, $z(t)$ $\dot{x}(t)$, $\dot{y}(t)$, and $\dot{z}(t)$. Note that

$$^{c}\frac{d}{dt}\vec{r}_{D/C} = \begin{bmatrix} \dot{x} \\ \dot{y} \\ \dot{z} \end{bmatrix}_c$$

The coordinates just described constitute a rectangular Cartesian coordinate system. It should be noted that cylindrical coordinates may also be used for an LVLH

frame; in this case, y is replaced by $r_C \Delta\theta$, where r_C is the distance from the Earth's center to the chief, and $\Delta\theta$ is the polar angle between the deputy and the chief, as shown in Figure 1. Interpreting an LVLH solution as cylindrical can increase the accuracy, since the chief satellite is not really moving in a straight line down the y-axis. This is especially true in the circular chief problem, when r_C is constant and θ corresponds to the true longitude through which the chief is moving at a constant rate. However, the error due to using rectangular coordinates is often well within a given application's error tolerance, particularly if the application is using a linearized model, and thus already assuming small relative separation distances.

II. Literature Review

There is a vast amount of technical literature on relative satellite motion. This survey cannot be exhaustive, but it is intended to cover the most significant developments in a variety of areas. The first two sections describe models of unperturbed motion in the circular and elliptical chief problems. The third section explains some of the most significant practical applications that have been designed to use such models. The final two sections provide a brief survey of higher-fidelity models and review a few existing methods for making comparisons between models.

Circular Chief Problem

Hill-Clohessy-Wiltshire Model.

The first and best known relative satellite motion model is the HCW model mentioned in Chapter I. It was developed by Clohessy and Wiltshire in 1960 [16]. The equations of motion which they derived and solved are similar to those used by the famous American mathematician George Hill in 1878 to describe the Moon's motion relative to the Earth [40]. The HCW model assumes that each satellite is following Keplerian two-body motion and that the chief's orbit is circular; the equations of motion are linearized by assuming small relative distances. The HCW model has served as the basis for most real-life RPO missions. As we shall see, a key advantage of HCW is that its solution has easily discernible geometric features.

In 2001, Sabol, Burns, and McLaughlin published a study closely examining the geometry of HCW dynamics [75]. They noted that even very small differences in semi-

major axis between the chief and deputy would result in different periods (see Eq. (D.1)) and therefore would cause the two satellites to drift apart in the y-direction over time. They further asserted that, under HCW dynamics, every relative satellite trajectory which does not drift in this way is shaped like an ellipse. They also proposed a number of potentially useful formation flying geometries, including a projected circular orbit (PCO), in which several satellites orbit together in such a way that they appear to remain on a circle in the y-z plane.

In 2004, Lovell, Tragesser, and Tollefson [61] and Lovell and Tragesser [60] identified the ROEs, six parameters that could be used to define HCW relative satellite motion in a geometrically intuitive way. They showed the transformations between ROEs and other possible realizations: Cartesian initial conditions (that is, values of the position and velocity components at epoch time) and orbit-element differences (that is, differences in the values of the chief's and deputy's classical orbit elements). They also showed that the HCW solution written in terms of ROEs can be used to calculate impulsive maneuvers as part of an autonomous guidance algorithm.

Also in 2004, Press used ROEs to describe the physical geometry of an HCW relative orbit [71]. He showed that an instantaneous relative trajectory is confined to a plane and is defined by the intersection of that plane with a 2x1 elliptical cylinder orthogonal to the x-y plane. The relative orbit plane and the elliptical cylinder may be drifting at the same rate in the y-direction.

Quadratic Models.

In 1963, London published a new relative satellite motion model accurate over longer distances than the HCW model [57]. He still assumed a circular chief orbit, but retained second-order terms in the relative distance. London's equations of motion are more complex than the HCW equations, but they can be solved by the method of successive approximations. The resulting solution includes secular terms (containing t and t^2) in the y-direction and mixed-secular terms (of the form $\alpha_1 t \sin(\alpha_2 t + \alpha_3)$) in all three directions.

In 1999, Sedwick, Miller, and Kong, in the process of studying HCW dynamics perturbed by the J2 term of the Earth's gravitational field, developed an unperturbed quadratic equation of motion for the radial direction [81]. They illustrated that, for some relative satellite motion applications, the linearization error is negligible compared to the differential J2 effect.

More recently, in 2003, Karlgaard and Lutze used spherical instead of rectangular or cylindrical coordinates to derive equations of relative motion [48]. They retained up to quadratic terms in the relative position and velocity components. They solved the equations using the method of multiple scales; part of their rationale for this method was that it eliminates the mixed-secular terms in the x- and z-directions found in London's solution.

About the same time, Gurfil and Kasdin used orbit-element differences to create arbitrarily high-order nonlinear corrections to the HCW model [36, 37]. Then, by

truncating the infinite series relating the deputy's true anomaly to time, they created a time-explicit solution that is second-order in the orbit-element differences.

Elliptical Chief Problem

Lawden's Equations: the First Generation.

The first generation of linearized models for the elliptical chief problem was developed via three independent paths during the period from the 1950s through the mid-1980s. Only one of the three paths was pursuing a relative satellite motion model. The other two paths used equivalent equations of motion while attempting to model other spaceflight phenomena, such as a spacecraft's deviation from a reference trajectory. This system of equivalent equations has been expressed in a variety of coordinate types (rectangular and cylindrical) and independent variables (time, chief true anomaly, and chief eccentric anomaly). Derivations of several forms of these equations can be found in Schaub and Junkins [79].

Path One.

The first to derive and solve the equations was Lawden in 1954 (in-plane components only) [55] and 1963 (all three components) [56]. His purpose was to describe the primer vector for optimal spacecraft trajectory design. Lawden's equations are perhaps the best-known elliptical-chief model. Written for LVLH-frame coordinates, they use the chief's true anomaly as the independent variable, so that the first equation defines x'', a scalar second derivative with respect to chief true anomaly, rather than $\ddot{x}$, and so on. Lawden's 1963 book lays out a complete theory of optimal trajectory design; the sections of present interest concern spacecraft in an inverse-square gravity field.

Lawden presented a closed-form solution for position and velocity in terms of arbitrary integration constants. He also presented the equations and solution in an alternate form where each coordinate is scaled by the chief's orbit radius; note that this scale factor is not a constant (see Eq. (D.2)). When the solution is written for unscaled coordinates, its terms contain a cumbersome definite integral which is singular for circular chief orbits. However, the 1954 article gave a closed-form expression for this integral that is valid for chief eccentricities between zero and one.

A key characteristic of all exact solutions to Lawden's equations is that their coefficients are time-varying, but not explicitly. Instead, the coefficients vary with the chief's true anomaly. Thus, because Kepler's equation (Eq. (D.4)) is transcendental, the solutions cannot be completely explicit in time.

A little-noticed contribution from Lawden's book was his study of the primer vector solution in coordinates parallel to the reference perifocal frame. This solution (which is mathematically equivalent to studying the deputy's relative motion in a non-rotating frame fixed to the chief and parallel to the chief's perifocal frame) proves to be much simpler, showing a small variation from circular motion.

Path Two.

The second path began with De Vries, also in 1963 [26]. De Vries was the first to address the elliptical chief problem directly. Like Clohessy and Wiltshire, he linearized the two-body problem by assuming small relative distances to create time-domain differential equations in the chief's LVLH coordinates. However, because he did not assume a circular chief orbit, the coefficients of these equations of motion include time-

varying quantities (chief orbit radius and chief true anomaly). In order to solve this system of equations, De Vries attempted to transform them into the true-anomaly domain. However, the out-of-plane component of this transformed system is incorrect [94].

Two years later, Tschauner and Hempel tackled the relative satellite motion problem in a paper whose title translates to "Rendezvous with a Target in an Elliptical Orbit" [94]. They corrected De Vries's mistake to create a three-dimensional system of true-anomaly-domain equations of relative motion. After they scaled these equations to the chief's orbit radius, they could be solved simply in closed form. Tschauner and Hempel's equations of motion, in both scaled and unscaled form, are mathematically the same as those used by Lawden. In fact, some authors refer to Lawden's equations as the Tschauner-Hempel equations. Later, Tschauner studied the equivalent system of equations transformed to the chief eccentric anomaly domain [93].

In 1966, Shulman and Scott presented an alternate derivation for the linearized equations of motion [88]. They proceeded to find a closed-form solution. They also mapped the arbitrary integration constants of that solution to Cartesian initial conditions for the special case when epoch time occurs at chief perigee. Importantly, they published graphical results of numerical simulations comparing their model (a linearized model complete in the chief's eccentricity, like Lawden's equations) to the full nonlinear Keplerian equations integrated numerically and to a variety of low-eccentricity approximations. Some of these numerical results show the effect of the mixed-secular terms in the x-direction.

In 1983, Wolfsberger, Weiß, and Rangnitt presented a general closed-form solution to Lawden's equations (which they knew only from Tschauner and Hempel) [105]. These solutions take the form of a linear system in the Cartesian initial conditions, and can be initialized with an epoch time anywhere along the chief orbit. They continue to use rotating LVLH coordinates primarily, although they did calculate and plot an example relative trajectory in inertial chief-fixed coordinates, allowing a visual comparison.

Path Three.

The third path began with Stern's research in 1963 [90]. Stern independently developed a model mathematically equivalent to De Vries's time-domain equations in order to describe spacecraft motion about a reference trajectory for the purpose of midcourse guidance. Before solving the system, he transformed to cylindrical coordinates and to chief true anomaly as the independent variable (except for the out-of-plane component, for which the chief's eccentric anomaly became the independent variable). Stern solved this transformed system directly in closed form. He then derived expressions for the in-plane relative position coordinates via orbit-element differences. He also showed the equivalence of the two methods, relating the arbitrary integration constants in the original solution to the orbit-element differences.

The next contribution to the third path was from Jones in 1980 [46]. He used the time-domain differential equations from Stern, and presented a slightly modified form of Stern's closed-form solution, including a state transition matrix (although the elements were not shown, simply the algorithm for calculating it). He also demonstrated that,

according to the linearized equations, small impulsive changes can result in secular variations (drift) in multiple states, not only along-track position.

Lawden's Equations: Later Developments.

In 1987, Carter and Humi became the first to unify two of the paths [14]. They recognized that Lawden's equations and solution are equivalent to those found by De Vries, Tschauner and Hempel, and those who followed. In 1990, Carter [11] found an improvement to the definite integral in Lawden's solution. Carter's new definite integral is no longer singular for circular chief orbits, allowing the solution to be applied to all chief eccentricities.

In 2002, Inalhan, Tillerson, and How built on the previous results, presenting time-domain and true-anomaly-domain versions of Lawden's equations and a non-singular version of the solution in terms of six integration constants [41]. They showed that setting one of the in-plane integration constants to zero corresponds to a boundedness condition; that is, it is an equivalent constraint to requiring the chief and deputy orbits to have the same semi-major axis, eliminating the secular drift terms. One of their most important contributions was a study of modeling error costs. Specifically, they showed that the fuel penalty could be significant for using an HCW-based formationkeeping control algorithm, even for Shuttle-type eccentricities (0.005).

Also in 2002, Yamanaka and Ankersen used a new approach to eliminate the definite integral in the solution to Lawden's equations [106]. Their new term is proportional to the transition time; thus the Yamanaka-Ankersen solution has coefficients

expressed in terms of both time and chief true anomaly. They organized the solution into a fairly complex state transition matrix.

In 2003, Broucke solved the time-domain version of Lawden's equations directly, without having to transform to chief true anomaly as the independent variable [8]. Instead, he replaced the time-varying coefficients first found by De Vries, taking their partial derivatives with respect to the chief's classical orbit elements. He showed a method for organizing the solution into a state transition matrix; the matrix still contains elements that vary with true anomaly, rather than explicitly with time.

Later, Sengupta [83] and Sengupta and Vadali [85, 86] summarized solutions to the elliptical chief problem. They solved the true-anomaly-domain equations of motion in terms of scaled and unscaled coordinates, using the Yamanaka-Ankersen method of eliminating the definite integrals. Their "velocity" solution is shown first in the true anomaly domain (i.e., they solve for $x'(t)$ instead of $\dot{x}(t)$, etc.). They included a generally applicable mapping from the solution's six constants of integration to Cartesian initial conditions; they also laid out an approach for developing a state transition matrix in these terms. Sengupta and Vadali also transformed the solution into a time-explicit version, retaining the infinite-series Fourier-Bessel expansions [6] of the coefficients; because the series are not truncated, they remain exact solutions to Lawden's equations, but may be difficult to implement practically. Finally, Sengupta and Vadali developed simple expressions for quantifying the amount of drift in unbounded-motion cases (i.e., mismatched semi-major axes); they showed that this drift, measured over an integer number of chief orbits, is a minimum when that measurement occurs at chief apogee.

In 2007, Irvin derived a new form of Lawden's equations using fractions of the chief orbit as a non-dimensional independent variable [42]. His research in the chief-orbit-fraction domain focused on applications of the circular chief problem, however.

Equivalent Forms.

Other linearized relative satellite motion models for the elliptical chief problem are physically equivalent to using Lawden's equations, even though they are not described in terms of Cartesian LVLH coordinates.

In 1994, Kelly, aware of both Lawden's and Tschauner and Hempel's work, created a physically equivalent model, but resolved in the coordinates of a non-orthogonal reference frame [50]. In Kelly's frame, the 2-direction is changed so that it is always parallel to the chief's inertial velocity vector. Kelly presented time-domain differential equations of motion linearized about the reference orbit, as well as a closed-form solution in the form of a relatively simple state transition matrix. He also gave the mapping between his coordinates and more traditional orthogonal LVLH coordinates. He further showed how his model lends itself to a simple impulsive maneuver scheme.

In 2006, Rathke and Izzo used a reference frame defined in the same way as Kelly's to describe the behavior of an asteroid after an impact [72]. They found secular terms only in the 2-direction. They asserted that their solution, when rotated into LVLH coordinates, is "an analytic and explicit solution of the Tschauner-Hempel equations".

Most linearized relative satellite motion models take the difference between the nonlinear Keplerian two-body motion of each satellite, rotate into an LVLH frame, and then truncate a binomial series expansion of the relative gravitational force term. In

1997, Der and Danchick took a different approach [25]. They used a linearized state transition matrix of the two-body problem itself (using universal variables), applying it to both satellites and then taking the difference. This resulted in a relative motion solution in ECI coordinates, which can be transformed into other reference frames via rotation matrices.

As we have seen from Stern, it is also possible to represent linearized two-body motion in terms of small differences between the chief and deputy orbit elements. This approach is physically equivalent to using Lawden's equations, but yields some additional insight into how the large-scale geometric features of the two orbits compare. This concept was rediscovered by a series of studies that, unaware of Stern's results, exploited orbit-element differences to model relative satellite motion.

One of the first studies to do so was that of Garrison, Gardner, and Axelrad in 1995 [32]. They derived a state transition matrix and LVLH trajectory equations linearized with respect to the orbit-element differences. Their numerical results were "nearly identical" to a numerical integration of Lawden's equations; they recognized that any differences between the two methods would have to be of second order.

The best-known work using orbit-element differences came in 2003 and 2004 from Schaub [77, 78] and Schaub and Junkins [79]. This research used a set of elements in which eccentricity and argument of perigee are replaced, so that the system is not singular for circular orbits. Schaub and Junkins included a linearized mapping between orbit-element differences and Cartesian coordinates, and they derived equations for Cartesian LVLH velocity by directly differentiating the position equations. They

examined the difference in mean anomaly, δM , as a function of time and of chief true anomaly, and derived an expression for drift ($\delta \dot{M}$) incorporating the effect of unequal orbit energies (mismatched semi-major axes).

In 2006, Lane and Axelrad transformed Broucke's approach to develop a three-dimensional linearized description of relative satellite motion in terms of classical orbit-element differences [54]. They showed that the in-plane position depends on the difference in right ascension of the ascending node, $\delta\Omega$, in a way that Broucke did not capture, because Broucke treated coplanar motion independently from cross-track motion.

The research of Sengupta and Vadali [86] also included orbit-element differences. Using classical orbit elements as well as a variety of nonsingular element sets, they derived expressions for relative position and velocity in terms of element differences, showing that the results are mathematically equivalent to their solutions of Lawden's equations. They included the mapping from the six constants of integration to these orbit-element differences.

Bounded-motion Analysis of Lawden's Equations.

Some of the most interesting and geometrically meaningful analysis of the elliptical chief problem has occurred in studies requiring bounded motion. A solution to Lawden's equations can be made bounded, or periodic, if it is subjected to one of the following equivalent constraints: requiring zero drift, equal orbit energies, or equal semi-major axes. The remaining solution terms are usually somewhat simpler.

In 2003, Zhang and Sun offered a linearized relative satellite motion model that assumes equal semi-major axes and small orbit-element differences [111]. They gave

position solutions in terms of these differences and in terms of Cartesian initial conditions. They further analyzed the geometry of the resulting trajectory and suggested formation designs not possible in the circular chief problem.

Schaub's research [78, 79] also included analysis of bounded motion. The linearized expression for semi-major axis difference, δa, can be set to zero and used as a boundedness condition. After this condition is imposed, the scaled non-dimensional position equations of Schaub's model give some geometrical insight into the trajectory.

The research of Lane and Axelrad [54] resulted in a simple bounded-motion model with parameters very similar to the ROEs of the circular chief problem. The eight parameters are not linearly independent, and they are defined in terms of five orbit-element differences (only five because δa is already set to zero in the boundedness condition). They analyzed three specific formation geometries possible in the bounded motion model. The most interesting is an in-track/cross-track formation, in which the deputy's motion follows an ellipse in the y-z plane with no associated x-motion, behavior impossible in the circular chief problem.

The research of Sengupta and Vadali [86] also included geometrically insightful bounded-motion analysis. They derived a boundedness condition from their solution to Lawden's equations by setting one of the constants of integration to zero; they expressed this condition in terms of both scaled and unscaled Cartesian coordinates. They next wrote a bounded version of the position solution using five design parameters; again, there are only five design parameters because one degree of freedom was used to eliminate drift. After analyzing the effect of these design parameters and comparing to

the bounded HCW model, Sengupta and Vadali observed five geometric effects of eccentricity: higher-frequency harmonics, amplitude scaling, phase shift, off-center formations, and skewness of the relative orbit "plane."

In 2008, Jiang, Li, Baoyin, and Gao used a unique celestial-sphere approach to derive a relative satellite-motion model [45]. They showed that in its linearized and bounded-motion form, their model is equivalent to a bounded-motion solution to Lawden's equations. They created a position solution using five parameters, relating these parameters to the integration constants used by Inalhan, Tillerson, and How, and then to Cartesian initial conditions. Next, they used a change of variable to $s(t)$, defined as

$$s(t) = \tan\frac{\nu(t)}{2}$$

In this way, they eliminated all trigonometric terms, creating a completely algebraic parameterized solution. This algebraic form lends itself to simple geometric analysis; Jiang et al. found that the trajectory's projection into each of the LVLH coordinate planes could be described by a quartic equation. They also found that such a bounded trajectory could have at most one self-intersection point; they derived expressions for locating such points, as well as for locating chief-deputy collision points (i.e., when the deputy crosses the LVLH frame's origin). They further proved that, except in a limited number of degenerate cases, a bounded relative trajectory is *not* confined to a plane, as is the case in the circular chief problem.

The most dramatic result from Jiang et al. was proving that, in three dimensions, a bounded relative trajectory is always confined to a quadric surface. The coefficients of the quadric-surface equation can be related to chief eccentricity and the five relative orbit parameters. Jiang et al. derived expressions for finding the geometric center of the quadric surface; for rotating from LVLH coordinates to quadric-surface principal-axis coordinates; and for determining in a particular case whether the quadric surface will be an elliptic cylinder, a hyperboloid of one sheet, or an elliptic cone. All self-intersecting relative trajectories are confined to the surface of an elliptic cone.

Low-eccentricity Approximations.

Since relative satellite motion models for the elliptical chief problem tend to be somewhat complex, there have been numerous efforts to simplify the equations of motion or their solutions by assuming small values for the chief's eccentricity. Many of these expand coefficients containing the chief's true anomaly, angular rate, and orbit radius in an eccentricity power series, truncating the results to retain only terms which are first-, second-, or third-order in eccentricity. The more terms retained, the more complex the result, but also the more accurate for a given level of chief eccentricity. This series-expansion approach can have the added operational advantage of rendering the solution completely explicit in time.

In 1965, Anthony and Sasaki solved their second-order equations of relative motion via the method of differential corrections [4]. That is, their relative motion solution was composed of the HCW solution plus a correction for first-order eccentricity plus another correction for quadratic terms in the displacement. Leaving out the

eccentricity correction resulted in a solution equivalent to London's. But leaving out the quadratic correction resulted in a linear model valid for first-order eccentricity. This linear model is time-explicit, containing periodic terms with frequencies $n_C t$ and $2n_C t$ (where n_C is the chief's mean motion) and mixed-secular terms. In numerical examples, the linear model did not perform as well as the quadratic, as expected, especially when it came to capturing drift in the radial direction; but the example formations were all on the scale of 50 miles or larger.

Jones [46] also addressed small-eccentricity orbits in his research, using a first-order truncated eccentricity power series. He gave the elements of the resulting state-transition matrix, and showed that the percentage error using this approximation is significantly improved over that using a circular orbit approximation (i.e., neglecting the chief eccentricity and using HCW dynamics alone).

In 2000, Melton found an approximate solution to the time-domain version of Lawden's equations in both rectangular and cylindrical coordinates [66]. Using Lagrange's generalized expansion theorem [6], he expanded the dynamics matrix, creating a time-explicit matrix equation of motion in the form of an eccentricity power series which can be truncated at the desired order. This form admits a solution in the form of a state transition matrix expanded in an eccentricity power series, truncated to the same order. The zeroth-order matrix corresponds to HCW dynamics. Melton listed the elements for the first- and second-order state transition matrices in both rectangular and cylindrical coordinates. Of course, the method described could be used to generate approximate solutions of arbitrarily high order. The first- and second-order elements

include periodic terms with frequencies $n_C t$, $2n_C t$, and $3n_C t$, plus mixed-secular terms. Melton believed that the mixed-secular terms in the x-direction lacked physical significance.

In 2003, Sabol, McLaughlin, and Luu proposed a new relative satellite motion model, which they entitled the COWPOKE Equations, standing for Cluster Orbits with Perturbations of Keplerian Elements [76]. In spite of the title, the original model did not include perturbing forces, making it an approximation of the two-body elliptical chief problem. The model used a linearized orbit-element difference approach to describe relative position in spherical coordinates; it then used Fourier-Bessel series expansions to make the equations explicit in time, allowing truncation at the desired power of chief eccentricity. They carefully analyzed the question of how many terms to retain in order to approximate well even for higher eccentricities; this is important because for values higher than about 0.03, the coefficients may increase faster than the powers of eccentricity decrease. Sabol et al. wrote out some of the required expansions to tenth order and the complete equations to first order. Their numerical simulations showed reasonable results for the first-order model at a chief eccentricity of 0.01 and for the tenth-order model at a chief eccentricity of 0.7.

In 2003, Vaddi, Vadali, and Alfriend extended previous approximations by adding corrections to the HCW solutions that are quadratic in the relative distance and third-order in the chief's eccentricity [97]. A linearized model is easily constructed by leaving out the quadratic corrections; Vaddi, et al., wrote out the linear equations in terms of Cartesian initial conditions for the special case when motion is bounded and epoch time

occurs at chief perigee. Interestingly, the out-of-plane equation contains no third-order terms. They also included a boundedness condition for this special case.

Schaub's research [78, 79] also examined a small-eccentricity approximation. Noting that the linearization of his orbit-element difference method already assumed a small value for the ratio of relative distance to chief orbit radius, he stated that powers of chief eccentricity smaller than that ratio could be neglected. He created a first-order approximation of chief orbit radius (see Eq. (D.2)) as $a_C\left(1-e_C\cos\nu_C\left(t\right)\right)$, where the subscript C indicates chief orbit elements. He was then able to write first-order approximations for δM and for the relative position coordinates.

In 2006, Ketema developed a complex nonlinear relative satellite motion model, and then created a linearized approximation by assuming small chief eccentricity and small differences in eccentricity and inclination [51]. After further assuming bounded motion, Ketema created a model with interesting geometric characteristics. In this model, the relative trajectory's projection into the chief orbit plane (the x-y plane) is shown to be an ellipse centered at $\left(0,-a_C\left(e_C+\delta e\right)\sin E_{C,0}\right)$, where $E_{C,0}$ is the chief's eccentric anomaly at epoch.

Quadratic Models.

As with the circular chief problem, a relative satellite motion model that includes quadratic terms in the relative distance increases accuracy over a linearized model, especially as the relative distance grows.

The model of Anthony and Sasaki [4] was the first such model. Their quadratic corrections include periodic terms with frequencies of $n_C t$ and $2n_C t$, mixed-secular

terms, and, in the along-track direction only, terms with a factor of t^2. They also showed how this model, continuing with the method of differential corrections, can be used effectively to solve rendezvous problems.

In 1967, Euler and Shulman derived true-anomaly-domain equations of relative motion directly analogous to Lawden's equations, but retaining quadratic gravity terms [28]. To solve, they used the known solutions to Lawden's equations as the homogeneous solution, converted the quadratic terms to forcing functions, and solved for the particular solutions in the x- and z-directions via variation of parameters. They were unable to find a closed-form particular solution in the y-direction.

The model developed by Vaddi, Vadali, and Alfriend [97] included quadratic corrections, as we have seen. They also analyzed the higher-order coupling between nonlinearity and eccentricity, although this coupling was not reflected in their model.

In 2006, Sengupta, Sharma, and Vadali extended the results of Euler and Shulman by finding a closed-form solution in all three relative components [84]. They were able to do so in the case of bounded motion. To solve, they used a perturbation approach involving a small parameter which depends on relative distance and chief eccentricity. Since bounded motion was important to their result, they derived an index to quantify drift, or rather, to quantify error as compared with the boundedness condition. They also noted that, strictly speaking, all two-body solutions are bounded, but that what we really need is 1:1 resonance between the chief and deputy orbit periods.

Applications of Relative Motion

Relative satellite motion models have been used for a variety of spaceflight applications. In 1981, Kelley, Cliff, and Lutze used HCW dynamics and a maneuver-scheme game scenario to analyze pursuit and evasion on orbit [49]. As we have seen, Rathke and Izzo [72] applied a linearized elliptical chief model to study asteroid deflection missions.

Some studies have applied a variety of models to develop relative guidance, navigation, and control applications [22, 27, 34, 47, 60, 63, 87, 89, 96, 100, 109].

Other studies have examined formation flying missions [9, 35, 63, 75, 95, 107, 111], such as the European PRISMA mission [22], NASA's Magnetosphere Multiscale mission [21, 34, 62, 80, 109], or a variety of Earth-observing synthetic-aperture or bistatic radar concepts [30, 52, 81].

The largest group of studies considered for this survey considered rendezvous and proximity operations (RPO) [7, 15, 31, 38, 42, 43, 44, 69, 83, 92, 104, 105, 110]. Specific studies have covered operations near the International Space Station, including Free Flyer missions [64, 74] and the European ATV resupply vehicle [89, 99]. Early autonomous RPO experiments have included the Japanese ETS-VII mission [68], the Air Force's XSS-11 mission [104], and Orbital Express, managed by DARPA and NASA [29, 100]. In 2005, Naasz planned for a robotic servicing mission to the Hubble Space Telescope by studying a parameterized version of the HCW model, using a variety of geometric constraints [67].

Higher-fidelity Models

The present research focuses on linear or quadratic approximations of unperturbed two-body relative satellite motion. However, for a model to be accurate over long distances or long time scales, it must consider a variety of other factors. The literature contains many examples of such high-fidelity models.

High-order nonlinear models can be accurate even without a closeness assumption that requires the deputy to remain within a certain distance from the chief [17, 18, 19, 20, 37, 47, 51, 53, 70, 87, 111]. These models tend to be complex, and several require determining both the chief and deputy orbit elements prior to calculating the relative motion.

In 2009, Segal and Gurfil developed a nonlinear six-degree-of-freedom model that included spacecraft rotation effects [82].

Many models consider the differential effects of the J2 [3, 23, 33, 39, 50, 77, 78, 81, 83, 108] term of the Earth's gravity field. Wiesel accounted for higher-order gravity terms, as well [103]. Other models considered the differential effects of air drag in low-altitude orbits [5, 13, 23, 77, 103]. Lovell, Horneman, Tragesser, and Tollefson incorporated the J2 and differential drag effects on ROEs [59].

Finally, even though the present research does not consider eccentricity greater than or equal to 1, some researchers have considered relative satellite motion on parabolic, hyperbolic, or rectilinear Keplerian orbits [10].

Model Comparisons

A few studies in the literature have been devoted to comparing relative satellite motion models or to developing criteria for such comparisons.

For example, in 1998, Carter provided a fairly comprehensive bibliography and taxonomy of models developed to that point [12]. He was one of the few authors aware of the third path of development in the first generation of linearized elliptical chief models (Stern [90] and Jones [46]).

In 2003, Melton numerically compared four models to HCW and to numerically integrated fully nonlinear equations of motion [65]. The models he compared are Yamanaka-Ankersen [106], Broucke [8], Melton [66], and Karlgaard-Lutze [48]. The first two performed the same; this is understandable, since both are versions of Lawden's equations. Except for chief eccentricities below about 0.2, the first two performed noticeably better than the third; this, too, is understandable, since Melton's model is an approximation (second-order, in this case) to Lawden's equations. The fourth model performed much better than HCW, also as expected.

In 2005, Alfriend and Yan showed that the accuracy of a relative satellite motion model increases with its complexity [2]. They compared a variety of models and discovered that the scale of the relative trajectory and the chief eccentricity are key parameters for characterizing their accuracy. Their evaluation considered not only eccentricity, but also J2 and high-order nonlinear effects.

Also in 2005, Lovell, Chavez, and Johnson compared the Yamanaka-Ankersen model to HCW dynamics and to numerically simulated fully nonlinear two-body motion

[58]. They found that for the examples considered, for chief eccentricity about 0.001, the HCW model was significantly less accurate. They also found that the accuracy of the Yamanaka-Ankersen model began to drop off at values of chief eccentricity above about 0.6. Since any version of Lawden's equations, including Yamanaka-Ankersen, is a linearized model, it cannot capture the high-order coupling between eccentricity and the nonlinear terms [97]; it is possible that this effect could explain the results from Lovell et al.

Summary

One goal of this thesis is to analyze the ROE realization of the HCW model for the circular chief problem, identifying some of the features which provide operational efficacy. The other main goal is to find a new model for the elliptical chief problem which retains the advantages of ROEs.

After searching the extensive literature for such a model, we found that none had all of the following characteristics: simple parameterized trajectory equations, parameters with geometrically intuitive interpretations, validity for eccentric chief orbits, and validity for drifting relative trajectories.

Many existing models exhibit one or more of these characteristics, but none exhibit all. Chapter IV will explore several possible approaches for developing a satisfactory model.

III. Relative Orbit Elements for the Circular Chief Problem

As we have seen, the most commonly applied relative satellite motion model is the Hill-Clohessy-Wiltshire (HCW) model for the circular chief problem, and Relative Orbit Elements (ROEs) are a particularly useful realization of that model. The goal of this chapter is to describe the characteristics of ROEs which provide such a high degree of geometrical insight and operational efficacy. After an intuitive derivation of the ROE parameters, we will also see that the instantaneous trajectory of the deputy satellite is an ellipse, viewed in three-dimensional space.

The HCW Model

Derivations and solutions of the HCW equations of motion can be found in many astrodynamics texts [79, 98, 102]. Assuming no external forces (except, of course, inverse-square gravity), the scalar equations of motion are

$$\begin{aligned} \ddot{x} - 2n_C\dot{y} - 3{n_C}^2 x &= 0 \\ \ddot{y} + 2n_C\dot{x} &= 0 \\ \ddot{z} + {n_C}^2 z &= 0 \end{aligned} \tag{3.1}$$

where n_C is the chief's mean motion. In the circular chief problem, n_C is also equal to its angular rate at every point in the orbit. Using the notation introduced in Chapter I, the angular velocity of the chief's LVLH frame with respect to inertial space is

$$\vec{\omega}_{C/I} = \begin{bmatrix} 0 \\ 0 \\ n_C \end{bmatrix}_c$$

Note that the z-motion is uncoupled from the in-plane motion.

If we use the relative position and velocity at epoch time t_0 as initial conditions, denoted by the subscript 0, then the position solution to the HCW equations is

$$\begin{aligned} x(t) &= \frac{\dot{x}_0}{n_C}\sin\left[n_C\left(t-t_0\right)\right] - \left(3x_0 + \frac{2\dot{y}_0}{n_C}\right)\cos\left[n_C\left(t-t_0\right)\right] + 4x_0 + \frac{2\dot{y}_0}{n_C} \\ y(t) &= \left(6x_0 + \frac{4\dot{y}_0}{n_C}\right)\sin\left[n_C\left(t-t_0\right)\right] + \frac{2\dot{x}_0}{n_C}\cos\left[n_C\left(t-t_0\right)\right] - \left(6n_C x_0 + 3\dot{y}_0\right)\left(t-t_0\right) \\ &\quad + y_0 - \frac{2\dot{x}_0}{n_C} \\ z(t) &= z_0\cos\left[n_C\left(t-t_0\right)\right] + \frac{\dot{z}_0}{n_C}\sin\left[n_C\left(t-t_0\right)\right] \end{aligned} \tag{3.2}$$

Again using the notation of Chapter I for relative position and velocity, the position can be expressed in terms of state transition sub-matrices, so that

$$\vec{r}_{D/C}\left(t\right) = \Phi_{rr}\left(t,t_0\right)\vec{r}_{D/C}\left(t_0\right) + \Phi_{rv}\left(t,t_0\right)\,{}^{c}\frac{d}{dt}\vec{r}_{D/C}\left(t_0\right) \tag{3.3}$$

where

$$\Phi_{rr}(t,t_0)=\begin{bmatrix} -3\cos\left[n_C(t-t_0)\right]+4 & 0 & 0 \\ 6\sin\left[n_C(t-t_0)\right]-6n_C(t-t_0) & 1 & 0 \\ 0 & 0 & \cos\left[n_C(t-t_0)\right] \end{bmatrix}$$

$$\Phi_{rv}(t,t_0)=\begin{bmatrix} \dfrac{\sin\left[n_C(t-t_0)\right]}{n_C} & -\dfrac{2\cos\left[n_C(t-t_0)\right]}{n_C}+\dfrac{2}{n_C} & 0 \\ \dfrac{2\cos\left[n_C(t-t_0)\right]}{n_C}-\dfrac{2}{n_C} & \dfrac{4\sin\left[n_C(t-t_0)\right]}{n_C}-3(t-t_0) & 0 \\ 0 & 0 & \dfrac{\sin\left[n_C(t-t_0)\right]}{n_C} \end{bmatrix} \tag{3.4}$$

Likewise, the velocity solution can be written as

$$^{c}\frac{d}{dt}\vec{r}_{D/C}(t)=\Phi_{vr}(t,t_0)\vec{r}_{D/C}(t_0)+\Phi_{vv}(t,t_0)\,^{c}\frac{d}{dt}\vec{r}_{D/C}(t_0) \tag{3.5}$$

where

$$\Phi_{vr}(t,t_0)=\begin{bmatrix} 3n_C\sin\left[n_C(t-t_0)\right] & 0 & 0 \\ 6n_C\cos\left[n_C(t-t_0)\right]-6n_C & 0 & 0 \\ 0 & 0 & -n_C\sin\left[n_C(t-t_0)\right] \end{bmatrix}$$

$$\Phi_{vv}(t,t_0)=\begin{bmatrix} \cos\left[n_C(t-t_0)\right] & 2\sin\left[n_C(t-t_0)\right] & 0 \\ -2\sin\left[n_C(t-t_0)\right] & 4\cos\left[n_C(t-t_0)\right]-3 & 0 \\ 0 & 0 & \cos\left[n_C(t-t_0)\right] \end{bmatrix} \tag{3.6}$$

A Geometric Parameterization of the Solution

This section is a detailed derivation of the six ROEs: x_d, $y_d(t)$, a_e, β_0 or $\beta(t)$, $z_{\max}$, and ψ_0 or γ [60]. To characterize the geometry of the HCW relative trajectory, we must examine the various terms in Eqs. (3.2). The x-equation is periodic, with the third

and fourth terms constant, representing a constant offset in the x-direction. This x-offset is x_d, the first ROE:

$$x_d = 4x_0 + \frac{2\dot{y}_0}{n_C}$$

The first two terms of the y-equation are periodic, the third term represents a secular drift in the y-direction, and the fourth and fifth terms are constant.

Note that the drift in the y-direction equals $-\frac{3}{2} n_C x_d \left(t - t_0\right)$. Thus, we can state the HCW condition for bounded motion in either of the following ways:

$$\begin{aligned} x_d &= 0 \\ 2n_C x_0 + \dot{y}_0 &= 0 \end{aligned} \tag{3.7}$$

The y-motion, then, is periodic about a drifting offset term, given by y_d, the second ROE:

$$y_d = y_0 - \frac{2\dot{x}_0}{n_C} - \frac{3}{2} n_C x_d \left(t - t_0\right) \tag{3.8}$$

To deal with the periodic terms in the x-, y-, and z-equations, we must use the following principle, the Harmonic Addition Theorem. (See Appendix B.) A periodic function defined as

$$f(\theta) = A\sin\theta + B\cos\theta \tag{3.9}$$

can be equivalently written both as

$$f(\theta) = \sqrt{A^2 + B^2}\,\sin(\theta + atan2(B, A)) \tag{3.10}$$

and as

$$f(\theta) = -\sqrt{A^2 + B^2}\,\cos(\theta + atan2(A, -B)) \tag{3.11}$$

where atan2 is the quadrant-specific inverse tangent function. Both of these forms, Eqs. (3.10) and (3.11), are periodic functions whose amplitude ($\sqrt{A^2 + B^2}$), initial phase ($atan2(B, A)$ or $atan2(A, -B)$), and time-varying phase parameter (θ) are all readily apparent.

The periodic terms of the y-equation from Eqs. (3.2) can be re-written using Eq. (3.10), yielding

$$y(t) = \sqrt{\left(6x_0 + \frac{4\dot{y}_0}{n_C}\right)^2 + \left(\frac{2\dot{x}_0}{n_C}\right)^2}\,\sin\left[n_C\left(t - t_0\right) + atan2\left(\frac{2\dot{x}_0}{n_C}, 6x_0 + \frac{4\dot{y}_0}{n_C}\right)\right] + y_d$$

The amplitude of the y-oscillation can be written as a_e, another ROE:

$$a_e = 2\sqrt{\left(3x_0 + \frac{2\dot{y}_0}{n_C}\right)^2 + \left(\frac{\dot{x}_0}{n_C}\right)^2}$$

Also, factoring $\frac{2}{n_C}$ out of both arguments of the atan2 function, we can describe a constant phase parameter

$$\beta_0 = atan2(\dot{x}_0, 3n_C x_0 + 2\dot{y}_0)$$

We can use β_0 as one of the ROEs, or instead we can define a time-varying phase parameter

$$\beta = \beta_0 + n_C\left(t - t_0\right) \tag{3.12}$$

Then we can describe the along-track motion as

$$y(t) = a_e \sin\beta + y_d \tag{3.13}$$

Next, we can use Eq. (3.11) to re-write the x-equation from Eqs. (3.2), yielding

$$x(t) = -\sqrt{\left(\frac{\dot{x}_0}{n_C}\right)^2 + \left(3x_0 + \frac{2\dot{y}_0}{n_C}\right)^2}\cos\left[n_C\left(t - t_0\right) + atan2\left(\frac{\dot{x}_0}{n_C}, 3x_0 + \frac{2\dot{y}_0}{n_C}\right)\right] + x_d$$

Note that the amplitude of the x-oscillation equals $\frac{-a_e}{2}$. Also, multiplying both arguments of the atan2 function by n_C, we see that the x-motion is 90 degrees out of phase with the y-motion, such that

$$x(t) = -\frac{a_e}{2}\cos\beta + x_d \tag{3.14}$$

Finally, applying Eq. (3.10) to Eq. (3.2), we can re-write the z-equation as

$$z(t) = \sqrt{z_0{}^2 + \left(\frac{\dot{z}_0}{n_C}\right)^2}\,\sin\left[n_C\left(t - t_0\right) + atan2\left(z_{0,}\,\frac{\dot{z}_0}{n_C}\right)\right]$$

Thus, the deputy's cross-track motion is a simple sinusoid motion with amplitude $z_{\max}$, first identified as a useful parameter by Clohessy and Wiltshire [16], and adopted later as another ROE:

$$z_{\max} = \sqrt{z_0{}^2 + \left(\frac{\dot{z}_0}{n_C}\right)^2} \tag{3.15}$$

For the sixth and final ROE, we could define a constant phase parameter

$$\psi_0 = atan2\left(z_{0,}\,\frac{\dot{z}_0}{n_C}\right) \tag{3.16}$$

Or, alternatively, we could use the constant phase difference between the cross-track oscillation and the along-track oscillation:

$$\gamma = \psi_0 - \beta_0$$

Thus, the z-motion is

$$z(t) = z_{\max} \sin(\beta + \gamma) \tag{3.17}$$

We have now used ROEs to describe the deputy's relative trajectory in three parametric equations (Eqs. (3.13), (3.14), and (3.17)), as did Lovell and Tragesser [60].

The Three-dimensional Geometry of the Relative Trajectory

Projection into the Orbit Plane.

To understand the physical geometry of the deputy's motion, as seen from the chief, we look first at the trajectory's projection into the chief's orbit plane, the x-y plane.

First let us consider the degenerate case when a_e equals zero. The deputy's relative position is simply $\left(x_d, y_d\left(t\right)\right)$, meaning the projected trajectory is simply a point, possibly drifting in the y-direction.

If a_e is not zero, we can re-write Eq. (3.13) as

$$\frac{y(t) - y_d}{a_e} = \sin\beta \tag{3.18}$$

and then square both sides, obtaining

$$\frac{\left(y(t) - y_d\right)^2}{a_e{}^2} = \sin^2\beta \tag{3.19}$$

Next, rewriting Eq. (3.14) as

$$\frac{x(t)-x_d}{a_e/2} = -\cos\beta \tag{3.20}$$

and again squaring both sides yields

$$\frac{\left(x(t)-x_d\right)^2}{\left(a_e/2\right)^2} = \cos^2\beta \tag{3.21}$$

Adding Eqs. (3.19) and (3.21) and then applying the trigonometric identity in Eq. (A.1),

$$\frac{(x(t)-x_d)^2}{\left(a_e/2\right)^2} + \frac{\left(y(t)-y_d\right)^2}{a_e{}^2} = 1 \tag{3.22}$$

This is the equation of an ellipse in the x-y plane centered at point (x_d , y_d), a point which is drifting because of the secular term in the definition of y_d , Eq. (3.8). The ellipse's semi-major axis is a_e and lies along the y-axis; the semi-minor axis is $a_e/2$ and lies along the x-axis. Thus the deputy's in-plane motion can be described as an instantaneous 2x1 ellipse.

Instantaneous Plane of the Trajectory.

To understand the trajectory in three dimensions, I will follow an argument used by Press [71] to describe stationary satellite formations (in which the deputy's along-track

secular drift is constrained to be zero). Here, I will extend Press's result by describing the general case, with drift allowed.

We have already used Eq. (3.22) to describe an instantaneous ellipse in the x-y plane. Viewed in three dimensions, however, Eq. (3.22) describes an elliptical cylinder orthogonal to the x-y plane. Thus, at any given time, the deputy's relative trajectory is confined to the surface of this elliptical cylinder.

Next, we can use the trigonometric identity in Eq. (A.2) to expand Eq. (3.17), obtaining

$$z(t) = z_{\max}\left(\cos\beta\sin\gamma + \sin\beta\cos\gamma\right) \tag{3.23}$$

We can then substitute Eqs. (3.18) and (3.20) into Eq. (3.23) to obtain

$$z(t) = z_{\max}\left\{-\frac{x(t)-x_d}{a_e/2}\sin\gamma + \frac{y(t)-y_d}{a_e}\cos\gamma\right\}$$

Rearranging,

$$0 = \left(-2\sin\gamma\right)\left(x(t)-x_d\right) + (\cos\gamma)(y(t)-y_d) - \frac{a_e}{z_{\max}}(z(t)-0) \tag{3.24}$$

This is the equation of a plane passing through the point (x_d , y_d ,0), the center point of the x-y projected ellipse. The plane has normal vector

$$\vec{N} = \begin{bmatrix} -2\sin\gamma \\ \cos\gamma \\ -a_e / z_{\max} \end{bmatrix}_c \tag{3.25}$$

Thus at any time, Eq. (3.24) must be true, and the deputy's motion must be confined to the plane it describes. This plane is constant in orientation, since $\vec{N}$ is a constant vector, but it drifts along with the center point of the x-y projected ellipse. Note that the z-component of $\vec{N}$ is always negative; thus $\vec{N}$ always points "below" the chief's orbit plane.

The deputy's relative trajectory in 3-D must therefore be on the intersection of this plane with the elliptical cylinder described by Eq. (3.22). The orientation of this plane with the **c**-frame can be easily understood from Eq. (3.25). In fact, the 3-D instantaneous trajectory and its drift can be completely described by the chief's mean motion (n_C) and the five non-periodic ROEs of the deputy's relative motion (constants x_d , $z_{\max}$, a_e , and γ , and secular element y_d). The deputy's motion within its 3-D trajectory can be completely described by the sixth ROE, β .

The True Ellipse.

We know (see Appendix C) that any trajectory equations which satisfy the following form must describe an ellipse:

$$
\begin{aligned}
x(t) &= au_x \cos\theta + bv_x \sin\theta + C_x \\
y(t) &= au_y \cos\theta + bv_y \sin\theta + C_y \\
z(t) &= au_z \cos\theta + bv_z \sin\theta + C_z
\end{aligned}
\tag{3.26}
$$

If we can show that this form is satisfied by the deputy's **c**-frame parametric equations, then we will have proven that the deputy's relative trajectory is an instantaneous ellipse. However, we must consider carefully what form of the parametric equations to use.

The derivation in Appendix C uses a and b as the semi-major and semi-minor axis lengths, and it defines the first two basis vectors of the principal-axis reference frame as aligned with the ellipse's major and minor axes. However, it makes no statement about whether the major axis corresponds to a and the reference frame's 1-direction or to b and the reference frame's 2-direction. All we know is that θ is a phase parameter moving in a positive rotation from the 1-direction to the 2-direction, as shown in Figure 2.

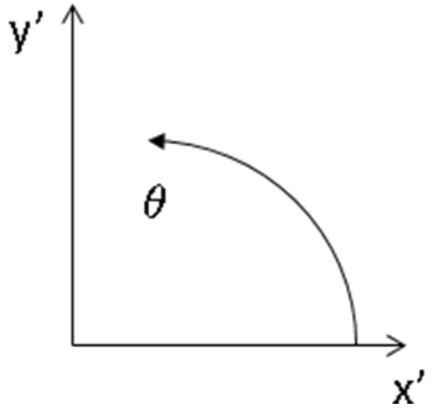

Figure 2. Direction of theta

If we wish to map correctly into the ellipse's principal-axis frame from the **c**-frame, we must use an appropriate phase parameter. β is not ideal because it rotates in a negative sense starting from the negative x-axis, as shown in Figure 3. To prove this, let us introduce a new definition of β, equivalent to Eq. (3.12). Replacing the initial conditions within the definition of β_0 with time-varying components, and assuming for illustration purposes that t_0 is zero, we see that

$$\beta = atan2(\dot{x}, 3n_C x + 2\dot{y})$$

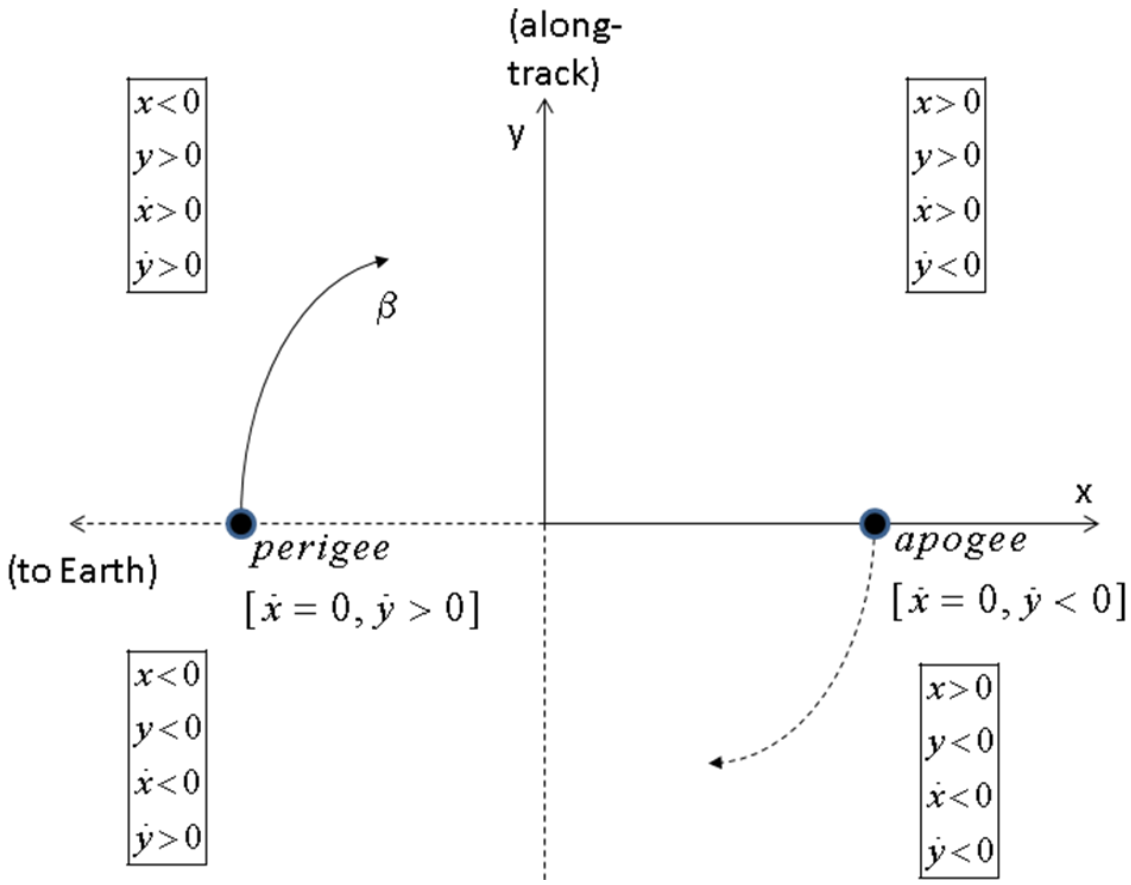

Figure 3. Direction of beta

We know that β is rotating negatively (clockwise in Figure 3) because when the deputy is at perigee, it is at a lower altitude than the chief. Thus, it is moving faster than the chief, and the y-coordinate of its position must be increasing; in other words, $\dot{y}$ must be greater than zero. The opposite is true at apogee.

Where we begin measuring the rotation of β, it must take on a zero value. This occurs where the sine of $\dot{x}$ equals zero; in other words, where $\dot{x}$ equals zero. This is true at the maximum and minimum values of x; examining the 2x1 projected ellipse in the x-y plane makes it clear that these values occur at apogee and perigee, respectively. To determine where β begins its rotation, we must find a way to discriminate between these two possible points.

A phase angle moves through its first quadrant where both arguments of its atan2 function are positive, just after the phase angle equals zero. β moves through its first quadrant where both the sine of $\dot{x}$ and the cosine of $3n_C x + 2\dot{y}$ take on positive values; we must determine whether this is true just after perigee or just after apogee. The sine of $\dot{x}$ near zero is positive only where $\dot{x}$ is positive; that is, where x is increasing. This is *not* true in the quadrant clockwise from the apogee point; it *is* true in the quadrant clockwise from the perigee point, as shown in Figure 3.

Thus, β rotates in a negative sense, starting from the negative x-axis.

To address the concern about the direction of rotation, we can constrain the third principal axis $\hat{w}$ to have an opposite sense from the third LVLH axis, $\hat{c}_3$, so that

$$\hat{w} = \frac{\vec{N}}{\left\| \vec{N} \right\|_2}$$

Still, β is a phase variable measured from the negative x-axis, while θ from Eqs. (3.26) is a phase variable measured from one of the principal axes of the three-dimensional trajectory. If and only if the negative x-axis aligns with the projection in the x-y plane of one of the principal axes, we can equate β to θ and compare Eqs. (3.13), (3.14), and (3.17) directly to Eqs. (3.26).

Likewise, if and only if the deputy's position at epoch corresponds to one of the principal axes, we can equate θ to $n_C \left(t - t_0 \right)$ and compare Eqs. (3.2) directly to Eqs. (3.26).

However, to be completely general, we must locate the principal axes of the instantaneous ellipse in three-dimensional space whose existence we are ultimately seeking to prove. Again following Press's treatment [71], we can define the deputy's distance from the center of its instantaneous relative trajectory as

$$d\left(t\right) = \sqrt{\left(x\left(t\right) - x_d\right)^2 + \left(y\left(t\right) - y_d\left(t\right)\right)^2 + z\left(t\right)^2}$$

Using Eqs. (3.13), (3.14), and (3.17),

$$d\left(t\right) = \sqrt{a_e{}^2 \sin^2 \beta + \frac{a_e{}^2}{4} \cos^2 \beta + z_{\max}{}^2 \sin^2 \left(\beta + \gamma\right)}$$

If the instantaneous relative trajectory is indeed an ellipse, then $d(t)$ will have maximum and minimum values at the endpoints of this ellipse's semi-major and semi-minor axes, respectively. To locate the extrema of $d(t)$, we can set its β-derivative equal to zero,

$$\frac{d}{d\beta} d(t) = 0$$

Differentiating, and assigning β_a to be the value of β corresponding to the 1-direction of the principal axis frame,

$$0 = \frac{1}{2d(t)} \left[\begin{array}{l} 2a_e{}^2 \sin\beta_a \cos\beta_a - \frac{a_e{}^2}{2} \sin\beta_a \cos\beta_a \\ +2z_{\max}{}^2 \sin(\beta_a + \gamma)\cos(\beta_a + \gamma) \end{array} \right] \tag{3.27}$$

Of course, because Eq. (3.27) is true whenever the numerator of the right-hand side is zero, we can simplify and use the trigonometric identities in Eqs. (A.2) and (A.11) to say

$$\begin{aligned} 0 &= 3a_e{}^2 \sin\beta_a \cos\beta_a \\ &\quad +4z_{\max}{}^2 \left[\sin\beta_a \cos\gamma + \cos\beta_a \sin\gamma\right]\left[\cos\beta_a \cos\gamma - \sin\beta_a \sin\gamma\right] \end{aligned} \tag{3.28}$$

Expanding, rearranging, and applying the trigonometric identities from Eqs. (A.1) (A.10), and (A.11), we find that

$$\tan\left(2\beta_a\right) = \frac{-{z_{\max}}^2 \sin\left(2\gamma\right)}{\frac{3}{4}{a_e}^2 + {z_{\max}}^2 \cos\left(2\gamma\right)} \tag{3.29}$$

During one chief orbit, as β goes from zero to 2π, the function $\tan\left(2\beta\right)$ repeats four times; in other words, $\tan\left(2\beta\right)$ is periodic with a period of $\pi/2$. Thus for any given value of $\tan\left(2\beta\right)$, such as the constant right-hand side of Eq. (3.29), the solution set will contain four values of β separated by $\pi/2$. Since we have defined β_a to correspond with the 1-direction of the principal-axis frame, we can assign the second solution

$$\beta_b = \beta_a + \frac{\pi}{2}$$

to correspond with the 2-direction. The remaining two solutions will correspond with the negative 1- and 2-axes.

Solving Eq. (3.29),

$$\beta_a = \frac{1}{2}\tan^{-1}\left(\frac{-{z_{\max}}^2 \sin\left(2\gamma\right)}{\frac{3}{4}{a_e}^2 + {z_{\max}}^2 \cos\left(2\gamma\right)}\right)$$

Press's analysis [71] stopped after finding two of the solutions for β in a slightly different form. However, we must continue in order to define the mapping between reference frames.

Since our goal was to find a phase variable measured from the principal-axis frame's 1-direction, we can now find the general form:

$$\theta = \beta - \beta_a$$

This allows us to re-write the deputy's **c**-frame parametric trajectory equations (Eqs. (3.13), (3.14), and (3.17)) as follows, using the trigonometric identities from Eqs. (A.2) and (A.11):

$$\begin{aligned} x(t) &= \frac{-a_e}{2}\left[\cos\beta_a\cos\theta - \sin\beta_a\sin\theta\right] + x_d \\ y(t) &= a_e\left[\sin\beta_a\cos\theta + \cos\beta_a\sin\theta\right] + y_d(t) \\ z(t) &= z_{\max}\left[\sin(\beta_a+\gamma)\cos\theta + \cos(\beta_a+\gamma)\sin\theta\right] \end{aligned}$$

This form can be compared directly to Eqs. (3.26), showing that the instantaneous relative trajectory viewed in three dimensions is, in fact, an ellipse, with

$$a\hat{u} = \begin{bmatrix} \frac{-a_e}{2}\cos\beta_a \\ a_e\sin\beta_a \\ z_{\max}\sin(\beta_a+\gamma) \end{bmatrix}_c \tag{3.30}$$

$$b\hat{v} = \begin{bmatrix} \frac{a_e}{2}\sin\beta_a \\ a_e\cos\beta_a \\ z_{\max}\cos(\beta_a+\gamma) \end{bmatrix}_c \tag{3.31}$$

$$C = \begin{bmatrix} x_d \\ y_d(t) \\ 0 \end{bmatrix}_c$$

We can perform two simple checks on these results. First, we could find $a\hat{u}$ and $b\hat{v}$ by substituting the solutions for β_a and β_b directly into Eqs. (3.13), (3.14), and (3.17) and subtracting the coordinates of the center from the resulting position coordinates; the results match Eqs. (3.30) and (3.31).

Second, we could calculate the dot product of $a\hat{u}$ and $b\hat{v}$ to verify orthogonality:

$$\begin{aligned} a\hat{u} \cdot b\hat{v} &= 3a_e{}^2 \sin\beta_a \cos\beta_a \\ &\quad +4z_{\max}{}^2 \left[\sin\beta_a \cos\gamma + \cos\beta_a \sin\gamma\right]\left[\cos\beta_a \cos\gamma - \sin\beta_a \sin\gamma\right] \end{aligned}$$

From Eq. (3.28), we can see that this dot product is indeed zero.

Note that we now have a general method for transforming from principal-axis coordinates into **c**-frame coordinates and vice versa. If we call the principal-axis frame **r**, the necessary rotation matrices are

$$\begin{aligned} R^{r\to c} &= \left[\left[\hat{u}\right]_c \quad \left[\hat{v}\right]_c \quad \left[\hat{w}\right]_c\right] \\ R^{c\to r} &= \left[R^{r\to c}\right]^T \end{aligned}$$

where

$$\hat{u} = \frac{a\hat{u}}{\left\| a\hat{u} \right\|_2}$$
$$\hat{v} = \frac{b\hat{v}}{\left\| b\hat{v} \right\|_2}$$

Brief Example.

One geometrical insight we can gain using the results of this chapter concerns a case involving only in-plane motion, no drift, and motion centered about the origin. In this case, the maximum displacement of the deputy from the chief equals a_e. We know (see Eq. (D.6)) that the deputy's orbit radius from perigee is $a_D\left(1-e_D\right)$. Also, since boundedness indicates that the chief and deputy orbits have equal semi-major axes, then we can say the distance between the deputy's perigee point and the chief's orbit radius equals $a_D e_D$. As we can see from Figure 3, this perigee displacement equals the semi-minor axis of the relative ellipse, which equals $\frac{a_e}{2}$. Finally, we have an expression for the maximum distance between chief and deputy:

$$\rho_{\max} = a_e = 2a_D e_D \tag{3.32}$$

IV. Parameterized Models of the Elliptical Chief Problem

Objectives

As with any dynamics model, every relative satellite motion model is an approximation, incorporating certain assumptions that affect the range of validity for the model. For example, the HCW model's assumption of a circular chief orbit means that, for a given application's error tolerance, there is a value of chief orbit eccentricity beyond which the HCW model is invalid.

Each model represents a balance between accuracy and simplicity. Choosing the best model for an application depends on getting that balance right. For example, if a spacecraft performing RPO is to have an autonomous impulsive maneuver scheme, its on-board planning computer must use a parameterized relative motion model that can be easily optimized (e.g., for elapsed time or velocity-change magnitude) to determine the timing, magnitude, and direction of the next impulse. Likewise, if the proximity operations mission has geometrically defined constraints, such as field-of-view restrictions, the model's parameters should have a simple relationship to the geometry of the relative trajectory. These simplicity requirements must be balanced against accuracy; if the spacecraft is to perform RPO near satellites whose orbits have non-negligible eccentricity, the HCW model may be inadequate.

Finding a good relative motion model whose parameters yield significant geometric insight for such an application (an impulsive maneuver scheme for autonomous RPO) is the goal of the present chapter. Having seen that ROEs constitute a

satisfactory model for the circular chief problem, we will examine a novel method (the Virtual Chief method) to see whether it is a similarly satisfactory answer to the elliptical chief problem.

In other words, we wish to relax the eccentricity restriction of the HCW model. Specifically, the end result should be a relative motion model with four characteristics. First, the model should have a closed-form solution that is geometrically intuitive, yielding a high degree of insight into the physical trajectory of the deputy with respect to the chief.

Second, the model should lend itself to a high degree of operational efficacy. In other words, developing impulsive maneuver schemes and relative navigation algorithms should not involve a high degree of complexity or computational cost.

Third, assumptions of small eccentricity, small separation distances (relative to the chief orbit radius), and Keplerian two-body dynamics are permissible. Otherwise, the model should not exclude any classes of relative orbit problems. For example, it should accommodate drifting trajectories, non-repeating trajectories which experience a secular drift due to a difference in semi-major axes. (Of course, this accommodation may last only a finite time, until the drift causes any small-separation assumption to be exceeded.) Also, the model should permit the chief and deputy orbits to have widely different arguments of perigee and right ascensions of the ascending nodes (if the orbits are near-equatorial), provided the small-separation assumption is not violated.

Fourth, if the chief's eccentricity is zero, the model should reduce to the HCW equations.

Possible Approaches

The search for an appropriate relative motion model could have proceeded along any of five possible approaches.

Neglect Chief Eccentricity.

The first approach would be to use the HCW model, ignore the eccentricity of the chief's orbit, and accept the resulting error. This approach, although used for some applications, translates into fuel penalties even for small eccentricities [41].

Lawden's Equations.

The second approach would be to use Lawden's equations, attempting to find geometrically meaningful parameters in some of the existing solutions. A time-domain version of these equations, similar to the notation of De Vries [26] or of Inalhan, Tillerson, and How [41], can be written as

$$\begin{bmatrix} \dot{x} \\ \dot{y} \\ \dot{z} \\ \ddot{x} \\ \ddot{y} \\ \ddot{z} \end{bmatrix}_c = \begin{bmatrix} 0 & 0 & 0 & 1 & 0 & 0 \\ 0 & 0 & 0 & 0 & 1 & 0 \\ 0 & 0 & 0 & 0 & 0 & 1 \\ A_{41} & \ddot{\nu}_C & 0 & 0 & 2\dot{\nu}_C & 0 \\ -\ddot{\nu}_C & A_{52} & 0 & -2\dot{\nu}_C & 0 & 0 \\ 0 & 0 & A_{63} & 0 & 0 & 0 \end{bmatrix} \begin{bmatrix} x \\ y \\ z \\ \dot{x} \\ \dot{y} \\ \dot{z} \end{bmatrix}_c \tag{4.1}$$

where

$$A_{41} = \dot{\nu}_C^{\,2} + 2n_C^{\,2}\left(\frac{1+e_C\cos\nu_C}{1-e_C^{\,2}}\right)^3$$
$$A_{52} = \dot{\nu}_C^{\,2} - n_C^{\,2}\left(\frac{1+e_C\cos\nu_C}{1-e_C^{\,2}}\right)^3 \qquad (4.2)$$
$$A_{63} = -n_C^{\,2}\left(\frac{1+e_C\cos\nu_C}{1-e_C^{\,2}}\right)^3$$

As a linearized two-body model, Lawden's equations would likely yield very accurate results over small relative distances and short timescales up to moderately large eccentricities (i.e., around 0.6) [58, 97]. However, these solutions are often complicated, and the resulting geometry is difficult to describe, especially if drift is allowed.

The case where chief and deputy orbits have the same semi-major axis (bounded motion) is a different matter. Using p_C as the semilatus rectum of the chief's orbit, Sengupta and Vadali [86] gave the following boundedness condition from their solution to Lawden's equations (converted to the notation of this thesis):

$$0 = \frac{1}{p_C}\left(2+e_C\cos\nu_C(t)\right)\left(1+e_C\cos\nu_C(t)\right)^2 x(t) + e_C\sqrt{\frac{p_C}{\mu}}\sin\nu_C(t)\,\dot{x}(t)$$
$$-\frac{e_C}{p_C}\sin\nu_C(t)\left(1+e_C\cos\nu_C(t)\right)^2 y(t) + \left(1+e_C\cos\nu_C(t)\right)\sqrt{\frac{p_C}{\mu}}\,\dot{y}(t)$$

After evaluating at epoch time t_0, applying the two-body orbit properties in Eqs. (D.7) and (D.11), and multiplying by constant factor a_C, the above equation becomes

$$
\begin{aligned}
0 = & \frac{2+e_C \cos\nu_{C,0}}{\left(1-e_C{}^2\right)}\left(1+e_C \cos\nu_{C,0}\right)^2 x_0 + \frac{e_C}{n_C}\sin\nu_{C,0}\left(1-e_C{}^2\right)^{1/2}\dot{x}_0 \\
& -\frac{e_C \sin\nu_{C,0}}{\left(1-e_C{}^2\right)}\left(1+e_C \cos\nu_{C,0}\right)^2 y_0 + \frac{\left(1-e_C{}^2\right)^{1/2}}{n_C}\left(1+e_C \cos\nu_{C,0}\right)\dot{y}_0
\end{aligned}
\tag{4.3}
$$

where epoch conditions are indicated by the subscript 0.

To check this result, we can use an alternate but equivalent approach from the linearized orbit-element difference method. Bounded motion requires simply that δa equal zero. Using the linearized mapping between orbit-element differences and Cartesian coordinates from Schaub and Junkins [79], after some manipulation,

$$
\begin{aligned}
\delta a = & \frac{2\left(2+e_C \cos\nu_C(t)\right)}{\left(1-e_C{}^2\right)^2}\left(1+e_C \cos\nu_C(t)\right)^2 x(t) + \frac{2e_C \sin\nu_C(t)}{n_C\left(1-e_C{}^2\right)^{1/2}}\dot{x}(t) \\
& -\frac{2e_C \sin\nu_C(t)}{\left(1-e_C{}^2\right)^2}\left(1+e_C \cos\nu_C(t)\right)^2 y(t) + \frac{2\left(1+e_C \cos\nu_C(t)\right)}{n_C\left(1-e_C{}^2\right)^{1/2}}\dot{y}(t)
\end{aligned}
$$

Setting δa to zero, evaluating at t_0, and multiplying by the constant factor $\frac{1}{2}\left(1-e_C{}^2\right)$ causes the above equation to equal Eq. (4.3), showing that the two methods are equivalent.

As we have seen, for bounded motion using Lawden's equations, there has been some recent success describing the geometrical impact of the constants of integration [54] and defining a set of five design parameters [86]. The discovery that any bounded-motion solution lies on a definable quadric surface [45] is certainly geometrically

meaningful. However, because an RPO maneuver scheme may benefit from using drifting trajectories, these options were not pursued.

First- and Second-order Eccentricity Approximations.

The third approach would be to attempt to simplify the solution to Lawden's equations by making a further approximation. For example, a series expansion of the chief's true anomaly could retain only terms that are first- or second-order in the chief's eccentricity (see Eq. (D.12)). As we have seen, this technique has been used for numerical comparisons often in the literature, and Melton applied this method to derive a state transition matrix of relative motion which can be initialized at any time during the chief's orbit [66].

Change of Reference Frames.

The fourth approach would be to attempt to achieve a simpler representation of the relative motion by using some chief-centered reference frame other than the traditional rotating LVLH frame. For some applications, a variety of non-orthogonal reference frames have proven useful [50]. Also, using an inertial coordinate frame (for example, a frame parallel to the chief's perifocal frame) has shown promise in highlighting simple geometric features [56, 67], but this idea has not been widely explored in the literature.

The Virtual Chief Method.

The fifth approach is the Virtual Chief method. It is an attempt to avoid the complexity of existing elliptical-chief models and take advantage of the simplicity of the HCW model and its closed-form solution. This method uses a virtual chief, a third

satellite (besides the chief and deputy) whose orbit elements are the same as those of the actual chief, except for eccentricity, which is zero. The virtual chief is a theoretical object, and may not physically exist. It is defined in the same way as the "reference platform" of Fasano and D'Errico's higher-fidelity model. Their model is first-order in the eccentricity and second-order in the relative distance, and it incorporates higher-order gravity effects [30]. The linearized, unperturbed Virtual Chief method is the approach selected for the current study, although adding second-order terms could constitute an alternative approach.

The Virtual Chief Equations

The Virtual Chief method is applicable to the elliptical chief problem, but it assumes a small eccentricity for the orbits of both chief and deputy. This eccentricity restriction is folded into the small-separation restriction, because we assume that both the chief and deputy will remain near the virtual chief. Using the subscript O for the virtual chief and the subscript C for the chief, we could define the virtual chief's orbit in terms of semi-major axis a, inclination i, eccentricity e, right ascension of the ascending node Ω, and mean anomaly M, as

$$\begin{bmatrix} a_O \\ i_O \\ e_O \\ \Omega_O \\ M_O \end{bmatrix} = \begin{bmatrix} a_C \\ i_C \\ 0 \\ \Omega_C \\ M_C \end{bmatrix} \tag{4.4}$$

Note that even though there is no perigee for the circular orbit, we have defined the mean anomaly M_O to be equal to the chief's mean anomaly. Thus, at the chief's perigee, both mean anomalies will equal zero.

Reference Frames for the Actual and Virtual Chief.

Let there be an LVLH reference frame **c** fixed to the chief, and an LVLH frame **o** at the virtual chief. By the definition of the virtual chief, its orbit is coplanar with that of the chief. Thus,

$$\hat{c}_3 = \hat{o}_3$$

As a result, the angular separation between **c** and **o** can be described by a rotation about the third axis through an angle Δu, representing the difference in arguments of latitude between the chief and the virtual chief (see Figure 4).

Since both arguments of latitude are measured from the ascending node shared by both orbits, and since M_O and ν_C (the chief's true anomaly) are both measured from the chief's perigee point, we can say that

$$\begin{aligned} u_O &= \omega_C + M_O \\ u_C &= \omega_C + \nu_C \\ \Delta u &= u_C - u_O = \nu_C - M_O \end{aligned} \tag{4.5}$$

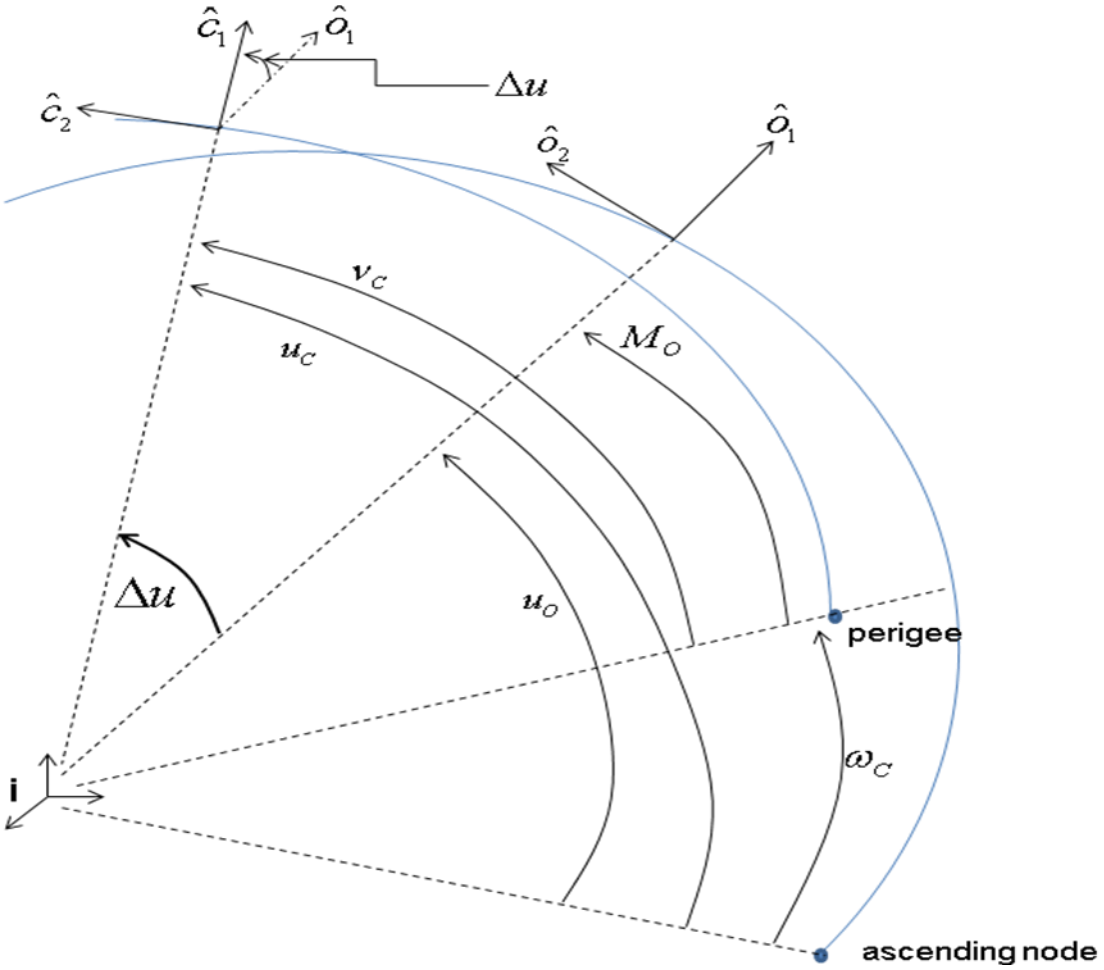

Figure 4. Reference Frames

Finally, since we know that both mean anomalies are always equal, we can construct the following rotation matrix that will convert **o**-frame coordinates into **c**-frame coordinates:

$$R^{o\to c} = \begin{bmatrix} \cos(\nu_C - M_C) & \sin(\nu_C - M_C) & 0 \\ -\sin(\nu_C - M_C) & \cos(\nu_C - M_C) & 0 \\ 0 & 0 & 1 \end{bmatrix}$$

Let the angular velocity of the **c**-frame with respect to the **o**-frame be $\vec{\omega}_{c/o}$. Since both orbits will always be coplanar, we know that the only component of $\vec{\omega}_{c/o}$ will be in the out-of-plane direction. In fact, the magnitude of this component will be the time rate of change of Δu :

$$\vec{\omega}_{c/o} = \left(\frac{d}{dt} \Delta u \right) \hat{o}_3 = \left(\frac{d}{dt} \Delta u \right) \hat{c}_3$$

Finding the chief's mean anomaly from Eq. (D.3), and using $\dot{\nu}_C$ as the time derivative of the chief's true anomaly, we can calculate the time rate of change of Δu as follows:

$$\frac{d}{dt} \Delta u = \frac{d}{dt} \left(\nu_C - M_C \right) = \dot{\nu}_C - \frac{d}{dt} \left(n_C \left[t - t_p \right] \right) = \dot{\nu}_C - n_C$$

Thus,

$$\vec{\omega}_{c/o} = \left(\dot{\nu}_C - n_C \right) \hat{o}_3 = \left(\dot{\nu}_C - n_C \right) \hat{c}_3$$

The angular velocity of the **c**-frame with respect to inertial space is simply

$$\vec{\omega}_{c/i} = \dot{\nu}_C \hat{c}_3$$

Taking an inertial derivative and using $\ddot{\nu}_C$ as the second time derivative of the chief's true anomaly yields the angular acceleration:

$$ {}^{i}\frac{d}{dt}\vec{\omega}_{\mathcal{C}/i} = \ddot{\nu}_C \hat{c}_3 \tag{4.6} $$

If n_O is the virtual chief's mean motion, then examining the **o**-frame in a similar way results in

$$ \vec{\omega}_{\mathcal{O}/i} = n_O \hat{o}_3 = n_O \hat{c}_3 $$

Likewise,

$$ {}^{i}\frac{d}{dt}\vec{\omega}_{\mathcal{O}/i} = \vec{0} \tag{4.7} $$

Vector Equations.

In order to write the vector equation of relative motion for our model, we must find an expression for ${}^{c}\frac{d^2}{dt^2}\vec{r}_{D/C}$. If the positions of the chief and deputy, respectively, from the virtual chief are $\vec{r}_{C/O}$ and $\vec{r}_{D/O}$, then we can also make the simple vector subtraction statement that

$$ \vec{r}_{D/O} - \vec{r}_{C/O} = \vec{r}_{D/C} \tag{4.8} $$

Taking an **o**-frame time derivative,

$$ {}^{o}\frac{d}{dt}\vec{r}_{D/O} - {}^{o}\frac{d}{dt}\vec{r}_{C/O} = {}^{c}\frac{d}{dt}\vec{r}_{D/C} + \vec{\omega}_{c/o} \times \vec{r}_{D/C} $$

A further **o**-frame time derivative yields

$$ {}^{o}\frac{d^2}{dt^2}\vec{r}_{D/O} - {}^{o}\frac{d^2}{dt^2}\vec{r}_{C/O} = {}^{c}\frac{d^2}{dt^2}\vec{r}_{D/C} + 2\vec{\omega}_{c/o} \times {}^{c}\frac{d}{dt}\vec{r}_{D/C} + \vec{\omega}_{c/o} \times (\vec{\omega}_{c/o} \times \vec{r}_{D/C}) + {}^{c}\frac{d}{dt}\vec{\omega}_{c/o} \times \vec{r}_{D/C} $$

Rearranging will provide the nonlinear vector equation of relative motion we have been seeking:

$$ {}^{c}\frac{d^2}{dt^2}\vec{r}_{D/C} = {}^{o}\frac{d^2}{dt^2}\vec{r}_{D/O} - {}^{o}\frac{d^2}{dt^2}\vec{r}_{C/O} - 2\vec{\omega}_{c/o} \times {}^{c}\frac{d}{dt}\vec{r}_{D/C} - \vec{\omega}_{c/o} \times (\vec{\omega}_{c/o} \times \vec{r}_{D/C}) - {}^{c}\frac{d}{dt}\vec{\omega}_{c/o} \times \vec{r}_{D/C} \quad (4.9) $$

Eq. (4.9) is the Virtual Chief vector equation of motion. It now remains to provide scalar values for the **c**-frame components of each term.

Scalar Equations.

First, let us denote the position coordinates of the chief and deputy, respectively, with the capital subscripts C and D; and let us do likewise for the **o**-frame relative velocity and acceleration components (for example, ${}^{o}\frac{d^2}{dt^2}\vec{r}_{D/O}$ will be written as $\begin{bmatrix} \ddot{x}_D & \ddot{y}_D & \ddot{z}_D \end{bmatrix}_o^T$).

Next, let us make use of the HCW equations (Eqs. (3.1)) to describe the motion of the chief and deputy relative to the virtual chief. Since the virtual chief is in a circular

orbit, the assumptions of the HCW equations are not violated, as long as the magnitudes of $\vec{r}_{C/O}$ and $\vec{r}_{D/O}$ remain small. Thus, we find that

$$
{}^{o}\frac{d^2}{dt^2}\vec{r}_{D/O} = \begin{bmatrix} 2n_O\dot{y}_D + 3n_O{}^2 x_D \\ -2n_O\dot{x}_D \\ -n_O{}^2 z_D \end{bmatrix}_o
$$

$$
{}^{o}\frac{d^2}{dt^2}\vec{r}_{C/O} = \begin{bmatrix} 2n_O\dot{y}_C + 3n_O{}^2 x_C \\ -2n_O\dot{x}_C \\ -n_O{}^2 z_C \end{bmatrix}_o
$$

Of course, since the orbits of the chief and the virtual chief have the same semi-major axis, it follows that

$$
n_O = n_C
$$

Furthermore, since we know that the orbits of the chief and the virtual chief are coplanar, we can say that

$$
z_C = \dot{z}_C = \ddot{z}_C = 0
$$

In addition, since we know ${}^{o}\frac{d^2}{dt^2}\vec{r}_{D/O}$ and ${}^{o}\frac{d^2}{dt^2}\vec{r}_{C/O}$ only in **o**-frame coordinates, we must apply the rotation matrix $R^{o\to c}$ before substituting into Eq. (4.9). In other words,

$$
\left[{}^{o}\frac{d^2}{dt^2}\vec{r}_{D/O} - {}^{o}\frac{d^2}{dt^2}\vec{r}_{C/O} \right]_c = R^{o\to c}\left(\left[{}^{o}\frac{d^2}{dt^2}\vec{r}_{D/O} \right]_o - \left[{}^{o}\frac{d^2}{dt^2}\vec{r}_{C/O} \right]_o \right)
$$

Next we must find ${}^{c}\frac{d}{dt}\vec{\omega}_{c/o}$. We can again make a simple vector subtraction statement,

$$\vec{\omega}_{c/o} = \omega_{c/i} - \omega_{o/i}$$

Taking a **c**-frame time derivative,

$${}^{c}\frac{d}{dt}\vec{\omega}_{c/o} = {}^{i}\frac{d}{dt}\vec{\omega}_{c/i} - \vec{\omega}_{c/i}\times\vec{\omega}_{c/i} - {}^{i}\frac{d}{dt}\vec{\omega}_{o/i} + \vec{\omega}_{c/i}\times\vec{\omega}_{o/i} = {}^{i}\frac{d}{dt}\vec{\omega}_{c/i} - {}^{i}\frac{d}{dt}\vec{\omega}_{o/i}$$

Substituting from Eqs. (4.6) and (4.7),

$${}^{c}\frac{d}{dt}\vec{\omega}_{c/o} = \begin{bmatrix} 0 \\ 0 \\ \ddot{\nu}_C \end{bmatrix}_c$$

Now we are prepared to rewrite Eq. (4.9) in matrix format. Substituting from results above,

$$\begin{bmatrix} \ddot{x} \\ \ddot{y} \\ \ddot{z} \end{bmatrix}_c = \begin{bmatrix} \cos(\nu_C - M_C) & \sin(\nu_C - M_C) & 0 \\ -\sin(\nu_C - M_C) & \cos(\nu_C - M_C) & 0 \\ 0 & 0 & 1 \end{bmatrix} \left(\begin{bmatrix} 2n_C\dot{y}_D + 3{n_C}^2 x_D \\ -2n_C\dot{x}_D \\ -{n_C}^2 z_D \end{bmatrix}_o - \begin{bmatrix} 2n_C\dot{y}_C + 3{n_C}^2 x_C \\ -2n_C\dot{x}_C \\ 0 \end{bmatrix}_o \right)$$
$$-2\begin{bmatrix} 0 \\ 0 \\ \dot{\nu}_C - n_C \end{bmatrix}_c \times \begin{bmatrix} \dot{x} \\ \dot{y} \\ \dot{z} \end{bmatrix}_c - \begin{bmatrix} 0 \\ 0 \\ \dot{\nu}_C - n_C \end{bmatrix}_c \times \left(\begin{bmatrix} 0 \\ 0 \\ \dot{\nu}_C - n_C \end{bmatrix}_c \times \begin{bmatrix} x \\ y \\ z \end{bmatrix}_c \right) - \begin{bmatrix} 0 \\ 0 \\ \ddot{\nu}_C \end{bmatrix}_c \times \begin{bmatrix} x \\ y \\ z \end{bmatrix}_c$$

Collecting terms and performing the cross products,

$$\begin{bmatrix} \ddot{x} \\ \ddot{y} \\ \ddot{z} \end{bmatrix}_c = \begin{bmatrix} \cos(\nu_C - M_C) & \sin(\nu_C - M_C) & 0 \\ -\sin(\nu_C - M_C) & \cos(\nu_C - M_C) & 0 \\ 0 & 0 & 1 \end{bmatrix} \begin{bmatrix} 2n_C\left(\dot{y}_D - \dot{y}_C\right) + 3{n_C}^2\left(x_D - x_C\right) \\ -2n_C\left(\dot{x}_D - \dot{x}_C\right) \\ -{n_C}^2 z_D \end{bmatrix}_o + \begin{bmatrix} 2\left(\dot{\nu}_C - n_C\right)\dot{y} + \left(\dot{\nu}_C - n_C\right)^2 x + \ddot{\nu}_C y \\ -2\left(\dot{\nu}_C - n_C\right)\dot{x} + \left(\dot{\nu}_C - n_C\right)^2 y - \ddot{\nu}_C x \\ 0 \end{bmatrix}_c \tag{4.10}$$

We can derive expressions in terms of x, y, and z to replace the factors $\left(x_D - x_C\right)$, $\left(\dot{x}_D - \dot{x}_C\right)$, $\left(\dot{y}_D - \dot{y}_C\right)$, and z_D in Eq. (4.10) by using the rotation matrix $R^{o\to c}$. From Eq. (4.8),

$$\left[\vec{r}_{D/C}\right]_c = R^{o\to c}\left[\vec{r}_{D/O} - \vec{r}_{C/O}\right]_o$$

Since $R^{o\to c}$ is a rotation matrix, and therefore orthogonal,

$$\left[\vec{r}_{D/O} - \vec{r}_{C/O}\right]_o = \left[R^{o\to c}\right]^T\left[\vec{r}_{D/C}\right]_c \tag{4.11}$$

Inserting the appropriate component values and evaluating,

$$\begin{bmatrix} x_D - x_C \\ y_D - y_C \\ z_D - z_C \end{bmatrix}_o = \begin{bmatrix} \cos\left(\nu_C - M_C\right)x - \sin\left(\nu_C - M_C\right)y \\ \sin\left(\nu_C - M_C\right)x + \cos\left(\nu_C - M_C\right)y \\ z \end{bmatrix}_o \tag{4.12}$$

Next, we rotate the **o**-frame derivative of Eq. (4.8) in the same way:

$$\left[{}^{o}\frac{d}{dt}\vec{r}_{D/O} - {}^{o}\frac{d}{dt}\vec{r}_{C/O} \right]_o = \left[R^{o\to c} \right]^T \left[{}^{c}\frac{d}{dt}\vec{r}_{D/C} + \vec{\omega}_{c/o} \times \vec{r}_{D/C} \right]_c \tag{4.13}$$

Inserting the appropriate values,

$$\begin{bmatrix} \dot{x}_D - \dot{x}_C \\ \dot{y}_D - \dot{y}_C \\ \dot{z}_D - \dot{z}_C \end{bmatrix}_o = \begin{bmatrix} \cos(\nu_C - M_C) & -\sin(\nu_C - M_C) & 0 \\ \sin(\nu_C - M_C) & \cos(\nu_C - M_C) & 0 \\ 0 & 0 & 1 \end{bmatrix} \left(\begin{bmatrix} \dot{x} \\ \dot{y} \\ \dot{z} \end{bmatrix}_c + \begin{bmatrix} 0 \\ 0 \\ \dot{\nu}_C - n_C \end{bmatrix}_c \times \begin{bmatrix} x \\ y \\ z \end{bmatrix}_c \right)$$

Calculating,

$$\begin{bmatrix} \dot{x}_D - \dot{x}_C \\ \dot{y}_D - \dot{y}_C \\ \dot{z}_D - \dot{z}_C \end{bmatrix}_o = \begin{bmatrix} \cos(\nu_C - M_C)\left[\dot{x} - (\dot{\nu}_C - n_C)\, y\right] - \sin(\nu_C - M_C)\left[\dot{y} + (\dot{\nu}_C - n_C)\, x\right] \\ \sin(\nu_C - M_C)\left[\dot{x} - (\dot{\nu}_C - n_C)\, y\right] + \cos(\nu_C - M_C)\left[\dot{y} + (\dot{\nu}_C - n_C)\, x\right] \\ \dot{z} \end{bmatrix}_o \tag{4.14}$$

Now we can substitute from Eqs. (4.12) and (4.14) into Eq. (4.10):

$$\begin{bmatrix} \ddot{x} \\ \ddot{y} \\ \ddot{z} \end{bmatrix}_c = \begin{bmatrix} 2(\dot{\nu}_C - n_C)\,\dot{y} + (\dot{\nu}_C - n_C)^2\, x + \ddot{\nu}_C y \\ -2(\dot{\nu}_C - n_C)\,\dot{x} + (\dot{\nu}_C - n_C)^2\, y - \ddot{\nu}_C x \\ 0 \end{bmatrix}_c + \begin{bmatrix} \cos(\nu_C - M_C) & \sin(\nu_C - M_C) & 0 \\ -\sin(\nu_C - M_C) & \cos(\nu_C - M_C) & 0 \\ 0 & 0 & 1 \end{bmatrix}$$

$$\begin{bmatrix} 2n_C\left\{\sin(\nu_C - M_C)\left[\dot{x} - (\dot{\nu}_C - n_C)\, y\right] + \cos(\nu_C - M_C)\left[\dot{y} + (\dot{\nu}_C - n_C)\, x\right]\right\} \\ +3{n_C}^2\left\{\cos(\nu_C - M_C)\, x - \sin(\nu_C - M_C)\, y\right\} \\ \hdotsfor{1} \\ -2n_C\left\{\cos(\nu_C - M_C)\left[\dot{x} - (\dot{\nu}_C - n_C)\, y\right] - \sin(\nu_C - M_C)\left[\dot{y} + (\dot{\nu}_C - n_C)\, x\right]\right\} \\ \hdotsfor{1} \\ -{n_C}^2 z \end{bmatrix}_o$$

Simplifying and performing the matrix product gives

$$\begin{bmatrix} \ddot{x} \\ \ddot{y} \\ \ddot{z} \end{bmatrix}_c = \begin{bmatrix} 2\dot{\nu}_C\dot{y} + \left(\dot{\nu}_C - n_C\right)^2 x + \ddot{\nu}_C y + 2n_C\left(\dot{\nu}_C - n_C\right)x + 3{n_C}^2\cos^2(\nu_C - M_C)x \\ \qquad -3{n_C}^2\cos(\nu_C - M_C)\sin\left(\nu_C - M_C\right)y \\ \hdashline -2\dot{\nu}_C\dot{x} + \left(\dot{\nu}_C - n_C\right)^2 y - \ddot{\nu}_C x + 2n_C\left(\dot{\nu}_C - n_C\right)y \\ -3{n_C}^2\sin(\nu_C - M_C)\cos\left(\nu_C - M_C\right)x + 3{n_C}^2\sin^2(\nu_C - M_C)y \\ \hdashline -{n_C}^2 z \end{bmatrix}_c \tag{4.15}$$

This is a set of scalar equations of relative motion that depend on time (through M_c, ν_C, $\dot{\nu}_C$, and $\ddot{\nu}_C$) and known constants n_C and t_p. Note that the out-of-plane equation is identical to the HCW out-of-plane equation. Eq. (4.15) can be further simplified and written conveniently as a linear time-varying system in the following form:

$$\begin{bmatrix} \dot{x} \\ \dot{y} \\ \dot{z} \\ \ddot{x} \\ \ddot{y} \\ \ddot{z} \end{bmatrix}_c = \begin{bmatrix} 0 & 0 & 0 & 1 & 0 & 0 \\ 0 & 0 & 0 & 0 & 1 & 0 \\ 0 & 0 & 0 & 0 & 0 & 1 \\ A_{41} & A_{42} & 0 & 0 & 2\dot{\nu}_C & 0 \\ A_{51} & A_{52} & 0 & -2\dot{\nu}_C & 0 & 0 \\ 0 & 0 & -{n_C}^2 & 0 & 0 & 0 \end{bmatrix} \begin{bmatrix} x \\ y \\ z \\ \dot{x} \\ \dot{y} \\ \dot{z} \end{bmatrix}_c \tag{4.16}$$

where

$$\begin{aligned} A_{41} &= \dot{\nu}_C{}^2 - {n_C}^2 + 3{n_C}^2\cos^2(\nu_C - M_C) \\ A_{42} &= \ddot{\nu}_C - 3{n_C}^2\cos(\nu_C - M_C)\sin\left(\nu_C - M_C\right) \\ A_{51} &= -\ddot{\nu}_C - 3{n_C}^2\sin(\nu_C - M_C)\cos\left(\nu_C - M_C\right) \\ A_{52} &= \dot{\nu}_C{}^2 - {n_C}^2 + 3{n_C}^2\sin^2(\nu_C - M_C) \end{aligned}$$

The time dependence of the system in Eq. (4.16) is implicit. The time dependence through M_C could easily be made explicit through Eq. (D.3). However, showing the time dependence through ν_C and its derivatives requires solving Kepler's transcendental equation (Eq. (D.4)).

Note that if we wished to account for differential drag, thrust, or other forces affecting the relative motion, we could do so by adding the appropriate terms to the right-hand side of Eq. (4.16). Note also that this model resembles the time-domain Lawden's equations, Eqs. (4.1) and (4.2), but with additional terms.

Finally, note that Eq. (4.16) reduces to the HCW equations when the chief's eccentricity is zero. To show this, simply substitute the following circular-chief equivalent values for the chief true anomaly and its successive time derivatives: M_C, n_C, and 0.

The Virtual Chief Solution

Eq. (4.16) represents a system of second-order differential equations whose dynamics matrix $A(t)$ is known. When the closed-form solution to the system takes the form of a state transition matrix $\Phi(t,t_0)$, that matrix must obey the following:

$$\dot{\Phi}(t,t_0) = A(t)\Phi(t,t_0) \tag{4.17}$$

The initial condition for Eq. (4.17) is that $\Phi(t_0,t_0)$ is the identity matrix [73].

However, rather than solve the differential equations directly, we shall once again take advantage of the known HCW motion. The HCW position and velocity solutions, whose state transition matrix forms are shown in Eqs. (3.3) and (3.5), can be applied to the **o**-frame motion of the chief relative to the virtual chief:

$$\begin{aligned}\left[\vec{r}_{C/O}(t)\right]_o &= \Phi_{rr}(t,t_0)\left[\vec{r}_{C/O}(t_0)\right]_o + \Phi_{rv}(t,t_0)\left[{}^o\frac{d}{dt}\vec{r}_{C/O}(t_0)\right]_o \\ \left[{}^o\frac{d}{dt}\vec{r}_{C/O}(t)\right]_o &= \Phi_{vr}(t,t_0)\left[\vec{r}_{C/O}(t_0)\right]_o + \Phi_{vv}(t,t_0)\left[{}^o\frac{d}{dt}\vec{r}_{C/O}(t_0)\right]_o\end{aligned} \tag{4.18}$$

A similar construction can be used to define the motion of the deputy relative to the virtual chief,

$$\begin{aligned}\left[\vec{r}_{D/O}(t)\right]_o &= \Phi_{rr}(t,t_0)\left[\vec{r}_{D/O}(t_0)\right]_o + \Phi_{rv}(t,t_0)\left[{}^o\frac{d}{dt}\vec{r}_{D/O}(t_0)\right]_o \\ \left[{}^o\frac{d}{dt}\vec{r}_{D/O}(t)\right]_o &= \Phi_{vr}(t,t_0)\left[\vec{r}_{D/O}(t_0)\right]_o + \Phi_{vv}(t,t_0)\left[{}^o\frac{d}{dt}\vec{r}_{D/O}(t_0)\right]_o\end{aligned} \tag{4.19}$$

Vector Solution.

To find the solution in vector form, we begin by differencing the chief and deputy motions expressed in Eqs. (4.18) and (4.19) as follows:

$$\begin{aligned}\left[\vec{r}_{D/O}(t)-\vec{r}_{C/O}(t)\right]_o &= \Phi_{rr}(t,t_0)\left[\vec{r}_{D/O}(t_0)-\vec{r}_{C/O}(t_0)\right]_o \\ &\quad +\Phi_{rv}(t,t_0)\left[{}^o\frac{d}{dt}\vec{r}_{D/O}(t_0)-{}^o\frac{d}{dt}\vec{r}_{C/O}(t_0)\right]_o\end{aligned} \tag{4.20}$$

$$\left[{}^{o}\frac{d}{dt}\vec{r}_{D/O}(t) - {}^{o}\frac{d}{dt}\vec{r}_{C/O}(t) \right]_o = \Phi_{vr}(t,t_0)\left[\vec{r}_{D/O}(t_0) - \vec{r}_{C/O}(t_0) \right]_o + \Phi_{vv}(t,t_0)\left[{}^{o}\frac{d}{dt}\vec{r}_{D/O}(t_0) - {}^{o}\frac{d}{dt}\vec{r}_{C/O}(t_0) \right]_o \tag{4.21}$$

For initial conditions, we can evaluate Eqs. (4.11) and (4.13) at epoch time t_0:

$$\begin{aligned} \left[\vec{r}_{D/O}(t_0) - \vec{r}_{C/O}(t_0) \right]_o &= \left[R^{o\to c}(t_0) \right]^T \left[\vec{r}_{D/C}(t_0) \right]_c \\ \left[{}^{o}\frac{d}{dt}\vec{r}_{D/O}(t_0) - {}^{o}\frac{d}{dt}\vec{r}_{C/O}(t_0) \right]_o &= \left[R^{o\to c}(t_0) \right]^T \left[{}^{c}\frac{d}{dt}\vec{r}_{D/C}(t_0) + \vec{\omega}_{c/o}(t_0)\times\vec{r}_{D/C}(t_0) \right]_c \end{aligned} \tag{4.22}$$

Note that each side of the first of Eqs. (4.22) equals $\left[\vec{r}_{D/C}(t_0) \right]_o$, and each side of the second of Eqs. (4.22) equals $\left[{}^{o}\frac{d}{dt}\vec{r}_{D/C}(t_0) \right]_o$. Substituting into Eqs. (4.20) and (4.21),

$$\left[\vec{r}_{D/O}(t) - \vec{r}_{C/O}(t) \right]_o = \Phi_{rr}(t,t_0)\left[R^{o\to c}(t_0) \right]^T \left[\vec{r}_{D/C}(t_0) \right]_c + \Phi_{rv}(t,t_0)\left[R^{o\to c}(t_0) \right]^T \left[{}^{c}\frac{d}{dt}\vec{r}_{D/C}(t_0) + \vec{\omega}_{c/o}(t_0)\times\vec{r}_{D/C}(t_0) \right]_c \tag{4.23}$$

$$\left[{}^{o}\frac{d}{dt}\vec{r}_{D/O}(t) - {}^{o}\frac{d}{dt}\vec{r}_{C/O}(t) \right]_o = \Phi_{vr}(t,t_0)\left[R^{o\to c}(t_0) \right]^T \left[\vec{r}_{D/C}(t_0) \right]_c + \Phi_{vv}(t,t_0)\left[R^{o\to c}(t_0) \right]^T \left[\begin{array}{l} {}^{c}\frac{d}{dt}\vec{r}_{D/C}(t_0) \\ +\vec{\omega}_{c/o}(t_0)\times\vec{r}_{D/C}(t_0) \end{array} \right]_c \tag{4.24}$$

Then we can substitute Eqs. (4.23) and (4.24) into rearranged forms of Eqs. (4.11) and (4.13), yielding

$$\begin{aligned}\left[\vec{r}_{D/C}(t)\right]_c &= \left[R^{o\to c}(t)\right]\Phi_{rr}(t,t_0)\left[R^{o\to c}(t_0)\right]^T\left[\vec{r}_{D/C}(t_0)\right]_c \\ &\quad+\left[R^{o\to c}(t)\right]\Phi_{rv}(t,t_0)\left[R^{o\to c}(t_0)\right]^T\left[\begin{array}{l}{}^c\dfrac{d}{dt}\vec{r}_{D/C}(t_0)\\ +\vec{\omega}_{c/o}(t_0)\times\vec{r}_{D/C}(t_0)\end{array}\right]_c\end{aligned} \tag{4.25}$$

$$\begin{aligned}\left[{}^c\frac{d}{dt}\vec{r}_{D/C}(t)\right]_c &= \left[R^{o\to c}(t)\right]\Phi_{vr}(t,t_0)\left[R^{o\to c}(t_0)\right]^T\left[\vec{r}_{D/C}(t_0)\right]_c \\ &\quad+\left[R^{o\to c}(t)\right]\Phi_{vv}(t,t_0)\left[R^{o\to c}(t_0)\right]^T\left[\begin{array}{l}{}^c\dfrac{d}{dt}\vec{r}_{D/C}(t_0)\\ +\vec{\omega}_{c/o}(t_0)\times\vec{r}_{D/C}(t_0)\end{array}\right]_c \\ &\quad-\left[\vec{\omega}_{c/o}(t)\times\vec{r}_{D/C}(t)\right]_c\end{aligned} \tag{4.26}$$

Finally, substituting Eq. (4.25) into Eq. (4.26),

$$\begin{aligned}\left[{}^c\frac{d}{dt}\vec{r}_{D/C}(t)\right]_c &= \left[R^{o\to c}(t)\right]\Phi_{vr}(t,t_0)\left[R^{o\to c}(t_0)\right]^T\left[\vec{r}_{D/C}(t_0)\right]_c \\ &\quad+\left[R^{o\to c}(t)\right]\Phi_{vv}(t,t_0)\left[R^{o\to c}(t_0)\right]^T\left[{}^c\frac{d}{dt}\vec{r}_{D/C}(t_0)+\vec{\omega}_{c/o}(t_0)\times\vec{r}_{D/C}(t_0)\right]_c \\ &\quad-\left[\vec{\omega}_{c/o}(t)\times\left\{\begin{array}{l}\left[R^{o\to c}(t)\right]\Phi_{rr}(t,t_0)\left[R^{o\to c}(t_0)\right]^T\left[\vec{r}_{D/C}(t_0)\right]_c\\ +\left[R^{o\to c}(t)\right]\Phi_{rv}(t,t_0)\left[R^{o\to c}(t_0)\right]^T\left[\begin{array}{l}{}^c\dfrac{d}{dt}\vec{r}_{D/C}(t_0)\\ +\vec{\omega}_{c/o}(t_0)\times\vec{r}_{D/C}(t_0)\end{array}\right]_c\end{array}\right\}\right]_c\end{aligned} \tag{4.27}$$

Eqs. (4.25) and (4.27) are the solution we have been seeking, in vector form. The relative position and velocity at any time are given as a function of initial position, initial velocity, time, and a variety of time-varying elements from the rotation matrices and angular velocity vectors.

Scalar Solution.

The elements of all the matrices and vectors in Eqs. (4.25) and (4.27) are already known. Finding the scalar solution equations is then a straightforward matter of vector-matrix operations. Eq. (4.25) becomes

$$
\begin{aligned}
\begin{bmatrix} x(t) \\ y(t) \\ z(t) \end{bmatrix}_c = &\begin{bmatrix} \cos\left[\nu_C(t) - M_C(t)\right] & \sin\left[\nu_C(t) - M_C(t)\right] & 0 \\ -\sin\left[\nu_C(t) - M_C(t)\right] & \cos\left[\nu_C(t) - M_C(t)\right] & 0 \\ 0 & 0 & 1 \end{bmatrix} \\
&\begin{bmatrix} -3\cos\left[n_C(t-t_0)\right] + 4 & 0 & 0 \\ 6\sin\left[n_C(t-t_0)\right] - 6n_C(t-t_0) & 1 & 0 \\ 0 & 0 & \cos\left[n_C(t-t_0)\right] \end{bmatrix} \\
&\begin{bmatrix} \cos\left[\nu_{C,0} - M_{C,0}\right] & -\sin\left[\nu_{C,0} - M_{C,0}\right] & 0 \\ \sin\left[\nu_{C,0} - M_{C,0}\right] & \cos\left[\nu_{C,0} - M_{C,0}\right] & 0 \\ 0 & 0 & 1 \end{bmatrix} \begin{bmatrix} x_0 \\ y_0 \\ z_0 \end{bmatrix}_c \\
&+ \begin{bmatrix} \cos\left[\nu_C(t) - M_C(t)\right] & \sin\left[\nu_C(t) - M_C(t)\right] & 0 \\ -\sin\left[\nu_C(t) - M_C(t)\right] & \cos\left[\nu_C(t) - M_C(t)\right] & 0 \\ 0 & 0 & 1 \end{bmatrix} \\
&\begin{bmatrix} \dfrac{\sin\left[n_C(t-t_0)\right]}{n_C} & -\dfrac{2\cos\left[n_C(t-t_0)\right]}{n_C} + \dfrac{2}{n_C} & 0 \\ \dfrac{2\cos\left[n_C(t-t_0)\right]}{n_C} - \dfrac{2}{n_C} & \dfrac{4\sin\left[n_C(t-t_0)\right]}{n_C} - 3(t-t_0) & 0 \\ 0 & 0 & \dfrac{\sin\left[n_C(t-t_0)\right]}{n_C} \end{bmatrix} \\
&\begin{bmatrix} \cos\left[\nu_{C,0} - M_{C,0}\right] & -\sin\left[\nu_{C,0} - M_{C,0}\right] & 0 \\ \sin\left[\nu_{C,0} - M_{C,0}\right] & \cos\left[\nu_{C,0} - M_{C,0}\right] & 0 \\ 0 & 0 & 1 \end{bmatrix} \left\{ \begin{bmatrix} \dot{x}_0 \\ \dot{y}_0 \\ \dot{z}_0 \end{bmatrix}_c + \begin{bmatrix} 0 \\ 0 \\ \dot{\nu}_{C,0} - n_C \end{bmatrix}_c \times \begin{bmatrix} x_0 \\ y_0 \\ z_0 \end{bmatrix}_c \right\}
\end{aligned}
\tag{4.28}
$$

For the sake of brevity in the following development, we introduce constant intermediate parameters A, B, C, and D such that the initial conditions can be expressed as

$$\left[\vec{r}_{D/C}\left(t_0\right)\right]_o = \begin{bmatrix} A \\ B \\ z_0 \end{bmatrix}_o$$

$$\left[{}^o\frac{d}{dt}\vec{r}_{D/C}\left(t_0\right)\right]_o = \begin{bmatrix} n_C D \\ n_C C \\ \dot{z}_0 \end{bmatrix}_o$$

We can find the values of the intermediate parameters by calculating Eq. (4.22):

$$\begin{aligned}
A &= \cos\left[\nu_{C,0} - M_{C,0}\right] x_0 - \sin\left[\nu_{C,0} - M_{C,0}\right] y_0 \\
B &= \sin\left[\nu_{C,0} - M_{C,0}\right] x_0 + \cos\left[\nu_{C,0} - M_{C,0}\right] y_0 \\
C &= \frac{1}{n_C}\left\{\begin{matrix} \sin\left[\nu_{C,0} - M_{C,0}\right]\left[\dot{x}_0 - \left(\dot{\nu}_{C,0} - n_C\right) y_0\right] \\ +\cos\left[\nu_{C,0} - M_{C,0}\right]\left[\dot{y}_0 + \left(\dot{\nu}_{C,0} - n_C\right) x_0\right] \end{matrix}\right\} \\
D &= \frac{1}{n_C}\left\{\begin{matrix} \cos\left[\nu_{C,0} - M_{C,0}\right]\left[\dot{x}_0 - \left(\dot{\nu}_{C,0} - n_C\right) y_0\right] \\ -\sin\left[\nu_{C,0} - M_{C,0}\right]\left[\dot{y}_0 + \left(\dot{\nu}_{C,0} - n_C\right) x_0\right] \end{matrix}\right\}
\end{aligned} \tag{4.29}$$

Using these parameters to evaluate Eq. (4.28), we find that the three position components are

$$x(t)=\sin\left[\nu_C(t)-M_C(t)\right]\begin{Bmatrix}\left\{6\sin\left[n_C(t-t_0)\right]-6n_C(t-t_0)\right\}A+B\\+\left\{4\sin\left[n_C(t-t_0)\right]-3n_C(t-t_0)\right\}C\\+\left\{2\cos\left[n_C(t-t_0)\right]-2\right\}D\end{Bmatrix}$$
$$+\cos\left[\nu_C(t)-M_C(t)\right]\begin{Bmatrix}\left\{-3\cos\left[n_C(t-t_0)\right]+4\right\}A\\+\left\{-2\cos\left[n_C(t-t_0)\right]+2\right\}C+\sin\left[n_C(t-t_0)\right]D\end{Bmatrix} \tag{4.30}$$

$$y(t)=-\sin\left[\nu_C(t)-M_C(t)\right]\begin{Bmatrix}\left\{-3\cos\left[n_C(t-t_0)\right]+4\right\}A\\+\left\{-2\cos\left[n_C(t-t_0)\right]+2\right\}C+\sin\left[n_C(t-t_0)\right]D\end{Bmatrix}$$
$$+\cos\left[\nu_C(t)-M_C(t)\right]\begin{Bmatrix}\left\{6\sin\left[n_C(t-t_0)\right]-6n_C(t-t_0)\right\}A+B\\+\left\{4\sin\left[n_C(t-t_0)\right]-3n_C(t-t_0)\right\}C\\+\left\{2\cos\left[n_C(t-t_0)\right]-2\right\}D\end{Bmatrix} \tag{4.31}$$

$$z(t)=\cos\left[n_C(t-t_0)\right]z_0+\frac{\sin\left[n_C(t-t_0)\right]}{n_C}\dot{z}_0 \tag{4.32}$$

The velocity components are a little more complicated. Eq. (4.27) becomes

$$
\begin{bmatrix} \dot{x}(t) \\ \dot{y}(t) \\ \dot{z}(t) \end{bmatrix}_c = \begin{bmatrix} \cos[\nu_C(t) - M_C(t)] & \sin[\nu_C(t) - M_C(t)] & 0 \\ -\sin[\nu_C(t) - M_C(t)] & \cos[\nu_C(t) - M_C(t)] & 0 \\ 0 & 0 & 1 \end{bmatrix}
$$

$$
\begin{bmatrix} 3n_C \sin[n_C(t-t_0)] & 0 & 0 \\ 6n_C \cos[n_C(t-t_0)] - 6n_C & 0 & 0 \\ 0 & 0 & -n_C \sin[n_C(t-t_0)] \end{bmatrix} \begin{bmatrix} \cos[\nu_{C,0} - M_{C,0}] & -\sin[\nu_{C,0} - M_{C,0}] & 0 \\ \sin[\nu_{C,0} - M_{C,0}] & \cos[\nu_{C,0} - M_{C,0}] & 0 \\ 0 & 0 & 1 \end{bmatrix} \begin{bmatrix} x_0 \\ y_0 \\ z_0 \end{bmatrix}_c
$$

$$
+ \begin{bmatrix} \cos[\nu_C(t) - M_C(t)] & \sin[\nu_C(t) - M_C(t)] & 0 \\ -\sin[\nu_C(t) - M_C(t)] & \cos[\nu_C(t) - M_C(t)] & 0 \\ 0 & 0 & 1 \end{bmatrix}
$$

$$
\begin{bmatrix} \cos[n_C(t-t_0)] & 2\sin[n_C(t-t_0)] & 0 \\ -2\sin[n_C(t-t_0)] & 4\cos[n_C(t-t_0)] - 3 & 0 \\ 0 & 0 & \cos[n_C(t-t_0)] \end{bmatrix}
$$

$$
\begin{bmatrix} \cos[\nu_{C,0} - M_{C,0}] & -\sin[\nu_{C,0} - M_{C,0}] & 0 \\ \sin[\nu_{C,0} - M_{C,0}] & \cos[\nu_{C,0} - M_{C,0}] & 0 \\ 0 & 0 & 1 \end{bmatrix} \left\{ \begin{bmatrix} \dot{x}_0 \\ \dot{y}_0 \\ \dot{z}_0 \end{bmatrix}_c + \begin{bmatrix} 0 \\ 0 \\ \dot{\nu}_{C,0} - n_C \end{bmatrix}_c \times \begin{bmatrix} x_0 \\ y_0 \\ z_0 \end{bmatrix}_c \right\}
$$

$$
- \begin{bmatrix} 0 \\ 0 \\ \dot{\nu}_C(t) - n_C \end{bmatrix}_c \times \left\{ \begin{bmatrix} \cos[\nu_C(t) - M_C(t)] & \sin[\nu_C(t) - M_C(t)] & 0 \\ -\sin[\nu_C(t) - M_C(t)] & \cos[\nu_C(t) - M_C(t)] & 0 \\ 0 & 0 & 1 \end{bmatrix} \right.
$$

$$
\begin{bmatrix} -3\cos[n_C(t-t_0)] + 4 & 0 & 0 \\ 6\sin[n_C(t-t_0)] - 6n_C(t-t_0) & 1 & 0 \\ 0 & 0 & \cos[n_C(t-t_0)] \end{bmatrix}
$$

$$
\begin{bmatrix} \cos[\nu_{C,0} - M_{C,0}] & -\sin[\nu_{C,0} - M_{C,0}] & 0 \\ \sin[\nu_{C,0} - M_{C,0}] & \cos[\nu_{C,0} - M_{C,0}] & 0 \\ 0 & 0 & 1 \end{bmatrix} \begin{bmatrix} x_0 \\ y_0 \\ z_0 \end{bmatrix}_c
$$

$$
+ \begin{bmatrix} \cos[\nu_C(t) - M_C(t)] & \sin[\nu_C(t) - M_C(t)] & 0 \\ -\sin[\nu_C(t) - M_C(t)] & \cos[\nu_C(t) - M_C(t)] & 0 \\ 0 & 0 & 1 \end{bmatrix} \left(\frac{1}{n_C} \right)
$$

$$
\begin{bmatrix} \sin[n_C(t-t_0)] & -2\cos[n_C(t-t_0)] + 2 & 0 \\ 2\cos[n_C(t-t_0)] - 2 & 4\sin[n_C(t-t_0)] - 3(t-t_0) & 0 \\ 0 & 0 & \sin[n_C(t-t_0)] \end{bmatrix}
$$

$$
\left. \begin{bmatrix} \cos[\nu_{C,0} - M_{C,0}] & -\sin[\nu_{C,0} - M_{C,0}] & 0 \\ \sin[\nu_{C,0} - M_{C,0}] & \cos[\nu_{C,0} - M_{C,0}] & 0 \\ 0 & 0 & 1 \end{bmatrix} \left\{ \begin{bmatrix} \dot{x}_0 \\ \dot{y}_0 \\ \dot{z}_0 \end{bmatrix}_c + \begin{bmatrix} 0 \\ 0 \\ \dot{\nu}_{C,0} - n_C \end{bmatrix}_c \times \begin{bmatrix} x_0 \\ y_0 \\ z_0 \end{bmatrix}_c \right\} \right\}
$$

Evaluating with A, B, C, and D,

$$\begin{aligned}\dot{x}(t) = {} & \sin\left[\nu_C(t) - M_C(t)\right]\left\{\begin{array}{l}\left\{6n_C\cos\left[n_C(t-t_0)\right]-6n_C\right\}A \\ +n_C\left\{4\cos\left[n_C(t-t_0)\right]-3\right\}C - 2n_C\sin\left[n_C(t-t_0)\right]D\end{array}\right\} \\ & +\cos\left[\nu_C(t) - M_C(t)\right]\left\{\begin{array}{l}\left\{3n_C\sin\left[n_C(t-t_0)\right]\right\}A \\ +2n_C\sin\left[n_C(t-t_0)\right]C + n_C\cos\left[n_C(t-t_0)\right]D\end{array}\right\} \\ & +\left(\dot{\nu}_C(t) - n_C\right)\left\{\begin{array}{l}-\sin\left[\nu_C(t) - M_C(t)\right]\left\{\begin{array}{l}\left\{-3\cos\left[n_C(t-t_0)\right]+4\right\}A \\ +\left\{-2\cos\left[n_C(t-t_0)\right]+2\right\}C \\ +\sin\left[n_C(t-t_0)\right]D\end{array}\right\} \\ +\cos\left[\nu_C(t) - M_C(t)\right]\left\{\begin{array}{l}\left\{6\sin\left[n_C(t-t_0)\right]-6n_C(t-t_0)\right\}A+B \\ +\left\{4\sin\left[n_C(t-t_0)\right]-3n_C(t-t_0)\right\}C \\ +\left\{2\cos\left[n_C(t-t_0)\right]-2\right\}D\end{array}\right\}\end{array}\right\}\end{aligned} \tag{4.33}$$

$$\begin{aligned}\dot{y}(t) = {} & -\sin\left[\nu_C(t) - M_C(t)\right]\left\{\begin{array}{l}\left\{3n_C\sin\left[n_C(t-t_0)\right]\right\}A \\ +2n_C\sin\left[n_C(t-t_0)\right]C + n_C\cos\left[n_C(t-t_0)\right]D\end{array}\right\} \\ & +\cos\left[\nu_C(t) - M_C(t)\right]\left\{\begin{array}{l}\left\{6n_C\cos\left[n_C(t-t_0)\right]-6n_C\right\}A \\ +n_C\left\{4\cos\left[n_C(t-t_0)\right]-3\right\}C - 2n_C\sin\left[n_C(t-t_0)\right]D\end{array}\right\} \\ & -\left(\dot{\nu}_C(t) - n_C\right)\left\{\begin{array}{l}\sin\left[\nu_C(t) - M_C(t)\right]\left\{\begin{array}{l}\left\{6\sin\left[n_C(t-t_0)\right]-6n_C(t-t_0)\right\}A+B \\ +\left\{4\sin\left[n_C(t-t_0)\right]-3n_C(t-t_0)\right\}C \\ \left\{2\cos\left[n_C(t-t_0)\right]-2\right\}D\end{array}\right\} \\ +\cos\left[\nu_C(t) - M_C(t)\right]\left\{\begin{array}{l}\left\{-3\cos\left[n_C(t-t_0)\right]+4\right\}A \\ +\left\{-2\cos\left[n_C(t-t_0)\right]+2\right\}C \\ +\sin\left[n_C(t-t_0)\right]D\end{array}\right\}\end{array}\right\}\end{aligned} \tag{4.34}$$

$$\dot{z}(t) = -n_C \sin\left[n_C (t - t_0)\right] z_0 + \cos\left[n_C (t - t_0)\right] \dot{z}_0 \tag{4.35}$$

Thus, Eqs. (4.30)-(4.35) are the Virtual Chief solution. A comparison reveals that Eqs. (4.33)-(4.35) are indeed the time derivatives of Eqs. (4.30)-(4.32).

Note that the out-of-plane solution is identical to HCW, and that if the chief's eccentricity is zero, Eqs. (4.30) and (4.31) reduce to the in-plane components of Eqs. (3.2).

State Transition Matrix.

We can arrange the Virtual Chief solution into a new state transition matrix $\Phi(t, t_0)$, such that

$$\begin{bmatrix} x(t) \\ y(t) \\ z(t) \\ \dot{x}(t) \\ \dot{y}(t) \\ \dot{z}(t) \end{bmatrix}_c = \Phi(t, t_0) \begin{bmatrix} x_0 \\ y_0 \\ z_0 \\ \dot{x}_0 \\ \dot{y}_0 \\ \dot{z}_0 \end{bmatrix}_c$$

The matrix is

$$\Phi(t, t_0) = \begin{bmatrix} \Phi_{11} & \Phi_{12} & 0 & \Phi_{14} & \Phi_{15} & 0 \\ \Phi_{21} & \Phi_{22} & 0 & \Phi_{24} & \Phi_{25} & 0 \\ 0 & 0 & \cos\left[n_C (t - t_0)\right] & 0 & 0 & \dfrac{\sin\left[n_C (t - t_0)\right]}{n_C} \\ \Phi_{41} & \Phi_{42} & 0 & \Phi_{44} & \Phi_{45} & 0 \\ \Phi_{51} & \Phi_{52} & 0 & \Phi_{54} & \Phi_{55} & 0 \\ 0 & 0 & -n_C \sin\left[n_C (t - t_0)\right] & 0 & 0 & \cos\left[n_C (t - t_0)\right] \end{bmatrix} \tag{4.36}$$

The sixteen in-plane elements of $\Phi(t,t_0)$ would be too cumbersome to list here; they are found in Appendix E. It can be shown that $\Phi(t,t_0)$ satisfies Eq. (4.17), and that the time derivatives of Eqs. (4.30)-(4.35) are consistent with the differential equations, Eq. (4.16). Thus, the solution presented here is the unique solution to the linear time-varying system of the previous section [24].

Parameterization.

Our goal is to find a meaningfully parameterized model. Since the Virtual Chief out-of-plane motion is identical to HCW out-of-plane motion, we can adopt two ROEs, $z_{\max}$ and ψ_0 (defined in Eqs. (3.15) and (3.16)), and re-write Eq. (4.32) as

$$z(t) = z_{\max} \sin\left(n_C (t - t_0) + \psi_0\right) \tag{4.37}$$

We can rewrite the in-plane position equations in the following manner, using the constants of Eq. (4.29), as well as the trigonometric identities in Eqs. (A.7) through (A.10):

$$\begin{aligned} x(t) = &\left(\frac{3}{2}D\right)\sin\left[\nu_C(t) + n_C t_p - n_C t_0\right] + \left(-\frac{9}{2}A - 3C\right)\cos\left[\nu_C(t) + n_C t_p - n_C t_0\right] \\ &+ (B - 2D)\sin\left[\nu_C(t) - n_C t + n_C t_p\right] + (4A + 2C)\cos\left[\nu_C(t) - n_C t + n_C t_p\right] \\ &+ \left(\frac{1}{2}D\right)\sin\left[\nu_C(t) - 2n_C t + n_C t_p + n_C t_0\right] + \left(\frac{3}{2}A + C\right)\cos\left[\nu_C(t) - 2n_C t + n_C t_p + n_C t_0\right] \\ &- (6A + 3C)\, n_C (t - t_0)\sin\left[\nu_C(t) - n_C t + n_C t_p\right] \end{aligned}$$

$$
\begin{aligned}
y(t) = &\left(\frac{9}{2}A + 3C\right)\sin\left[\nu_C(t) + n_C t_p - n_C t_0\right] + \left(\frac{3}{2}D\right)\cos\left[\nu_C(t) + n_C t_p - n_C t_0\right] \\
&-(4A + 2C)\sin\left[\nu_C(t) - n_C t + n_C t_p\right] + (B - 2D)\cos\left[\nu_C(t) - n_C t + n_C t_p\right] \\
&-\left(\frac{3}{2}A + C\right)\sin\left[\nu_C(t) - 2n_C t + n_C t_p + n_C t_0\right] + \frac{1}{2}D\cos\left[\nu_C(t) - 2n_C t + n_C t_p + n_C t_0\right] \\
&-(6A + 3C)n_C(t - t_0)\cos\left[\nu_C(t) - n_C t + n_C t_p\right]
\end{aligned}
$$

Next, we can apply the Harmonic Addition Theorem (see Appendix B), yielding

$$
\begin{aligned}
x(t) = &\sqrt{\frac{9}{4}D^2 + \frac{81}{4}A^2 + 27AC + 9C^2}\,\sin\begin{bmatrix}\nu_C(t) + n_C t_p - n_C t_0 \\ +atan2(-3A - 2C, D)\end{bmatrix} \\
&+\sqrt{B^2 - 4BD + 4D^2 + 16A^2 + 16AC + 4C^2}\,\sin\begin{bmatrix}\nu_C(t) - n_C t + n_C t_p \\ +atan2(4A + 2C, B - 2D)\end{bmatrix} \\
&+\sqrt{\frac{1}{4}D^2 + \frac{9}{4}A^2 + 3AC + C^2}\,\sin\begin{bmatrix}\nu_C(t) - 2n_C t + n_C t_p + n_C t_0 \\ +atan2(3A + 2C, D)\end{bmatrix} \\
&-(6A + 3C)n_C(t - t_0)\sin\left[\nu_C(t) - n_C t + n_C t_p\right]
\end{aligned}
\tag{4.38}
$$

$$
\begin{aligned}
y(t) = &\sqrt{\frac{9}{4}D^2 + \frac{81}{4}A^2 + 27AC + 9C^2}\,\cos\begin{bmatrix}\nu_C(t) + n_C t_p - n_C t_0 \\ +atan2(-3A - 2C, D)\end{bmatrix} \\
&+\sqrt{B^2 - 4BD + 4D^2 + 16A^2 + 16AC + 4C^2}\,\cos\begin{bmatrix}\nu_C(t) - n_C t + n_C t_p \\ +atan2(4A + 2C, B - 2D)\end{bmatrix} \\
&+\sqrt{\frac{1}{4}D^2 + \frac{9}{4}A^2 + 3AC + C^2}\,\cos\begin{bmatrix}\nu_C(t) - 2n_C t + n_C t_p + n_C t_0 \\ +atan2(3A + 2C, D)\end{bmatrix} \\
&-(6A + 3C)n_C(t - t_0)\cos\left[\nu_C(t) - n_C t + n_C t_p\right]
\end{aligned}
\tag{4.39}
$$

Let us define the following parameters:

$$
\begin{aligned}
A_1 &= \frac{3}{2}\sqrt{D^2 + \left(3A + 2C\right)^2} \\
\phi_1 &= n_C t_0 + atan2\left(3A + 2C, D\right) \\
A_2 &= \sqrt{\left(B - 2D\right)^2 + \left(4A + 2C\right)^2} \\
\phi_2 &= atan2\left(4A + 2C, B - 2D\right) \\
A_3 &= -\left(6A + 3C\right) n_C
\end{aligned}
\tag{4.40}
$$

Obviously, these five parameters are not independent, but are defined by the four intermediate constants A, B, C, and D, which are defined by the four in-plane Cartesian initial conditions. Substituting these parameters into Eqs. (4.38) and (4.39), and using the definition of mean anomaly in Eq. (D.3), as well as the identities in Eqs. (A.12) through (A.15),

$$
\begin{aligned}
x\left(t\right) = {} & A_1 \sin\left[\nu_C\left(t\right) + n_C t_p - \phi_1\right] + A_2 \sin\left[\nu_C\left(t\right) - n_C t + n_C t_p + \phi_2\right] \\
& + \frac{1}{3} A_1 \sin\left[\nu_C\left(t\right) - 2n_C t + n_C t_p + \phi_1\right] + A_3\left(t - t_0\right)\sin\left[\nu_C\left(t\right) - n_C t + n_C t_p\right]
\end{aligned}
\tag{4.41}
$$

$$
\begin{aligned}
y\left(t\right) = {} & A_1 \cos\left[\nu_C\left(t\right) + n_C t_p - \phi_1\right] + A_2 \cos\left[\nu_C\left(t\right) - n_C t + n_C t_p + \phi_2\right] \\
& + \frac{1}{3} A_1 \cos\left[\nu_C\left(t\right) - 2n_C t + n_C t_p + \phi_1\right] + A_3\left(t - t_0\right)\cos\left[\nu_C\left(t\right) - n_C t + n_C t_p\right]
\end{aligned}
\tag{4.42}
$$

The parameterized solution as it now stands comprises Eqs. (4.41), (4.42), and (4.37). It requires knowledge of chief mean motion and time of chief perigee passage. (Of course, calculating the parameters from Cartesian initial conditions also requires knowledge of chief true anomaly at epoch and chief angular rate at epoch.) The seven parameters (A_1, ϕ_1, A_2, ϕ_2, A_3, $z_{\max}$, and ψ_0) can be reduced to six by defining A_3 in

terms of the others. The simplest method for doing so is to examine the right triangle suggested by the definition of ϕ_2. Its hypotenuse would equal A_2, and $\sin\phi_2$ would equal $(4A+2C)/A_2$. Thus,

$$\frac{3}{2}A_2\sin\phi_2 = 6A+3C \tag{4.43}$$

We can substitute Eq. (4.43) directly into the definition of A_3, yielding

$$A_3 = -\left(\frac{3}{2}A_2\sin\phi_2\right)n_C$$

We can recognize some of the terms in Eqs. (4.41) and (4.42) as representing the difference in argument of latitude between the chief and the virtual chief, $\Delta u(t)$. From Eqs. (4.4), (4.5), and (D.3),

$$\nu_C(t) - n_C t + n_C t_p = \Delta u(t) \tag{4.44}$$

This allows us to define the relative motion with six Virtual Chief parameters, A_1, ϕ_1, A_2, ϕ_2, $z_{\max}$, and ψ_0. The position equations become

$$
\begin{aligned}
x(t) &= A_1 \sin\left[\Delta u(t) + n_C t - \phi_1\right] + A_2 \sin\left[\Delta u(t) + \phi_2\right] \\
&\quad + \frac{1}{3} A_1 \sin\left[\Delta u(t) - n_C t + \phi_1\right] - \frac{3}{2} A_2 \sin\phi_2 n_C (t - t_0) \sin\left[\Delta u(t)\right] \\
y(t) &= A_1 \cos\left[\Delta u(t) + n_C t - \phi_1\right] + A_2 \cos\left[\Delta u(t) + \phi_2\right] \\
&\quad + \frac{1}{3} A_1 \cos\left[\Delta u(t) - n_C t + \phi_1\right] - \frac{3}{2} A_2 \sin\phi_2 n_C (t - t_0) \cos\left[\Delta u(t)\right] \\
z(t) &= z_{\max} \sin\left(n_C (t - t_0) + \psi_0\right)
\end{aligned}
\tag{4.45}
$$

Thus, the in-plane motion is seen to operate in three frequencies and involve mixed-secular terms of the form $\alpha_1 t \sin(\alpha_2 t + \alpha_3)$. This form is similar to the terms that concerned Melton in his own time-explicit solution [66]. However, in Eqs. (4.45) it is nothing more than the projection of the deputy's drift (which is along-track only in the virtual chief's frame) into the actual chief's frame.

The Virtual Chief parameters can be used to write the relative velocity solution, as well. Taking a time derivative of Eqs. (4.45), using the Harmonic Addition Theorem and the trigonometric identities from Eqs. (A.7) through (A.10), and then rearranging terms yields

$$
\begin{aligned}
\dot{x}(t) &= -A_2 n_C \sqrt{1 - \frac{3}{4}\sin^2\phi_2}\, \cos\left[\Delta u(t) + atan2\left(-\sin\phi_2, 2\cos\phi_2\right)\right] \\
&\quad - \frac{2}{3} A_1 n_C \cos\left[\Delta u(t) - n_C t + \phi_1\right] + \frac{3}{2} A_2 \sin\phi_2 n_C{}^2 (t - t_0) \cos\left[\Delta u(t)\right] \\
&\quad + \dot{\nu}_C(t) A_1 \cos\left[\Delta u(t) + n_C t - \phi_1\right] + \dot{\nu}_C(t) A_2 \cos\left[\Delta u(t) + \phi_2\right] \\
&\quad + \frac{1}{3} \dot{\nu}_C(t) A_1 \cos\left[\Delta u(t) - n_C t + \phi_1\right] - \frac{3}{2} \dot{\nu}_C(t) A_2 \sin\phi_2 n_C (t - t_0) \cos\left[\Delta u(t)\right]
\end{aligned}
\tag{4.46}
$$

$$\begin{aligned}\dot{y}(t) = {} & A_2 n_C \sqrt{1-\frac{3}{4}\sin^2\phi_2}\,\sin\left[\Delta u(t) + atan2\left(-\sin\phi_2, 2\cos\phi_2\right)\right] \\ & + \frac{2}{3}A_1 n_C \sin\left[\Delta u(t) - n_C t + \phi_1\right] - \frac{3}{2}A_2 \sin\phi_2 n_C{}^2 (t-t_0)\sin\left[\Delta u(t)\right] \\ & - \dot{\nu}_C(t) A_1 \sin\left[\Delta u(t) + n_C t - \phi_1\right] - \dot{\nu}_C(t) A_2 \sin\left[\Delta u(t) + \phi_2\right] \\ & - \frac{1}{3}\dot{\nu}_C(t) A_1 \sin\left[\Delta u(t) - n_C t + \phi_1\right] + \frac{3}{2}\dot{\nu}_C(t) A_2 \sin\phi_2 n_C (t-t_0)\sin\left[\Delta u(t)\right]\end{aligned} \tag{4.47}$$

$$\dot{z}(t) = z_{\max} n_C \cos\left(n_C (t-t_0) + \psi_0\right) \tag{4.48}$$

Eqs. (4.46)-(4.48) can also be derived directly from Eqs. (4.33)-(4.35).

The set of Virtual Chief parameters is a realization equivalent to the six Cartesian initial conditions, and there is a one-to-one mapping between the two sets. Using the chief's orbit elements as given values, the Virtual Chief parameters can be calculated from Cartesian initial conditions via Eqs. (3.15), (3.16), (4.29), and (4.40). The Cartesian initial conditions can be calculated from the Virtual Chief parameters by evaluating Eqs. (4.44)-(4.48) at t_0 :

$$\Delta u_0 = \nu_{C,0} - n_C t_0 + n_C t_p$$

$$x_0 = A_1 \sin\left[\Delta u_0 + n_C t_0 - \phi_1\right] + A_2 \sin\left[\Delta u_0 + \phi_2\right] + \frac{1}{3}A_1 \sin\left[\Delta u_0 - n_C t_0 + \phi_1\right]$$

$$y_0 = A_1 \cos\left[\Delta u_0 + n_C t_0 - \phi_1\right] + A_2 \cos\left[\Delta u_0 + \phi_2\right] + \frac{1}{3}A_1 \cos\left[\Delta u_0 - n_C t_0 + \phi_1\right]$$

$$z_0 = z_{\max} \sin\psi_0$$

$$\dot{x}_0 = -A_2 n_C \sqrt{1-\frac{3}{4}\sin^2\phi_2}\cos\left[\Delta u_0 + atan2\left(-\sin\phi_2, 2\cos\phi_2\right)\right] - \frac{2}{3}A_1 n_C \cos\left[\Delta u_0 - n_C t_0 + \phi_1\right]$$
$$+\dot{v}_{C,0}A_1\cos\left[\Delta u_0 + n_C t_0 - \phi_1\right] + \dot{v}_{C,0}A_2\cos\left[\Delta u_0 + \phi_2\right] + \frac{1}{3}\dot{v}_{C,0}A_1\cos\left[\Delta u_0 - n_C t_0 + \phi_1\right]$$

$$\dot{y}_0 = A_2 n_C \sqrt{1-\frac{3}{4}\sin^2\phi_2}\sin\left[\Delta u_0 + atan2\left(-\sin\phi_2, 2\cos\phi_2\right)\right] + \frac{2}{3}A_1 n_C \sin\left[\Delta u_0 - n_C t_0 + \phi_1\right]$$
$$-\dot{v}_{C,0}A_1\sin\left[\Delta u_0 + n_C t_0 - \phi_1\right] - \dot{v}_{C,0}A_2\sin\left[\Delta u_0 + \phi_2\right] - \frac{1}{3}\dot{v}_{C,0}A_1\sin\left[\Delta u_0 - n_C t_0 + \phi_1\right]$$

$$\dot{z}_0 = z_{\max} n_C \cos\psi_0$$

Each of the VC parameters has a geometric interpretation; the following descriptions are based on my observations. As with the circular-chief ROEs, $z_{\max}$ and ψ_0 are the amplitude and initial phase of the deputy's oscillatory out-of-plane motion. A_1 roughly indicates the scale of the periodic portion of the deputy's motion. In fact, an upper bound on the amplitude of such motion (depending on phasing, a particular case's amplitude may be smaller) is $(4/3)A_1 + A_2$. ϕ_1 and ϕ_2 are initial phase angles for in-plane motion; they control the deputy's starting point along its periodic trajectory, as well as the orientation and "skewness" of that trajectory. ϕ_2 also controls the rate of drift; when ϕ_2 equals 0 or π, there is no drift, and the drift rate is a maximum when ϕ_2 equals $\pi/2$ or $3\pi/2$. A_2 also scales the drift rate.

In addition, the approximate center of the periodic motion is $(0, A_2, 0)$; Eqs. (4.45) reveal why this is so. $\Delta u(t) + n_C t$ is an increasing function of t, and it can be

shown (see Appendix G) that for chief eccentricities less than about 0.31, $\Delta u(t) - n_C t$ is a decreasing one. Because of this, the trigonometric functions in Eqs. (4.45) whose arguments are $\Delta u(t) + n_C t - \phi_1$ or $\Delta u(t) - n_C t + \phi_1$ will cycle through the full range of values between positive and negative 1. Thus, the first term may take on any value between positive and negative A_1, and the third term any value between positive and negative $(1/3)A_1$, in both the x- and y-equations. But because $\Delta u(t)$ is a small oscillation about zero, the second term in the x-direction is always close to zero, and the second term in the y-direction is always close to A_2. Likewise, this effect explains why the drift term in the x-direction produces an oscillation of increasing amplitude about zero, but the drift term in the y-direction produces a small oscillation about a drift rate of $-(3/2)A_2 \sin\phi_2 n_C t$.

Bounded Motion.

Above, we eliminated A_3 from our parameter set. Let us examine the physical interpretation of A_3. If we restrict our problem to bounded motion (equal chief and deputy periods), then the drift terms in Eqs. (4.45) should vanish. In other words, a zero value for A_3 represents a boundedness condition for the Virtual Chief model. This condition can equivalently be expressed in any of the following three ways:

$$\begin{aligned} 0 &= 2A + C \\ 0 &= A_2 \sin\phi_2 \\ 0 &= \cos\left[\nu_{C,0} - M_{C,0}\right]\left(n_C + \dot{\nu}_{C,0}\right)x_0 + \sin\left[\nu_{C,0} - M_{C,0}\right]\dot{x}_0 \\ &\quad - \sin\left[\nu_{C,0} - M_{C,0}\right]\left(n_C + \dot{\nu}_{C,0}\right)y_0 + \cos\left[\nu_{C,0} - M_{C,0}\right]\dot{y}_0 \end{aligned} \tag{4.49}$$

If the chief's eccentricity is zero, this reduces to the HCW boundedness condition, Eq. (3.7). Also note that Eq. (4.49) is different from the boundedness condition derived from Lawden's equations, Eq. (4.3).

V. Numerical Results and Conclusions

Examples

The Virtual Chief relative satellite motion model developed in Chapter IV is intended to relax the eccentricity restriction of the HCW model. That is, a relative satellite trajectory predicted by the Virtual Chief model should be more accurate than one predicted by HCW for non-zero chief eccentricities. Another way of stating this requirement is that a Virtual Chief trajectory should be within a desired range of accuracy over a greater range of chief eccentricities than is an HCW model.

In order to illustrate the relative satellite motion predicted by these models, example trajectories are calculated numerically via MATLAB (see Appendix F) and depicted below. The trajectories labeled "Virtual Chief" are calculated using Eqs. (4.45). The curve labeled "2BP" follows the relative position predicted by unperturbed nonlinear Keplerian two-body motion. The curve labeled "HCW" is calculated by ignoring the eccentricity of the chief's orbit and using the traditional HCW state transition matrix (the first approach described at the beginning of Chapter IV). Plots of the trajectories are shown projected into each **c**-frame coordinate plane and in three dimensions. In each plot, an "o" marks the initial position, and an "x" indicates the direction of initial motion. Finally, the error in each trajectory (as compared to the "truth" model, 2BP) is shown versus time in each coordinate and in magnitude.

Conditions for Example I are shown in Table 1; note that the first two columns are inputs, and the third column is determined by the first two via Eqs. (4.45) evaluated at t_0. Step size refers to increments of chief true anomaly. In this example, Figures 5 and 6, all

three models show negligible drift. It is clear from the final plot in Figure 6 that during some portions of the simulated trajectory, the HCW prediction has a smaller error magnitude, and during other portions, the Virtual Chief prediction has a smaller error magnitude.

The error magnitude at each time step is simply the root sum square of the three error components at that time step (i.e., error magnitude^2 = x error^2 + y error^2 + z error^2). It is also possible to calculate an average error value over a given time period by taking a root mean square of the error magnitude values for all the time steps during the given period (i.e., for n time steps, rms error^2 = (1/n) * Σ error magnitude^2). Over the two chief orbits plotted for Example I, the root mean square error for the Virtual Chief trajectory is 15.0240191299859 meters, and the root mean square error for the HCW trajectory is 16.7326981169077 meters.

Table 1. Example I Conditions

$a_C = 8000000 \ (\mathrm{m})$	$A_1 = 2400 \ (\mathrm{m})$	$x_0 = -1.59999786667033 \ (\mathrm{m})$
$e_C = 0.001$	$\phi_1 = -\pi \ (\mathrm{rad})$	$y_0 = -799.998400002667 \ (\mathrm{m})$
$M_{C,0} = \frac{\pi}{2} \ (\mathrm{rad})$	$A_2 = 2400 \ (\mathrm{m})$	$z_0 = 1000 \ (\mathrm{m})$
Number of chief orbits: 2	$\phi_2 = 0$	$\dot{x}_0 = -1.41173271214503 \ (\mathrm{m/s})$
Simulation step size: $\pi/360 \ (\mathrm{rad})$	$z_{\max} = 1000 \ (\mathrm{m})$	$\dot{y}_0 = 0.00282346730660115 \ (\mathrm{m/s})$
$t_0 = 0$	$\psi_0 = \frac{\pi}{2} \ (\mathrm{rad})$	$\dot{z}_0 = 5.40274864382506e\text{-}017 \ (\mathrm{m/s})$

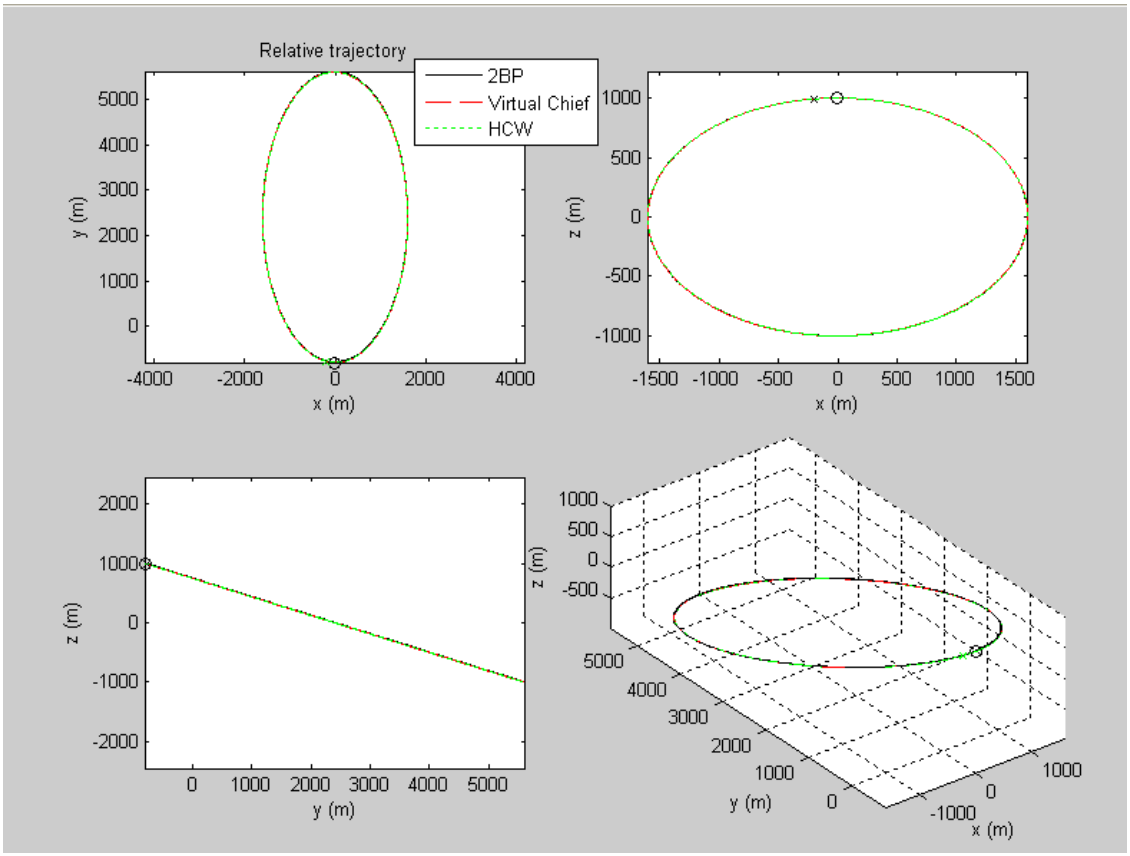

Figure 5. Example I Trajectory

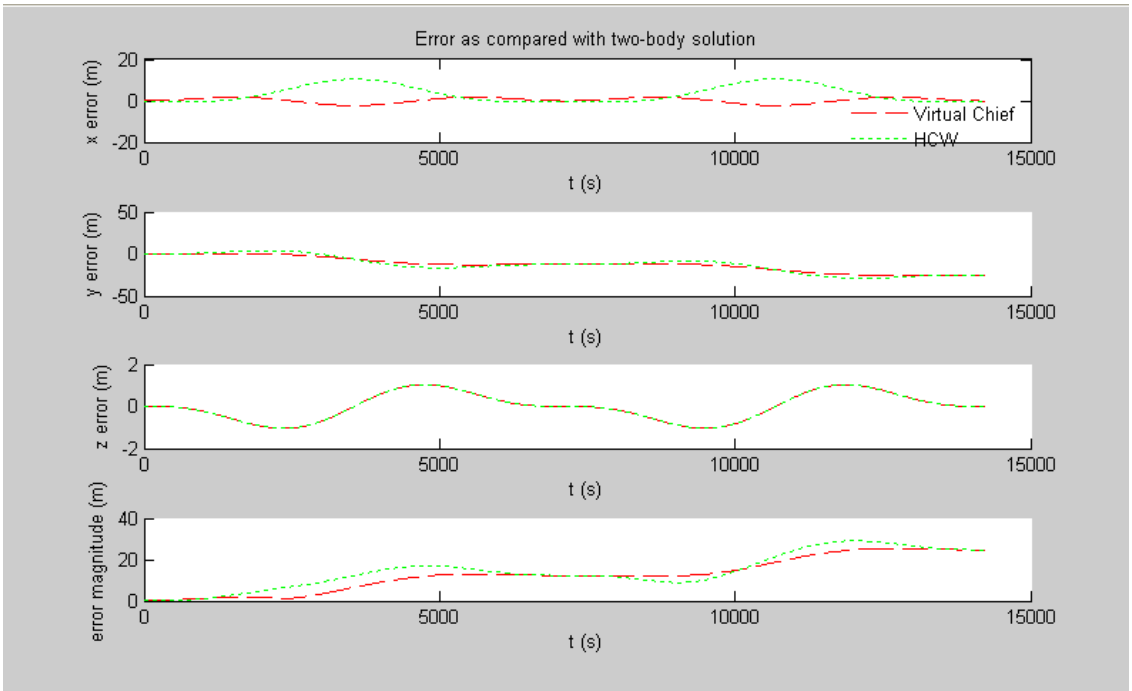

Figure 6. Example I Error

For some RPO missions, it is practical to set an error threshold for the deputy; when a deputy's position error exceeds the threshold distance from some desired relative trajectory, a correction maneuver must be initiated. Figure 7 shows a close-in view of the error magnitude during the first portion of the Example I simulation. If we arbitrarily select an error threshold of 15 meters, we see that in this particular case, the Virtual Chief trajectory does not exceed the threshold until after approximately 10,000 seconds, or about an orbit and a half. The HCW trajectory would exceed this threshold after about 4000 seconds.

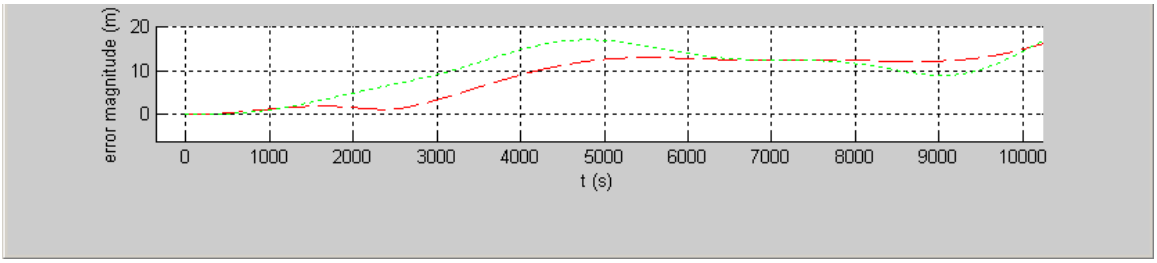

Figure 7. Example I Error Magnitude

Table 2. Example II Conditions

$a_C = 8000000 \ (\mathrm{m})$	$A_1 = 0$	$x_0 = 19.9993333633323 \ (\mathrm{m})$
$e_C = 0.005$	$\phi_1 = 0$	$y_0 = 1999.90000416646 \ (\mathrm{m})$
$M_{C,0} = \frac{\pi}{2} \ (\mathrm{rad})$	$A_2 = 2000 \ (\mathrm{m})$	$z_0 = 0$
Number of chief orbits: 2	$\phi_2 = 0$	$\dot{x}_0 = -0.000110280718448319 \ (\mathrm{m/s})$
Simulation step size: $\pi/360 \ (\mathrm{rad})$	$z_{\max} = 20 \ (\mathrm{m})$	$\dot{y}_0 = 1.10282556487623\mathrm{e}{-006} \ (\mathrm{m/s})$
$t_0 = 0$	$\psi_0 = 0$	$\dot{z}_0 = 0.0176467162534918 \ (\mathrm{m/s})$

Conditions for Example II are shown in Table 2. In Figures 8 and 9, the Virtual Chief prediction fails to capture the drift in the y-direction, and the x-direction oscillates in the opposite direction. In fact, the trajectory predicted by the Virtual Chief method is nearly a circle confined to the x-z plane, a physically unrealistic motion. The Virtual Chief prediction's error is clearly larger throughout the simulation; its root mean square error is 685.481869664407 meters. The root mean square error for the HCW trajectory is 212.449649464068 meters.

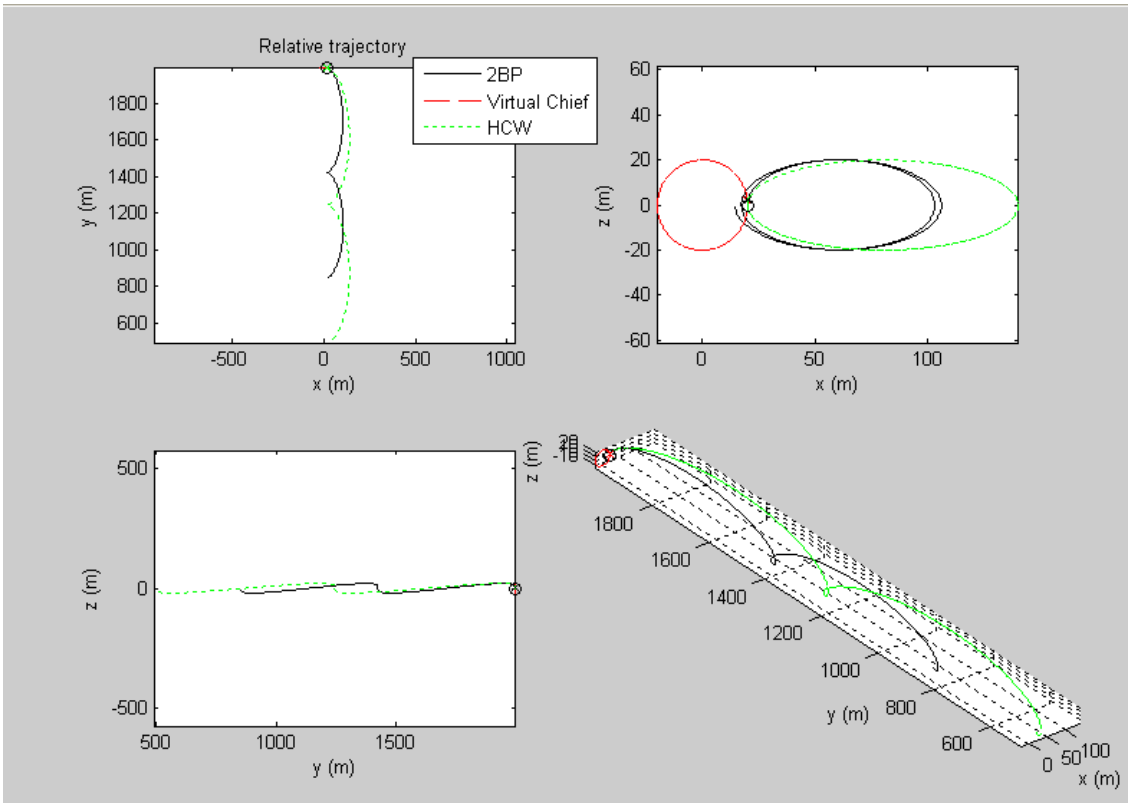

Figure 8. Example II Trajectory

Figure 10 shows a close-in view of the error magnitude plots during the first portion of the simulation. While in this case, the Virtual Chief trajectory would violate a

15-meter error threshold after about 10 minutes, the HCW trajectory would take about twice as long to do so.

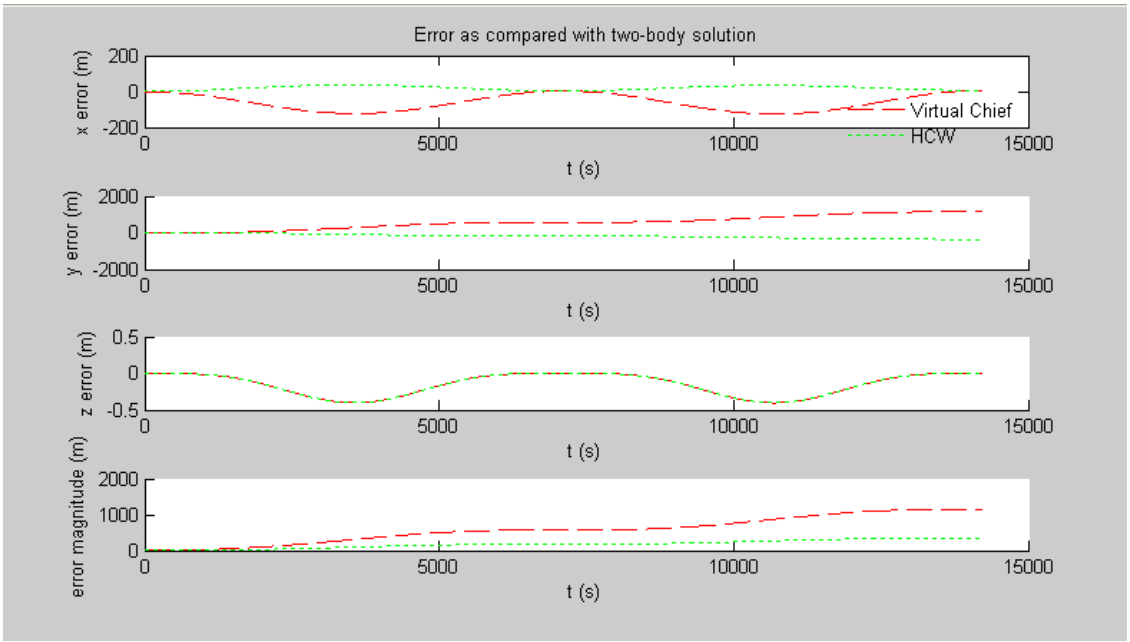

Figure 9. Example II Error

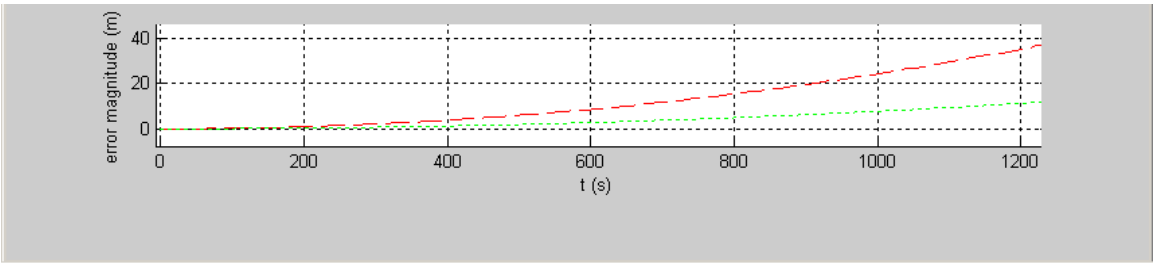

Figure 10. Example II Error Magnitude

Conditions for Example III are shown in Table 3. This in-plane-only example was carefully designed so that the deputy would follow the same trajectory as the chief, as seen by the virtual chief. In other words, $\vec{r}_{D/O}$ and $^{o}\frac{d}{dt}\vec{r}_{D/O}$ were selected to be nearly the opposite of the components of $\vec{r}_{C/O}$ and $^{o}\frac{d}{dt}\vec{r}_{C/O}$.

Table 3. Example III Conditions

$a_C = 8000000\ (\mathrm{m})$	$A_1 = 24000\ (\mathrm{m})$	$x_0 = -16000\ (\mathrm{m})$
$e_C = 0.001$	$\phi_1 = \frac{\pi}{2}\ (\mathrm{rad})$	$y_0 = 0$
$M_{C,0} = \pi\ (\mathrm{rad})$	$A_2 = 0$	$z_0 = 0$
Number of chief orbits: 2	$\phi_2 = -\frac{\pi}{2}\ (\mathrm{rad})$	$\dot{x}_0 = 0$
Simulation step size: $\pi/360\ (\mathrm{rad})$	$z_{\max} = 0$	$\dot{y}_0 = 28.2065465\ (\mathrm{m/s})$
$t_0 = 0$	$\psi_0 = 0$	$\dot{z}_0 = 0$

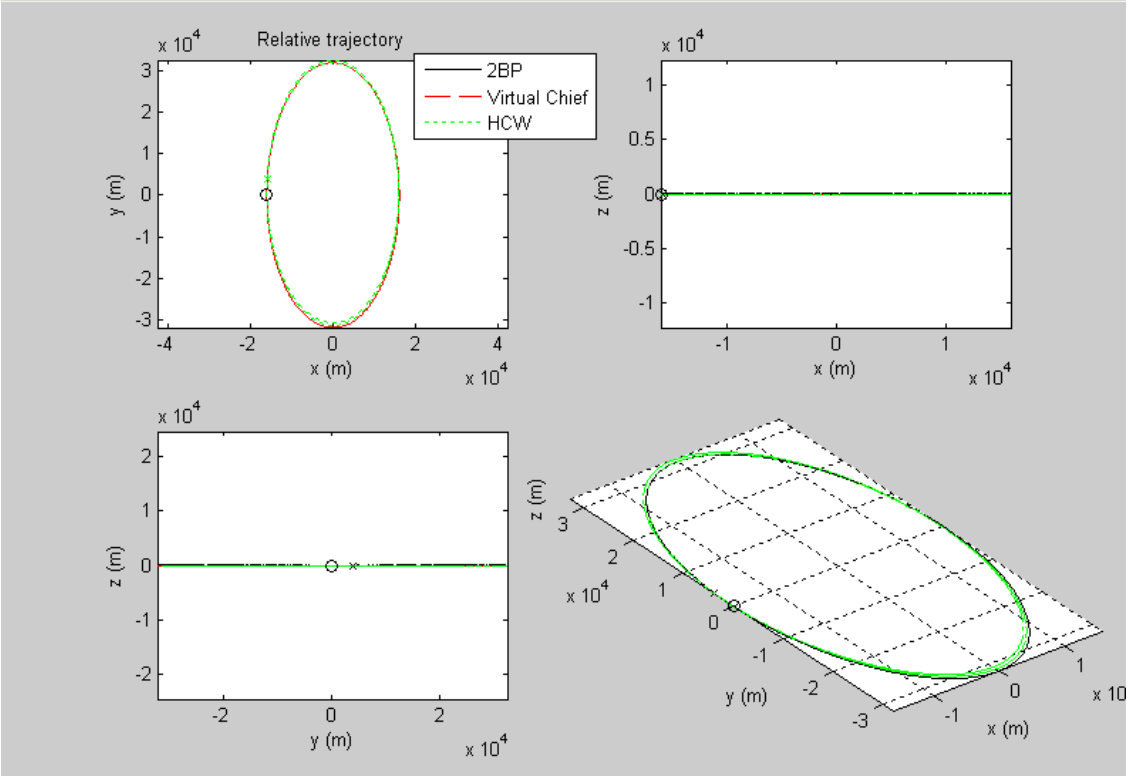

Figure 11. Example III Trajectory

Here, as shown in Figures 11 and 12, the Virtual Chief's prediction has the smaller error throughout the simulation. The root mean square error magnitude for the Virtual Chief and HCW predictions, respectively, are 0.182468634831835 meters and

720.129883483902 meters. Figure 13 shows a close-in view of the error magnitude plots. The HCW trajectory violates a 15-meter threshold after about 700 seconds, while in this simulation, the Virtual Chief trajectory's error never exceeds half a meter.

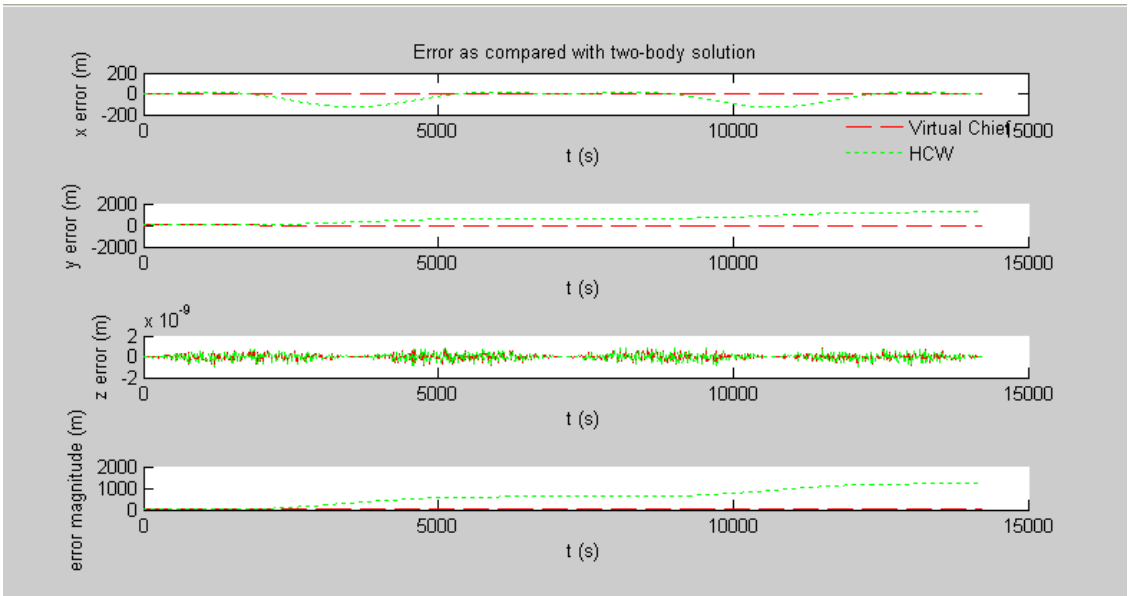

Figure 12. Example III Error

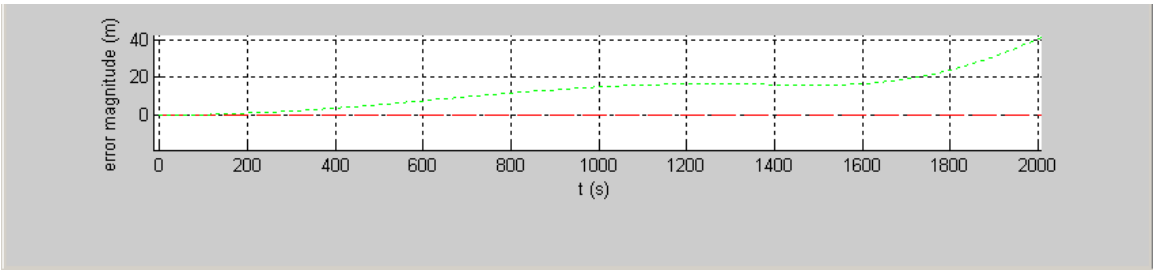

Figure 13. Example III Error Magnitude

Error Analysis: Phase 1

We have already established that every dynamics model represents a trade-off between simplicity and accuracy. Since the Virtual Chief method is more complex than

the HCW model, it is worth examining what we have gained in accuracy. Examples such as those in the previous section begin to suggest an answer.

Numerical simulations reveal that in some cases, the HCW model predicts the relative motion with better accuracy than the Virtual Chief method. To illustrate how the comparative accuracy changes by case, I conducted a series of simulations using the same Virtual Chief parameters as Example II above. In each case, the chief's semi-major axis was 16,778.137 km. The chief's eccentricity and mean anomaly at epoch were varied.

Table 4. Model Accuracy, Series 1

	$M_{C,0} = 0$	$\frac{\pi}{4}$	$\frac{\pi}{2}$	$\frac{3\pi}{4}$	$\frac{7\pi}{8}$	π	$\frac{9\pi}{8}$	$\frac{5\pi}{4}$	$\frac{3\pi}{2}$	$\frac{13\pi}{8}$	$\frac{7\pi}{4}$	$\frac{15\pi}{8}$
$e_C = 0$	tie	tie	tie	tie	tie	tie	tie	tie	tie	tie	tie	Tie
0.00010	H	H	H	H	H	V	V	V	V	V	V	V
0.00015	H	H	H	H	H	V	V	V	H	H	V	V
0.00020	H	H	H	H	H	V	V	H	H	H	H	V
0.00100	H	H	H	H	H	V	H	H	H	H	H	H
0.00500	H	H	H	H	H	H	H	H	H	H	H	H
0.01000	H	H	H	H	H	H	H	H	H	H	H	H

Table 4 summarizes the results, showing which model was more accurate, as measured by root mean square error. Each column is a different value of $M_{C,0}$ and each row a different value of e_C. An "H" indicates that, for that case, the HCW prediction had the lower root mean square error over the course of the simulation. A "V" indicates that the Virtual Chief prediction had the lower root mean square error. As previously noted,

when e_C is zero, the two models are identical. Inspection of Table 4 seems to indicate that, for these examples, the Virtual Chief method performed worse as chief eccentricity increased, and that it only performed better than HCW during the half-orbit from chief apogee to perigee.

In essence, I had been holding the relative motion problem constant and varying the chief orbit conditions to find some region where the Virtual Chief model represents a good choice. Since Table 4 does not suggest such a region, I attempted another series of simulations holding the chief orbit conditions constant and varying the in-plane Virtual Chief parameters.

This second series of simulations used a chief eccentricity of 0.00015 and a chief mean anomaly at epoch of $9\pi/8$, corresponding to a case in Table 4 for which the Virtual Chief model performed better. The results are presented in Table 5.

Table 5. Model Accuracy, Series 2

A_1 (m)	ϕ_1 (rad)	A_2 (m)	ϕ_2 (rad)	"Winner"
0	0	0	0	Tie
0	0	2	0	H
2	0	0	0	H
2	0	2	0	H
0	0	2	$\pi/4$	V
2	$\pi/4$	0	0	V
2	0	2	$\pi/4$	H
2	$\pi/4$	2	0	V
2	$\pi/4$	2	$\pi/4$	H

Thus, for the cases in Table 5, the Virtual Chief model did not consistently out-perform the HCW model. The results of Tables 4 and 5 imply that searching either the parameter space of the chief's orbit elements or the parameter space of the relative initial conditions (here, in the form of the Virtual Chief parameters) will not find a region of predictably good performance for the Virtual Chief model.

We can make a few statements about the modeling error in this study. The models compared (the two-body truth model, HCW, and Virtual Chief) have three possible error sources: unmodeled forces, eccentricity effects, and nonlinear effects. They correspond to the three assumptions underlying the equations of motion. First, the two-body assumption incurs errors from unmodeled differential forces (J2 and higher-order gravity terms, differential drag, etc.). This error is acceptable over short time scales, and is common to HCW, Virtual Chief, and the two-body truth model. Therefore, this error source has no effect in the current study.

Second, the circular chief assumption inherent to the HCW model incurs error because the chief's distance to the Earth and angular rate are not constant. This is the error which the Virtual Chief method was designed to remove or lessen. The two-body truth model does not incur this error. In the HCW model, this error can be approximated as an increasing function of actual chief eccentricity, $f_{ecc}(e_C)$.

Third, linearization of the gravity field incurs errors because the higher-order relative position terms are neglected (x^2, xy, etc.). The two-body truth model does not incur this error. In the HCW model, this error should tend to increase with the

displacement between deputy and chief. Thus, if f_{disp} is an increasing function of distance and ρ is $\sqrt{x^2+y^2+z^2}$, we can approximate the HCW error as

$$\delta_{HCW} \approx fn_1\left(f_{ecc}(e_C), f_{disp}(\rho)\right) \tag{5.1}$$

The Virtual Chief model is not immune to linearization error; in a sense, we are trying to fold the eccentricity error into the displacement error. The Virtual Chief displacement error has two contributions, because we linearized both the displacement from the actual chief to the virtual chief, ρ_C, *and* the displacement from the deputy to the virtual chief, ρ_D. Obviously, the error component dependent on ρ_D would vary by individual case.

Thus, we can approximate the Virtual Chief error as

$$\delta_{VC} \approx fn_2\left(f_{disp}(\rho_C), f_{disp}(\rho_D)\right) \tag{5.2}$$

Increasing e_C tends to increase δ_{HCW}, but also tends to increase ρ_C, and therefore has an effect on δ_{VC}. This effect would be consistent with the behavior seen in Table 4. It may also prevent the Virtual Chief method from being used to relax the HCW model's eccentricity restriction, at least in the general case.

Also, since the chief is in an orbit coplanar with that of the virtual chief, and since no along-track offset is present, the separation between the chief and the virtual chief is due entirely to the eccentricity difference. In fact, from the HCW in-plane solution to the

circular chief problem, we know that the chief's motion relative to the virtual chief describes a 2x1 ellipse with maximum separation occurring in the along-track direction. The value of this maximum displacement is found from Eq. (3.32) to be $2a_C e_C$. This tends to be a very large quantity, even for very low eccentricities and semi-major axes. If the deputy is far away from the chief, so that ρ approaches the value of $2a_C e_C$, then ρ_D is likely also very large. This would only be untrue if the trajectory is carefully designed so that the deputy remains as close to the virtual chief as does the actual chief, as in Example III.

For example, the conditions used to generate Table 4 gave the deputy a large positive along-track displacement from the chief; in other words, the deputy is leading the chief. During the half-orbit from perigee to apogee, the chief is itself leading the virtual chief, leading to a large displacement between the deputy and the virtual chief. However, during the half-orbit from apogee to perigee, the virtual chief is leading the chief, placing the virtual chief in the vicinity of the deputy. This may explain why, for the example of Table 4, the Virtual Chief prediction could only be more accurate during the second half-orbit.

Error Analysis: Phase 2

If there were some way to define a new parameter space (other than chief orbit elements and relative initial conditions) in which we could easily specify that the deputy must remain relatively close to the virtual chief, then it may be possible to discover a restricted region of good accuracy for the Virtual Chief model. As a test, let us use the

deputy's ROEs, as seen from the virtual chief; that is, the ROEs we would use to describe the HCW motion of the deputy in the **o**-frame. These deputy **o**-frame ROEs represent a combination of the information in both the chief's orbit elements and the deputy's relative initial conditions.

Note that the *chief's* **o**-frame ROEs are always zero except for a_e and β. Note also that the deputy's $z_{\max}$ is the same for both the **o**-frame HCW model and for the **c**-frame Virtual Chief model.

For the sake of simplicity, let us hold constant the chief's orbit using the same conditions as Example III above (Table 3) and examine bounded, in-plane-only relative motion. Let us further restrict the deputy to **o**-frame motion centered about the virtual chief, so that the only ROEs which can be non-zero are a_e and β. As shown in Figure 14, these restrictions are equivalent to varying only the deputy's **c**-frame x_0 value, while constraining $\dot{y}_0$ to equal $-2n_C x_0$. In the figure, the various dots along the x-axis are some of the sampled deputy initial positions. Note that, under these restrictions, the chief is always at apogee at epoch. Likewise, the deputy is at apogee or perigee at epoch.

By varying the deputy's x_0 under these conditions, we are effectively varying its a_e. The ratio of the deputy's **o**-frame a_e to the chief's **o**-frame a_e gives an indication of the relative closeness of the deputy to the virtual chief, which we expect to improve the Virtual Chief modeling error. In Table 6 below, the index column simply represents this a_e ratio.

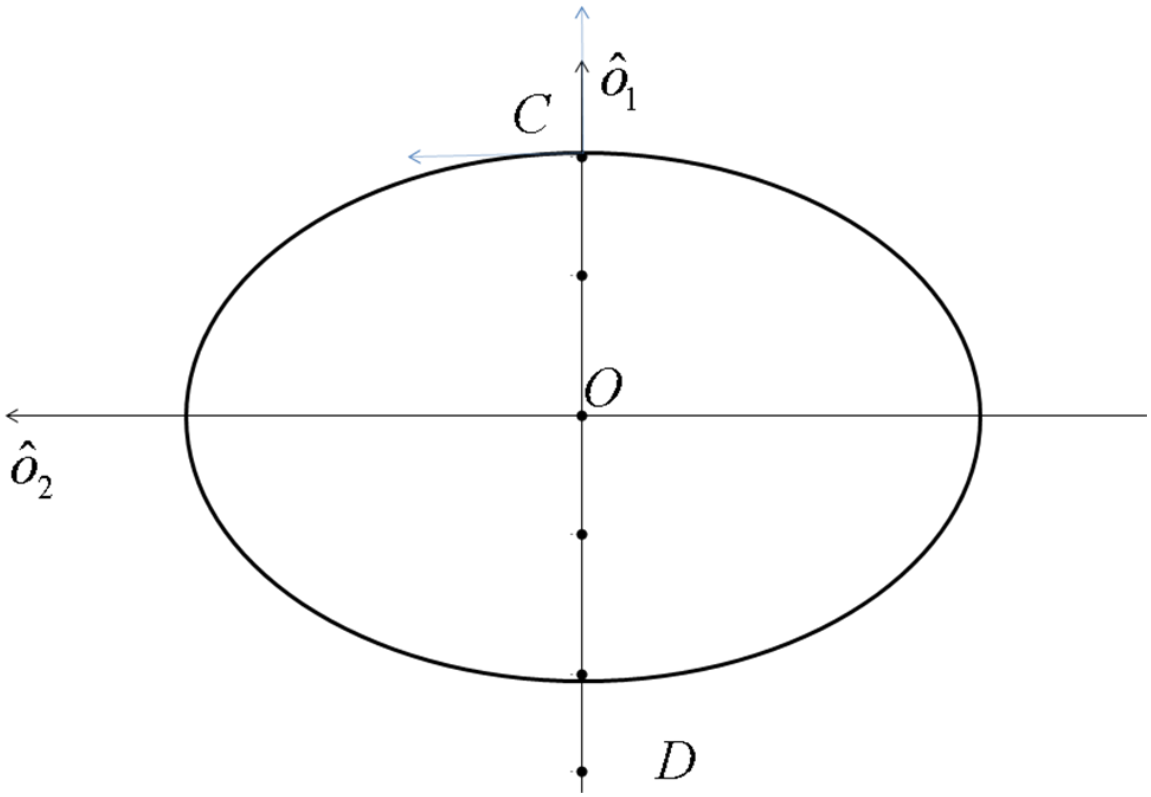

Figure 14. Phase 2 Geometry

Tables 6 give the simulation results for this phase of the study. All values are in meters, except for the index. The tables are organized by increasing index value. Note that when the index is zero, the deputy is co-located with the virtual chief. The other table entries occur in pairs; this is because the index will have the same value regardless of whether the deputy is at perigee or apogee.

Note that the Virtual Chief model performed with accuracy equal to or better than HCW for most of the cases in Table 6. These correspond to deputy **o**-frame a_e values both less than and greater than the chief's **o**-frame a_e; in other words, for deputy eccentricities both less than and greater than the chief's eccentricity. Since this one-dimensional search indicates a region of predictable accuracy for the Virtual Chief model,

we can begin to look for an analytical understanding of the modeling error by capturing the actual root mean square error values (the last two columns of Table 6).

Table 6. Phase 2 Results

x_0	Chief a_e	Deputy a_e	Index	VC rms error	HCW rms error
-8000	16000	0	0	90.76991438	450.51339369
-6000	16000	4000	0.25	85.00250365	354.74757485
-10000	16000	4000	0.25	85.22566297	535.01964956
-12000	16000	8000	0.5	68.35298262	608.25772993
-4000	16000	8000	0.5	67.94038372	247.73234487
-14000	16000	12000	0.75	40.13629411	670.22102227
-2000	16000	12000	0.75	39.60054922	129.47905476
0	16000	16000	1	0	0
-16000	16000	16000	1	0.182468635	720.12988348
2000	16000	20000	1.25	50.84427082	140.69177273
-18000	16000	20000	1.25	50.42206374	760.31085429
-20000	16000	24000	1.5	112.7794175	788.44127984
4000	16000	24000	1.5	112.9152819	292.58261425
6000	16000	28000	1.75	186.1960657	455.65838792
-22000	16000	28000	1.75	186.5534288	805.30781918
-24000	16000	32000	2	271.7596827	810.93090792
8000	16000	32000	2	270.6696696	629.90456028
16000	16000	48000	3	720.1537784	1438.2923102
-32000	16000	48000	3	727.2472372	722.05843779

Figures 15-18 illustrate the **c**-frame x-y plane trajectory predictions for four cases from Table 6. It is clear that HCW is always predicting bounded motion (repeating trajectories). The accuracy of the Virtual Chief prediction seems to depend, for these cases, on how well it captures the drift in the truth model. Figure 18 corresponds to the only case in Table 6 for which HCW showed superior accuracy.

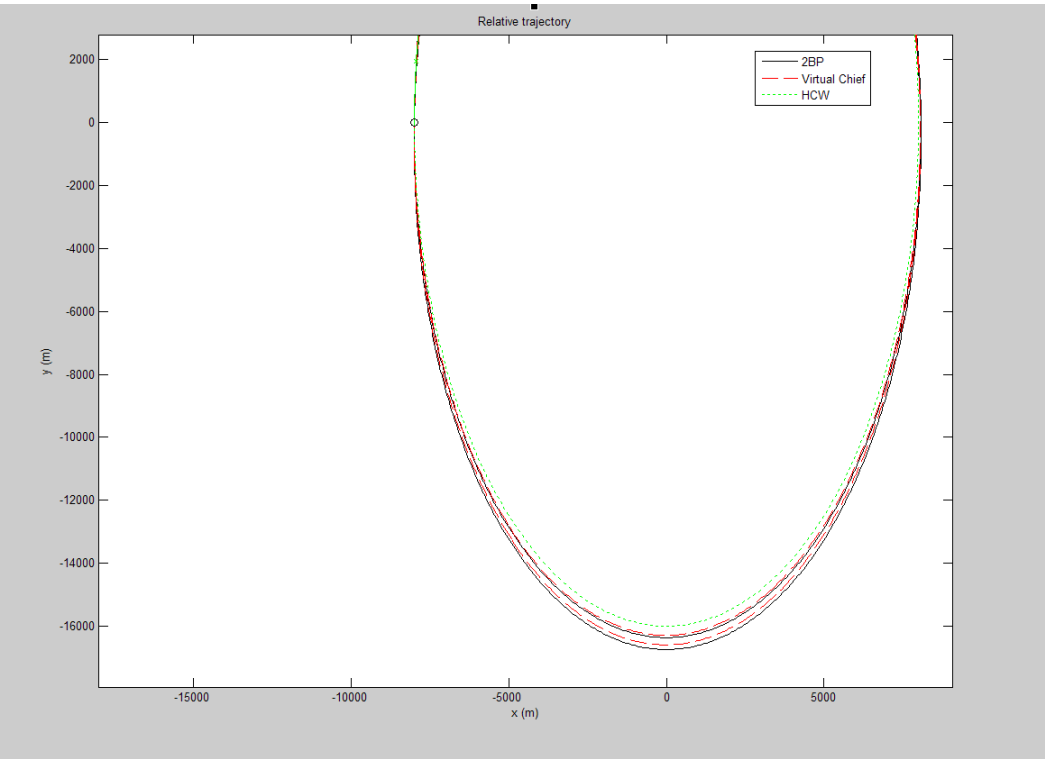

Figure 15. Index = 0

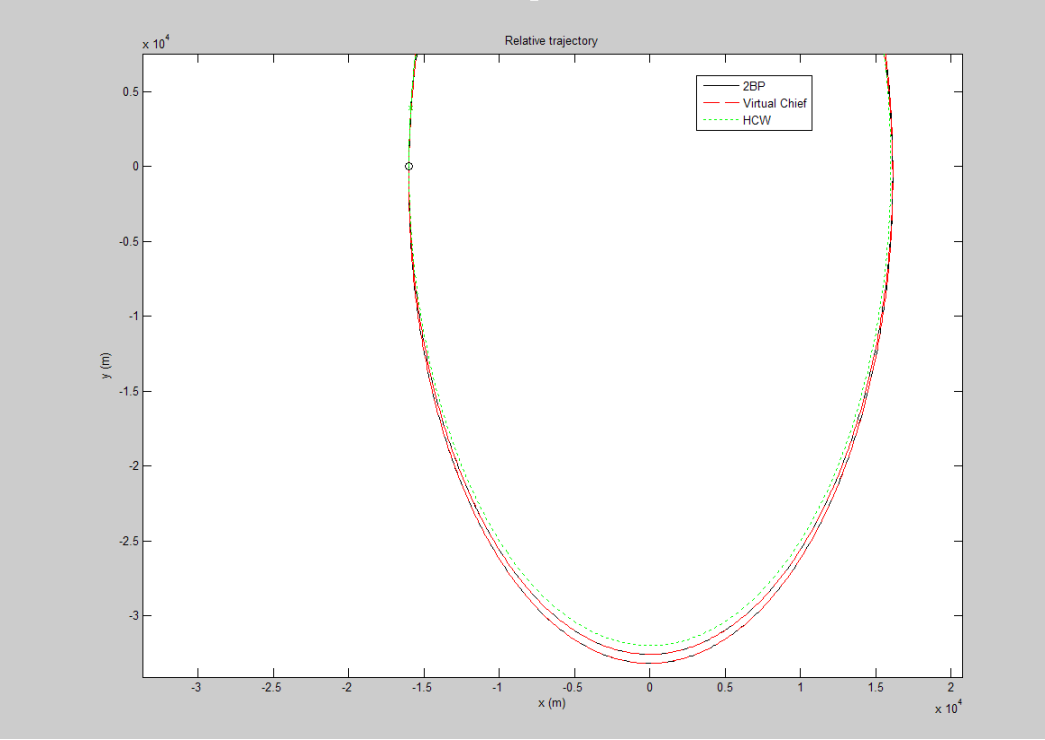

Figure 16. Index = 1

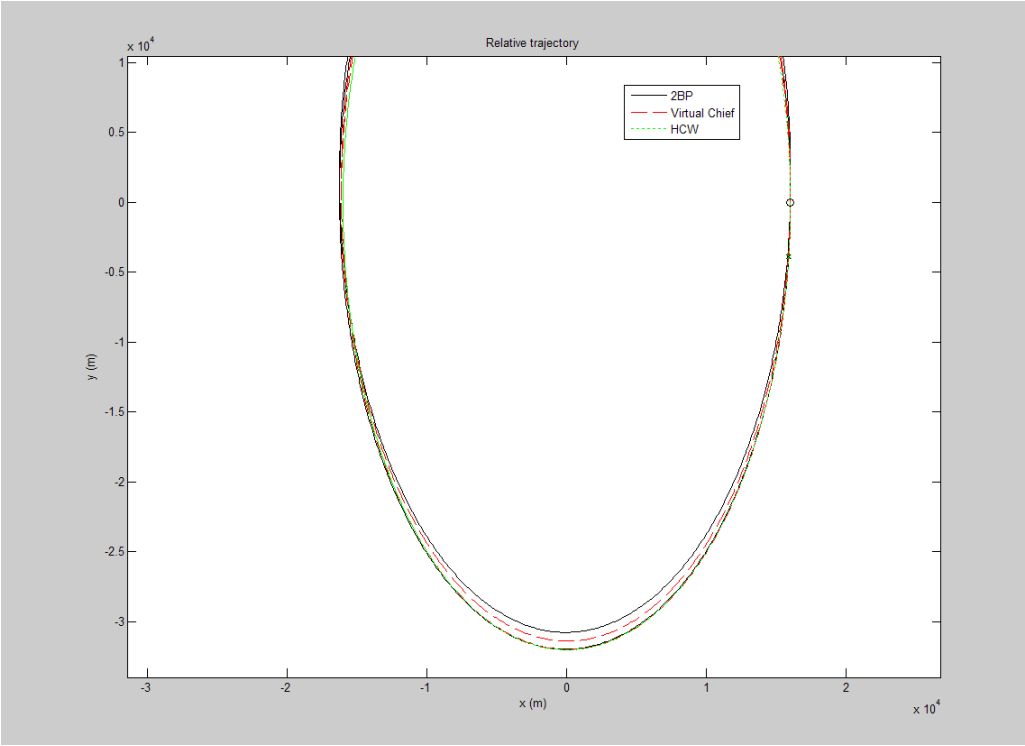

Figure 17. Index = 3 (x0 = 16 km)

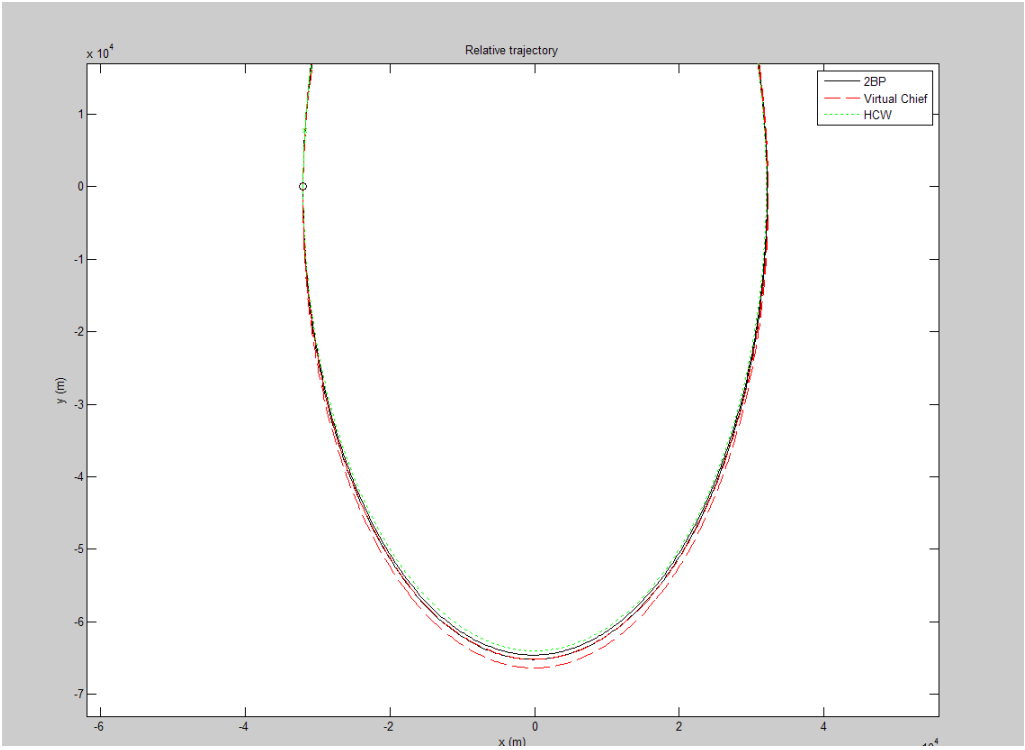

Figure 18. Index = 3 (x0 = -32 km)

We can also plot the root mean square error for each model against the deputy's **c**-frame x_0, as in Figure 19. Also depicted on the figure are analytic functions heuristically matched to the root mean square error data. For the cases in Phase 2, both the HCW error and the Virtual Chief error functions behave as a quadratic form:

$$\delta_{HCW} = 810 * abs\left(\left(\frac{x_0}{24000}+1\right)^2 - 1\right)$$

$$\delta_{VC} = 90 * abs\left(\left(\frac{x_0}{8000}+1\right)^2 - 1\right)$$

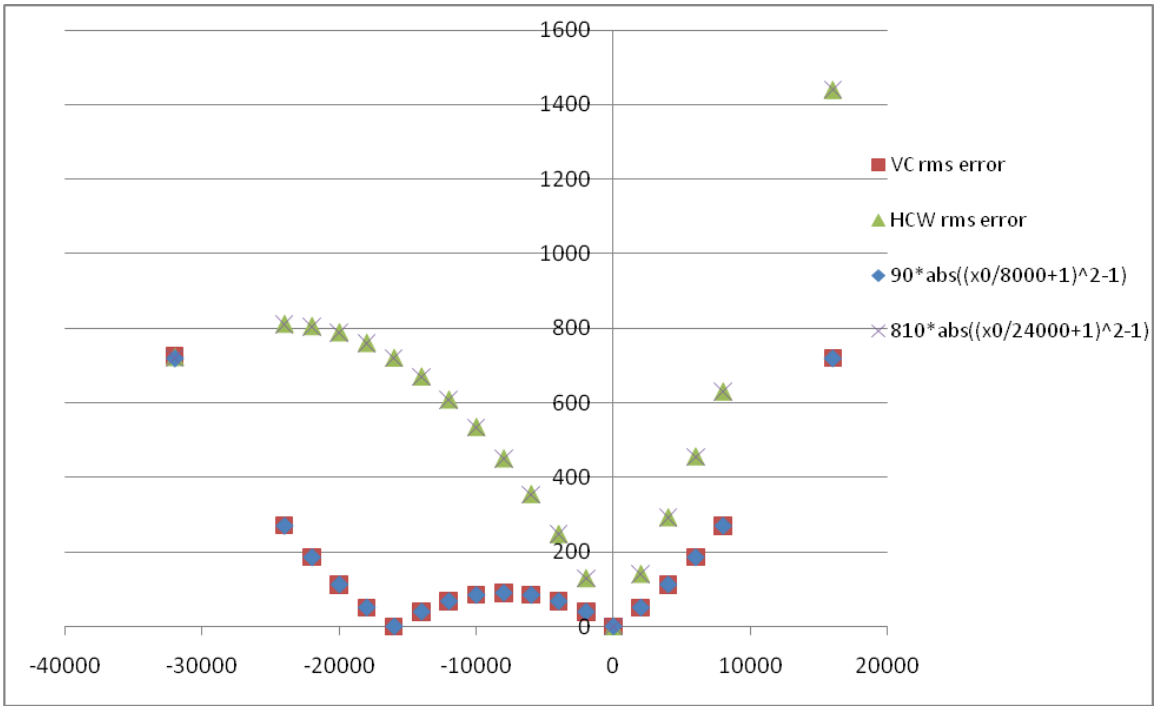

Figure 19. Phase 2 Error versus x0

Figure 20 shows a similar plot of the Virtual Chief error as a function of the Table 6 index value. Again, a heuristically derived quadratic function matches the error data:

$$\delta_{VC} = 90 * abs\left(index^2 - 1\right)$$

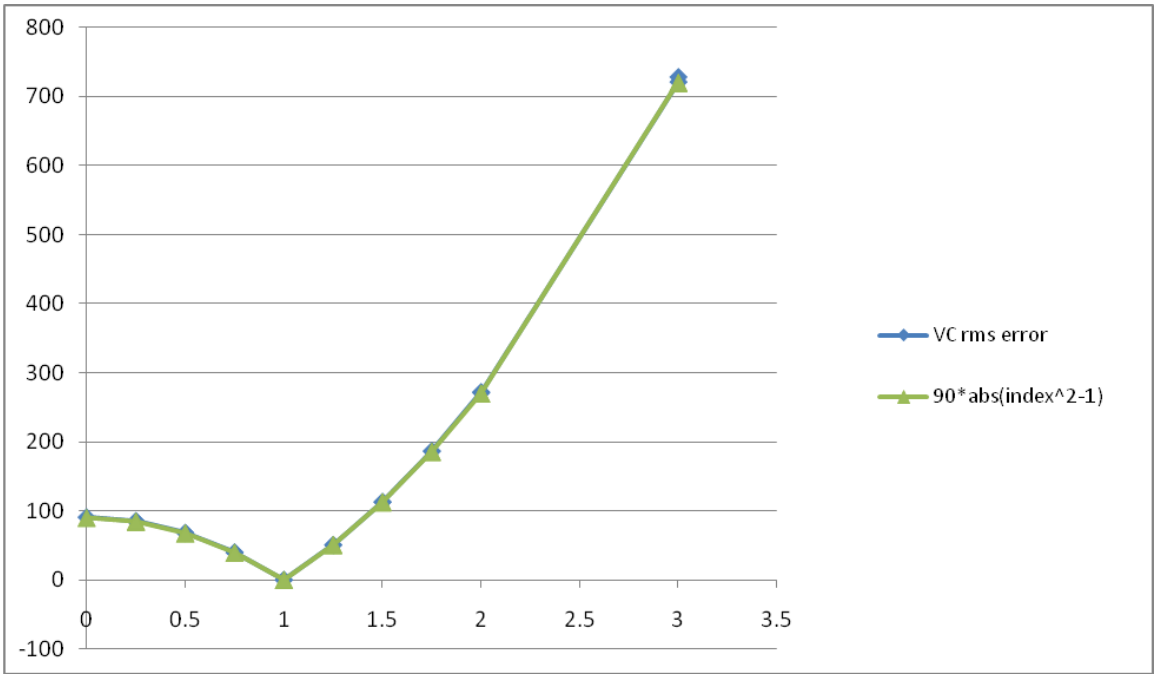

Figure 20. Phase 2 VC Error versus Index

One result from Phase 2 that is perhaps surprising is that δ_{VC} is not an increasing function of $\rho_D\left(t_0\right)$. Rather, the error is lowest when the a_e ratio is closest to unity. What we have achieved, though, is a region of predictable accuracy for the Virtual Chief model. It is clear from Figure 19 that, subject to the Phase 2 restrictions, for any value of x_0 greater than about -32,000 meters, the Virtual Chief root mean square error should be less than the HCW root mean square error.

Conclusions and Recommendations

Relative Orbit Elements constitute a useful realization of the HCW model for the circular chief problem. As we saw in Chapter III, they provide significant geometrical

insight into the relative motion. ROEs merit continued development to seek relative navigation techniques, autonomous maneuver planning algorithms, and other RPO applications.

The latter part of this study has developed an approximate relative satellite motion model for chief and deputy with slightly eccentric orbits. This model has a simple parameterization designed for a variety of applications, including autonomous RPO. The model achieves this simplicity at the risk of lower accuracy; in some cases, using the HCW model may be a better choice. In fact, in some cases, the new model tends to break down with increasing eccentricity.

The overarching goal was to find a simple parameterized model that provides geometrical insight and operational efficacy while predicting relative motion accurately at chief eccentricities higher than can the HCW model. Under the restrictions for the Phase 2 error analysis, this has been achieved for a predictable region. Further study is clearly indicated to expand this region of predictable accuracy. Specifically, we should search the deputy's **o**-frame ROE space under different cases, varying multiple parameters and characterizing the behavior of the root mean square error for both the Virtual Chief and the HCW models.

However, the broader goal of finding a simple model that is *generally* more accurate than HCW for elliptical orbits will have to be reached via a different approach. Any of the possible approaches listed at the beginning of Chapter IV remain open. With further study, these other options may prove a viable answer.

For example, the quadric surface of relative motion found by Jiang, et al. [45], might be adapted for drifting cases, so that the quadric surface's parameters are time-varying. Just as HCW predicts a drifting instantaneous ellipse, Lawden's equations may predict a drifting, oscillating instantaneous quadric surface.

Also, it may be possible to find geometrically meaningful parameters in a first-order, time-explicit approximate model, such as one derived from the first-order state transition matrix of Melton [66].

Alternatively, a linearized relative satellite motion model expressed in coordinates of a non-rotating rectangular reference frame, fixed to the chief and always parallel to the chief's perifocal frame, may prove to be simpler than existing LVLH-frame models.

We have already examined the fifth approach listed in Chapter IV, the Virtual Chief Method, in its linearized form. However, if a similar method were used to develop a quadratic model (second-order in the relative distances), the accuracy problems discovered in Chapter V would likely improve. This would be very close to the approach of Fasano and D'Errico [30]. However, this accuracy improvement would come at the expense of simplicity.

Appendix A: Identities

Common Trigonometric Identities

For convenience, the trigonometric identities used in this thesis are listed here:

$$\sin^2\alpha+\cos^2\alpha=1 \tag{A.1}$$

$$\sin(\alpha+\beta)=\cos\alpha\sin\beta+\sin\alpha\cos\beta \tag{A.2}$$

$$\sin\alpha=\sin\left(\pi-\alpha\right) \tag{A.3}$$

$$\cos\alpha=-\cos\left(\pi-\alpha\right) \tag{A.4}$$

$$\sin\left(-\alpha\right)=-\sin\alpha \tag{A.5}$$

$$\sin(\frac{\pi}{2}-\alpha)=\cos\alpha \tag{A.6}$$

$$\cos\alpha\cos\beta=\frac{1}{2}\left\{\cos\left(\alpha-\beta\right)+\cos\left(\alpha+\beta\right)\right\} \tag{A.7}$$

$$\sin\alpha\sin\beta=\frac{1}{2}\left\{\cos\left(\alpha-\beta\right)-\cos\left(\alpha+\beta\right)\right\} \tag{A.8}$$

$$\cos\alpha\sin\beta=\frac{1}{2}\left\{\sin\left(\alpha+\beta\right)-\sin\left(\alpha-\beta\right)\right\} \tag{A.9}$$

$$\sin\alpha\cos\beta = \frac{1}{2}\left\{\sin\left(\alpha+\beta\right)+\sin\left(\alpha-\beta\right)\right\} \tag{A.10}$$

$$\cos(\alpha+\beta) = \cos\alpha\cos\beta - \sin\alpha\sin\beta \tag{A.11}$$

$$\cos\left(\pi+\alpha\right) = -\cos\left(\alpha\right) \tag{A.12}$$

Identities for the atan2 Function

Similar identities for atan2, the quadrant-specific inverse tangent function, are less commonly found. The identities used in this thesis are listed below. They can often be understood graphically from right triangles and a unit circle, as shown in Figure 21.

$$atan2\left(-\beta,\alpha\right) = -atan2\left(\beta,\alpha\right) \tag{A.13}$$

$$atan2\left(\beta,-\alpha\right) = \pi - atan2\left(\beta,\alpha\right) \tag{A.14}$$

$$atan2\left(-\beta,-\alpha\right) = \pi + atan2\left(\beta,\alpha\right) \tag{A.15}$$

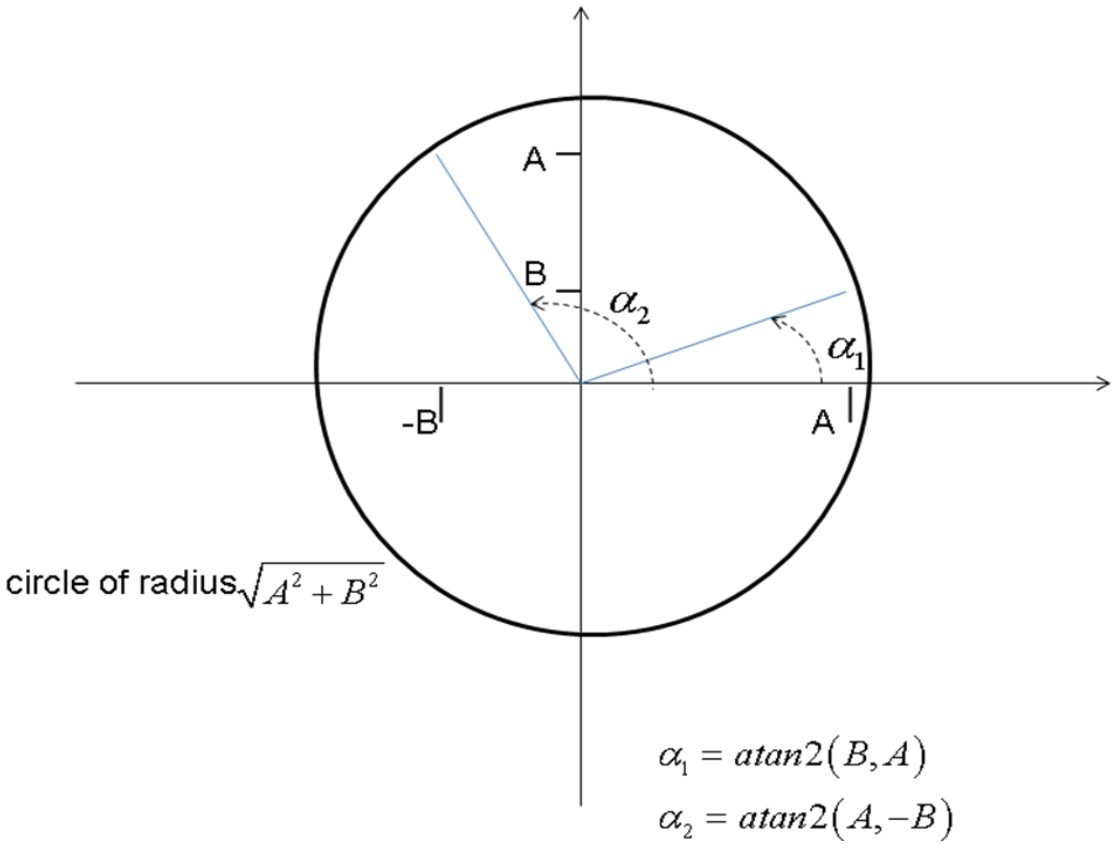

Figure 21. Eq. (A.16)

$$atan2(B,A) = atan2(A,-B) - \frac{\pi}{2} \tag{A.16}$$

Appendix B: Harmonic Addition Theorem

To deal with periodic terms in the trajectory equations, I used the principle stated in Eqs. (3.9) through (3.11) and repeated below, sometimes referred to as the Harmonic Addition Theorem [101]. A periodic function defined as

$$f(\theta) = A\sin\theta + B\cos\theta$$

can be equivalently written both as

$$f(\theta) = \sqrt{A^2 + B^2}\,\sin(\theta + atan2(B, A))$$

and as

$$f(\theta) = -\sqrt{A^2 + B^2}\,\cos(\theta + atan2(A, -B))$$

where atan2 is the quadrant-specific inverse tangent function.

The first step in deriving Eqs. (3.10) and (3.11) from Eq. (3.9) is to find the amplitude of the oscillation described by Eq. (3.9). Since Eq. (3.9) is written without an offset term, the oscillation is centered about zero, and the peak values of $f(\theta)$ will equal the amplitude. Each peak value is a local maximum where the derivative of $f(\theta)$ equals zero:

$$\dot{f}(\theta) = 0 = A\cos\theta - B\sin\theta$$

Rearranging,

$$A\cos\theta = B\sin\theta$$

Squaring both sides,

$$A^2\cos^2\theta = B^2\sin^2\theta \qquad \text{(B.1)}$$

Substituting the trigonometric identity in Eq. (A.1) into the right-hand side, Eq. (B.1) becomes

$$A^2\cos^2\theta = B^2 - B^2\cos^2\theta$$

Solving for the constant term,

$$B^2 = (A^2 + B^2)\cos^2\theta$$

Taking the square root,

$$B = \pm\sqrt{A^2 + B^2}\cos\theta$$

Rearranging,

$$\cos\theta = \frac{\pm B}{\sqrt{A^2 + B^2}} \tag{B.2}$$

Substituting the identity from Eq. (A.1) into the other side of Eq. (B.1) and then repeating the same steps as above yields the result

$$\sin\theta = \frac{\pm A}{\sqrt{A^2 + B^2}} \tag{B.3}$$

Eqs. (B.2) and (B.3) define the extrema of $f(\theta)$. If we choose the positive value from each, choose $\theta_{\max^+}$ as the corresponding value of θ, and substitute into Eq. (3.9), we can then write

$$f(\theta_{\max^+}) = A\left(\frac{A}{\sqrt{A^2 + B^2}}\right) + B\left(\frac{B}{\sqrt{A^2 + B^2}}\right)$$

where $f(\theta_{\max^+})$ represents the peak value, the amplitude we have been seeking. Simplifying,

$$f(\theta_{\max^+}) = \frac{A^2 + B^2}{\sqrt{A^2 + B^2}} = \sqrt{A^2 + B^2}$$

Now that we know the amplitude of $f(\theta)$, we can convert Eq. (3.9) into a single sinusoidal term by factoring out the amplitude:

$$f(\theta) = \sqrt{A^2 + B^2} \left\{ \frac{A}{\sqrt{A^2 + B^2}} \sin\theta + \frac{B}{\sqrt{A^2 + B^2}} \cos\theta \right\} \tag{B.4}$$

The coefficients inside the braces suggest a right triangle with legs of length A and B. Its hypotenuse would have length $\sqrt{A^2 + B^2}$. One of this triangle's angles would have a cosine equal to $\frac{A}{\sqrt{A^2 + B^2}}$, a sine equal to $\frac{B}{\sqrt{A^2 + B^2}}$, and a tangent equal to $\frac{B}{A}$. If we identify this angle as $atan2(B, A)$, then we can write Eq. (B.4) as

$$f(\theta) = \sqrt{A^2 + B^2} \left\{ \cos(atan2(B, A)) \sin\theta + \sin(atan2(B, A)) \cos\theta \right\} \tag{B.5}$$

Using the trigonometric identity from Eq. (A.2), this becomes

$$f(\theta) = \sqrt{A^2 + B^2} \sin(\theta + atan2(B, A))$$

which is Eq. (3.10).

Next, we can substitute Eq. (A.16) into Eq. (3.10), yielding

$$f(\theta) = \sqrt{A^2 + B^2} \sin(\theta + atan2(A, -B) - \frac{\pi}{2}) \tag{B.6}$$

If we apply the trigonometric identities from Eqs. (A.5) and (A.6), Eq. (B.6) becomes

$$f(\theta) = -\sqrt{A^2 + B^2}\cos\left(\theta + atan2(A, -B)\right)$$

which is Eq. (3.11).

Both of these forms, Eqs. (3.10) and (3.11), are periodic functions whose amplitude ($\sqrt{A^2 + B^2}$), initial phase ($atan2(B, A)$ or $atan2(A, -B)$), and time-varying phase parameter (θ) are all readily apparent.

Appendix C: An Ellipse Oriented Arbitrarily in Three Dimensions

In general, to define a curve or trajectory in 3-D space requires at least two equations. If the curve is an ellipse, then we can define a principal-axis reference frame with unit vectors $\hat{u}$, $\hat{v}$, and $\hat{w}$. In this frame, $\hat{u}$ and $\hat{v}$ are aligned with the ellipse's major and minor axes (although it is not yet necessary to specify which is which), and $\hat{w}$ is normal to the plane containing the ellipse.

Let position with respect to the ellipse center be defined by a vector with principal-axis frame coordinates x', y', and z':

$$\vec{r}_{D/EC} = x'\hat{u} + y'\hat{v} + z'\hat{w}$$

Then the two equations necessary to define the ellipse are

$$z' = 0$$
$$\frac{x'^2}{a^2} + \frac{y'^2}{b^2} = 1$$

Or, writing the system parametrically,

$$x' = a\cos\theta$$
$$y' = b\sin\theta$$

where a and b are the semi-major and semi-minor axis lengths and θ is a phase parameter.

Now let us allow the center of the ellipse to translate from the origin of the principal-axis frame to some point C whose principal-axis coordinates are

$$C = \begin{bmatrix} C_{x'} \\ C_{y'} \\ C_{z'} \end{bmatrix}$$

The form of the elliptical trajectory is therefore

$$\begin{bmatrix} x' \\ y' \\ z' \end{bmatrix} = \begin{bmatrix} a\cos\theta + C_{x'} \\ b\sin\theta + C_{y'} \\ C_{z'} \end{bmatrix}$$

In order to express this trajectory in arbitrary coordinates x, y, and z, we must construct a rotation matrix by writing the unit basis vectors of the principal-axis frame ($\hat{u}$, $\hat{v}$, and $\hat{w}$) in terms of their x-, y-, and z-coordinates. The system will then be

$$\begin{bmatrix} x \\ y \\ z \end{bmatrix} = \begin{bmatrix} \hat{u} \mid \hat{v} \mid \hat{w} \end{bmatrix} \begin{bmatrix} x' \\ y' \\ z' \end{bmatrix}$$

Let x-, y-, and z-coordinate values be specified by subscripts. Then the parametric equations of an elliptical trajectory in an arbitrary 3-D reference frame are

$$\begin{aligned} x(t) &= au_x \cos\theta + bv_x \sin\theta + C_x \\ y(t) &= au_y \cos\theta + bv_y \sin\theta + C_y \\ z(t) &= au_z \cos\theta + bv_z \sin\theta + C_z \end{aligned}$$

Any trajectory equations which satisfy this form must therefore describe an ellipse.

Appendix D: Two-body Orbit Properties

The following properties of Earth satellite orbits under the two-body assumption can be found in most astrodynamics texts. They are listed here for convenience, as well as to express them in notation consistent with this thesis.

The period P of an orbit is related to the Earth's gravitational parameter μ and the orbit's semi-major axis a as:

$$P = 2\pi\sqrt{\frac{a^3}{\mu}} \tag{D.1}$$

A satellite's orbit radius, or its distance from the Earth's center, at time t is $r(t)$. It can be found from the orbit's semi-major axis, the orbit's eccentricity e, and the satellite's true anomaly $\nu(t)$ as:

$$r(t) = \frac{a\left(1-e^2\right)}{1+e\cos\nu(t)} \tag{D.2}$$

A satellite's mean anomaly $M(t)$ is defined in terms of its mean motion n and time of perigee passage t_p as:

$$M(t) = n\left(t-t_p\right) \tag{D.3}$$

Kepler's equation: a satellite's mean anomaly is related to its eccentric anomaly $E(t)$ as:

$$M(t) = E(t) - e\sin E(t) \tag{D.4}$$

Eccentric anomaly is related to true anomaly as:

$$\nu(t) = 2atan2\left[\sqrt{\frac{1+e}{1-e}}\sin\frac{E(t)}{2}, \cos\frac{E(t)}{2}\right] \tag{D.5}$$

A satellite's orbit radius at perigee, r_p, is found as:

$$r_p = a(1-e) \tag{D.6}$$

The semilatus rectum p of a satellite's orbit is found as:

$$p = a\left(1-e^2\right) \tag{D.7}$$

The angular rate $\dot{\nu}(t)$ of a satellite's orbit is found as:

$$\begin{aligned}\dot{\nu}(t) &= \frac{na^2}{\left[r(t)\right]^2}\sqrt{1-e^2} \\ &= \frac{na^2}{a^2\left(1-e^2\right)^2}\sqrt{1-e^2}\left(1+e\cos\left[\nu(t)\right]\right)^2 \\ &= n\left(1-e^2\right)^{-3/2}\left(1+e\cos\left[\nu(t)\right]\right)^2\end{aligned} \tag{D.8}$$

The angular momentum h of a satellite's orbit is found as:

$$h = \sqrt{\mu p} \tag{D.9}$$

It is also true that

$$h = \left[r(t) \right]^2 \dot{\nu}(t) \tag{D.10}$$

Combining Eqs. (D.9) and (D.10), and then using Eqs. (D.2), (D.7), and (D.8),

$$\begin{aligned} \sqrt{\frac{p}{\mu}} &= \frac{\dot{\nu}(t)}{\mu} \left[r(t) \right]^2 \\ &= \frac{\sqrt{1-e^2}}{na} \end{aligned} \tag{D.11}$$

Kepler's equation (Eq. (D.4)) may be replaced by a Fourier-Bessel series expansion of the true anomaly [6], written as:

$$\begin{aligned} \nu_C(t) &= M_C(t) \\ &+2\sum_{k=1}^{\infty} \frac{1}{k} \left\{ \sum_{n=-\infty}^{\infty} \left[\sum_{j=0}^{\infty} (-1)^j \frac{\left(-\frac{1}{2} k e_C \right)^{n+2j}}{j!(n+j)!} \right] \left[\frac{1-\sqrt{1-e_C^{\,2}}}{e_C} \right]^{|k+n|} \right\} \sin\left(k M_C(t) \right) \end{aligned} \tag{D.12}$$

A satellite's mean motion is

$$n = \frac{2\pi}{P} = \sqrt{\frac{\mu}{a^3}}$$

Appendix E: Elements of the Virtual Chief State Transition Matrix

The sixteen in-plane elements of the state transition matrix in Eq. (4.36) are as follows:

$$
\begin{aligned}
\Phi_{11} = {} & \cos\left[\nu_C(t) - M_C(t)\right]\left[-3\cos\left[n_C(t-t_0)\right]+4\right]\cos\left[\nu_{C,0} - M_{C,0}\right] \\
& + \sin\left[\nu_C(t) - M_C(t)\right]\left\{\begin{array}{l}\left[6\sin\left[n_C(t-t_0)\right] - 6n_C(t-t_0)\right]\cos\left[\nu_{C,0} - M_{C,0}\right] \\ +\sin\left[\nu_{C,0} - M_{C,0}\right]\end{array}\right\} \\
& + \left(\dot{\nu}_{C,0} - n_C\right)\left\{\begin{array}{l}\cos\left[\nu_C(t) - M_C(t)\right]\left\{\begin{array}{l} -\dfrac{\sin\left[n_C(t-t_0)\right]}{n_C}\sin\left[\nu_{C,0} - M_{C,0}\right] \\ +\left\{-\dfrac{2\cos\left[n_C(t-t_0)\right]}{n_C} + \dfrac{2}{n_C}\right\}\cos\left[\nu_{C,0} - M_{C,0}\right]\end{array}\right\} \\ +\sin\left[\nu_C(t) - M_C(t)\right]\left\{\begin{array}{l} -\left\{\dfrac{2\cos\left[n_C(t-t_0)\right]}{n_C} - \dfrac{2}{n_C}\right\}\sin\left[\nu_{C,0} - M_{C,0}\right] \\ +\left\{\dfrac{4\sin\left[n_C(t-t_0)\right]}{n_C} - 3t\right\}\cos\left[\nu_{C,0} - M_{C,0}\right]\end{array}\right\}\end{array}\right\}
\end{aligned}
$$

$$\Phi_{12} = -\cos\left[\nu_C(t) - M_C(t)\right]\left[-3\cos\left[n_C(t-t_0)\right]+4\right]\sin\left[\nu_{C,0} - M_{C,0}\right]$$
$$+\sin\left[\nu_C(t) - M_C(t)\right]\begin{Bmatrix}-\left[6\sin\left[n_C(t-t_0)\right]-6n_C(t-t_0)\right]\sin\left[\nu_{C,0} - M_{C,0}\right]\\ +\cos\left[\nu_{C,0} - M_{C,0}\right]\end{Bmatrix}$$
$$-\left(\dot{\nu}_{C,0} - n_C\right)\begin{Bmatrix}\cos\left[\nu_C(t) - M_C(t)\right]\begin{Bmatrix}\dfrac{\sin\left[n_C(t-t_0)\right]}{n_C}\cos\left[\nu_{C,0} - M_{C,0}\right]\\ +\left\{-\dfrac{2\cos\left[n_C(t-t_0)\right]}{n_C}+\dfrac{2}{n_C}\right\}\sin\left[\nu_{C,0} - M_{C,0}\right]\end{Bmatrix}\\ +\sin\left[\nu_C(t) - M_C(t)\right]\begin{Bmatrix}\left\{\dfrac{2\cos\left[n_C(t-t_0)\right]}{n_C}-\dfrac{2}{n_C}\right\}\cos\left[\nu_{C,0} - M_{C,0}\right]\\ +\left\{\dfrac{4\sin\left[n_C(t-t_0)\right]}{n_C}\\ -3(t-t_0)\end{Bmatrix}\end{Bmatrix}$$

$$\Phi_{14} = \cos\left[\nu_C(t) - M_C(t)\right]\begin{Bmatrix}\dfrac{\sin\left[n_C(t-t_0)\right]}{n_C}\cos\left[\nu_{C,0} - M_{C,0}\right]\\ +\left[-\dfrac{2\cos\left[n_C(t-t_0)\right]}{n_C}+\dfrac{2}{n_C}\right]\sin\left[\nu_{C,0} - M_{C,0}\right]\end{Bmatrix}$$
$$+\sin\left[\nu_C(t) - M_C(t)\right]\begin{Bmatrix}\left[\dfrac{2\cos\left[n_C(t-t_0)\right]}{n_C}-\dfrac{2}{n_C}\right]\cos\left[\nu_{C,0} - M_{C,0}\right]\\ +\left[\dfrac{4\sin\left[n_C(t-t_0)\right]}{n_C}-3(t-t_0)\right]\sin\left[\nu_{C,0} - M_{C,0}\right]\end{Bmatrix}$$

$$\Phi_{15} = \cos\left[\nu_C(t) - M_C(t)\right]\begin{Bmatrix}-\dfrac{\sin\left[n_C(t-t_0)\right]}{n_C}\sin\left[\nu_{C,0} - M_{C,0}\right]\\ +\left[-\dfrac{2\cos\left[n_C(t-t_0)\right]}{n_C}+\dfrac{2}{n_C}\right]\cos\left[\nu_{C,0} - M_{C,0}\right]\end{Bmatrix}$$
$$+\sin\left[\nu_C(t) - M_C(t)\right]\begin{Bmatrix}-\left[\dfrac{2\cos\left[n_C(t-t_0)\right]}{n_C}-\dfrac{2}{n_C}\right]\sin\left[\nu_{C,0} - M_{C,0}\right]\\ +\left[\dfrac{4\sin\left[n_C(t-t_0)\right]}{n_C}-3(t-t_0)\right]\cos\left[\nu_{C,0} - M_{C,0}\right]\end{Bmatrix}$$

$$
\begin{aligned}
\Phi_{21} = & -\sin\left[\nu_C(t) - M_C(t)\right]\left[-3\cos\left[n_C(t-t_0)\right]+4\right]\cos\left[\nu_{C,0} - M_{C,0}\right] \\
& +\cos\left[\nu_C(t) - M_C(t)\right]\left\{\begin{array}{l}\left[6\sin\left[n_C(t-t_0)\right] - 6n_C(t-t_0)\right]\cos\left[\nu_{C,0} - M_{C,0}\right] \\ +\sin\left[\nu_{C,0} - M_{C,0}\right]\end{array}\right\} \\
& +\left(\dot{\nu}_{C,0} - n_C\right)\left\{\begin{array}{l} -\sin\left[\nu_C(t) - M_C(t)\right]\left\{\begin{array}{l} -\dfrac{\sin\left[n_C(t-t_0)\right]}{n_C}\sin\left[\nu_{C,0} - M_{C,0}\right] \\ +\left[-\dfrac{2\cos\left[n_C(t-t_0)\right]}{n_C} + \dfrac{2}{n_C}\right]\cos\left[\nu_{C,0} - M_{C,0}\right]\end{array}\right\} \\ +\cos\left[\nu_C(t) - M_C(t)\right]\left\{\begin{array}{l} -\left[\dfrac{2\cos\left[n_C(t-t_0)\right]}{n_C} - \dfrac{2}{n_C}\right]\sin\left[\nu_{C,0} - M_{C,0}\right] \\ +\left[\dfrac{4\sin\left[n_C(t-t_0)\right]}{n_C} \right]\cos\left[\nu_{C,0} - M_{C,0}\right] \\ \left[-3(t-t_0)\right]\end{array}\right\}\end{array}\right\}
\end{aligned}
$$

$$
\begin{aligned}
\Phi_{22} = & \sin\left[\nu_C(t) - M_C(t)\right]\left[-3\cos\left[n_C(t-t_0)\right]+4\right]\sin\left[\nu_{C,0} - M_{C,0}\right] \\
& +\cos\left[\nu_C(t) - M_C(t)\right]\left\{\begin{array}{l}-\left[6\sin\left[n_C(t-t_0)\right] - 6n_C(t-t_0)\right]\sin\left[\nu_{C,0} - M_{C,0}\right] \\ +\cos\left[\nu_{C,0} - M_{C,0}\right]\end{array}\right\} \\
& +\left(\dot{\nu}_{C,0} - n_C\right)\left\{\begin{array}{l} \sin\left[\nu_C(t) - M_C(t)\right]\left\{\begin{array}{l} \dfrac{\sin\left[n_C(t-t_0)\right]}{n_C}\cos\left[\nu_{C,0} - M_{C,0}\right] \\ +\left[-\dfrac{2\cos\left[n_C(t-t_0)\right]}{n_C} + \dfrac{2}{n_C}\right]\sin\left[\nu_{C,0} - M_{C,0}\right]\end{array}\right\} \\ -\cos\left[\nu_C(t) - M_C(t)\right]\left\{\begin{array}{l} \left[\dfrac{2\cos\left[n_C(t-t_0)\right]}{n_C} - \dfrac{2}{n_C}\right]\cos\left[\nu_{C,0} - M_{C,0}\right] \\ +\left[\dfrac{4\sin\left[n_C(t-t_0)\right]}{n_C} \right]\sin\left[\nu_{C,0} - M_{C,0}\right] \\ \left[-3(t-t_0)\right]\end{array}\right\}\end{array}\right\}
\end{aligned}
$$

$$\Phi_{24} = -\sin\left[\nu_C(t) - M_C(t)\right]\left\{\begin{array}{l}\dfrac{\sin\left[n_C(t-t_0)\right]}{n_C}\cos\left[\nu_{C,0} - M_{C,0}\right] \\ +\left[-\dfrac{2\cos\left[n_C(t-t_0)\right]}{n_C} + \dfrac{2}{n_C}\right]\sin\left[\nu_{C,0} - M_{C,0}\right]\end{array}\right\}$$

$$+\cos\left[\nu_C(t) - M_C(t)\right]\left\{\begin{array}{l}\left[\dfrac{2\cos\left[n_C(t-t_0)\right]}{n_C} - \dfrac{2}{n_C}\right]\cos\left[\nu_{C,0} - M_{C,0}\right] \\ +\left[\dfrac{4\sin\left[n_C(t-t_0)\right]}{n_C} - 3(t-t_0)\right]\sin\left[\nu_{C,0} - M_{C,0}\right]\end{array}\right\}$$

$$\Phi_{25} = -\sin\left[\nu_C(t) - M_C(t)\right]\left\{\begin{array}{l}-\dfrac{\sin\left[n_C(t-t_0)\right]}{n_C}\sin\left[\nu_{C,0} - M_{C,0}\right] \\ +\left[-\dfrac{2\cos\left[n_C(t-t_0)\right]}{n_C} + \dfrac{2}{n_C}\right]\cos\left[\nu_{C,0} - M_{C,0}\right]\end{array}\right\}$$

$$+\cos\left[\nu_C(t) - M_C(t)\right]\left\{\begin{array}{l}-\left[\dfrac{2\cos\left[n_C(t-t_0)\right]}{n_C} - \dfrac{2}{n_C}\right]\sin\left[\nu_{C,0} - M_{C,0}\right] \\ +\left[\dfrac{4\sin\left[n_C(t-t_0)\right]}{n_C} - 3(t-t_0)\right]\cos\left[\nu_{C,0} - M_{C,0}\right]\end{array}\right\}$$

$$
\begin{aligned}
\Phi_{41} &= \cos\left[\nu_C(t) - M_C(t)\right]\left[3n_C \sin\left[n_C(t-t_0)\right]\right]\cos\left[\nu_{C,0} - M_{C,0}\right] \\
&\quad + \sin\left[\nu_C(t) - M_C(t)\right]\left[6n_C \cos\left[n_C(t-t_0)\right] - 6n_C\right]\cos\left[\nu_{C,0} - M_{C,0}\right] \\
&\quad + \left(\dot{\nu}_{C,0} - n_C\right)\left\{\begin{array}{l}\cos\left[\nu_C(t) - M_C(t)\right]\left\{\begin{array}{l}-\cos\left[n_C(t-t_0)\right]\sin\left[\nu_{C,0} - M_{C,0}\right] \\ +2\sin\left[n_C(t-t_0)\right]\cos\left[\nu_{C,0} - M_{C,0}\right]\end{array}\right\} \\ +\sin\left[\nu_C(t) - M_C(t)\right]\left\{\begin{array}{l}2\sin\left[n_C(t-t_0)\right]\sin\left[\nu_{C,0} - M_{C,0}\right] \\ +\left[4\cos\left[n_C(t-t_0)\right] - 3\right]\cos\left[\nu_{C,0} - M_{C,0}\right]\end{array}\right\}\end{array}\right\} \\
&\quad - \left(\dot{\nu}_C(t) - n_C\right)\sin\left[\nu_C(t) - M_C(t)\right]\left[-3\cos\left[n_C(t-t_0)\right] + 4\right]\cos\left[\nu_{C,0} - M_{C,0}\right] \\
&\quad + \left(\dot{\nu}_C(t) - n_C\right)\cos\left[\nu_C(t) - M_C(t)\right]\left\{\begin{array}{l}\left[6\sin\left[n_C(t-t_0)\right] - 6n_C(t-t_0)\right]\cos\left[\nu_{C,0} - M_{C,0}\right] \\ +\sin\left[\nu_{C,0} - M_{C,0}\right]\end{array}\right\} \\
&\quad + \left(\dot{\nu}_C(t) - n_C\right)\left(\dot{\nu}_{C,0} - n_C\right)\left\{\begin{array}{l}-\sin\left[\nu_C(t) - M_C(t)\right]\left\{\begin{array}{l}-\dfrac{\sin\left[n_C(t-t_0)\right]}{n_C}\sin\left[\nu_{C,0} - M_{C,0}\right] \\ +\left[-\dfrac{2\cos\left[n_C(t-t_0)\right]}{n_C} + \dfrac{2}{n_C}\right]\cos\left[\nu_{C,0} - M_{C,0}\right]\end{array}\right\} \\ +\cos\left[\nu_C(t) - M_C(t)\right]\left\{\begin{array}{l}-\left[\dfrac{2\cos\left[n_C(t-t_0)\right]}{n_C} - \dfrac{2}{n_C}\right]\sin\left[\nu_{C,0} - M_{C,0}\right] \\ +\left[\begin{array}{l}\dfrac{4\sin\left[n_C(t-t_0)\right]}{n_C} \\ -3(t-t_0)\end{array}\right]\cos\left[\nu_{C,0} - M_{C,0}\right]\end{array}\right\}\end{array}\right\}
\end{aligned}
$$

$$
\begin{aligned}
\Phi_{42} = & -\cos\left[\nu_C(t) - M_C(t)\right]\left[3n_C \sin\left[n_C(t-t_0)\right]\right]\sin\left[\nu_{C,0} - M_{C,0}\right] \\
& -\sin\left[\nu_C(t) - M_C(t)\right]\left[6n_C \cos\left[n_C(t-t_0)\right] - 6n_C\right]\sin\left[\nu_{C,0} - M_{C,0}\right] \\
& -\left(\dot{\nu}_{C,0} - n_C\right)\left\{\begin{array}{l}
\cos\left[\nu_C(t) - M_C(t)\right]\left\{\begin{array}{l}\cos\left[n_C(t-t_0)\right]\cos\left[\nu_{C,0} - M_{C,0}\right] \\ +2\sin\left[n_C(t-t_0)\right]\sin\left[\nu_{C,0} - M_{C,0}\right]\end{array}\right\} \\
+\sin\left[\nu_C(t) - M_C(t)\right]\left\{\begin{array}{l}-2\sin\left[n_C(t-t_0)\right]\cos\left[\nu_{C,0} - M_{C,0}\right] \\ +\left[4\cos\left[n_C(t-t_0)\right] - 3\right]\sin\left[\nu_{C,0} - M_{C,0}\right]\end{array}\right\}
\end{array}\right\} \\
& +\left(\dot{\nu}_C(t) - n_C\right)\left\{\begin{array}{l}
\sin\left[\nu_C(t) - M_C(t)\right]\left[-3\cos\left[n_C(t-t_0)\right] + 4\right]\sin\left[\nu_{C,0} - M_{C,0}\right] \\
+\cos\left[\nu_C(t) - M_C(t)\right]\left\{\begin{array}{l}-\left[6\sin\left[n_C(t-t_0)\right] - 6n_C(t-t_0)\right]\sin\left[\nu_{C,0} - M_{C,0}\right] \\ +\cos\left[\nu_{C,0} - M_{C,0}\right]\end{array}\right\}
\end{array}\right\} \\
& -\left(\dot{\nu}_C(t) - n_C\right)\left(\dot{\nu}_{C,0} - n_C\right)\left\{\begin{array}{l}
-\sin\left[\nu_C(t) - M_C(t)\right]\left\{\begin{array}{l}\dfrac{\sin\left[n_C(t-t_0)\right]}{n_C}\cos\left[\nu_{C,0} - M_{C,0}\right] \\ +\left[-\dfrac{2\cos\left[n_C(t-t_0)\right]}{n_C} + \dfrac{2}{n_C}\right]\sin\left[\nu_{C,0} - M_{C,0}\right]\end{array}\right\} \\
+\cos\left[\nu_C(t) - M_C(t)\right]\left\{\begin{array}{l}\left[\dfrac{2\cos\left[n_C(t-t_0)\right]}{n_C} - \dfrac{2}{n_C}\right]\cos\left[\nu_{C,0} - M_{C,0}\right] \\ +\left[\begin{array}{l}\dfrac{4\sin\left[n_C(t-t_0)\right]}{n_C} \\ -3(t-t_0)\end{array}\right]\sin\left[\nu_{C,0} - M_{C,0}\right]\end{array}\right\}
\end{array}\right\}
\end{aligned}
$$

$$
\begin{aligned}
\Phi_{44} = & \cos\left[\nu_C(t) - M_C(t)\right]\left\{\cos\left[n_C(t-t_0)\right]\cos\left[\nu_{C,0} - M_{C,0}\right] + 2\sin\left[n_C(t-t_0)\right]\sin\left[\nu_{C,0} - M_{C,0}\right]\right\} \\
& +\sin\left[\nu_C(t) - M_C(t)\right]\left\{\begin{array}{l}-2\sin\left[n_C(t-t_0)\right]\cos\left[\nu_{C,0} - M_{C,0}\right] \\ +\left[4\cos\left[n_C(t-t_0)\right] - 3\right]\sin\left[\nu_{C,0} - M_{C,0}\right]\end{array}\right\} \\
& +\left(\dot{\nu}_C(t) - n_C\right)\left\{\begin{array}{l}
-\sin\left[\nu_C(t) - M_C(t)\right]\left\{\begin{array}{l}\dfrac{\sin\left[n_C(t-t_0)\right]}{n_C}\cos\left[\nu_{C,0} - M_{C,0}\right] \\ +\left[-\dfrac{2\cos\left[n_C(t-t_0)\right]}{n_C} + \dfrac{2}{n_C}\right]\sin\left[\nu_{C,0} - M_{C,0}\right]\end{array}\right\} \\
+\cos\left[\nu_C(t) - M_C(t)\right]\left\{\begin{array}{l}\left[\dfrac{2\cos\left[n_C(t-t_0)\right]}{n_C} - \dfrac{2}{n_C}\right]\cos\left[\nu_{C,0} - M_{C,0}\right] \\ +\left[\dfrac{4\sin\left[n_C(t-t_0)\right]}{n_C} - 3(t-t_0)\right]\sin\left[\nu_{C,0} - M_{C,0}\right]\end{array}\right\}
\end{array}\right\}
\end{aligned}
$$

$$\Phi_{45} = \cos\left[\nu_C(t) - M_C(t)\right]\begin{Bmatrix} -\cos\left[n_C(t-t_0)\right]\sin\left[\nu_{C,0} - M_{C,0}\right] \\ +2\sin\left[n_C(t-t_0)\right]\cos\left[\nu_{C,0} - M_{C,0}\right] \end{Bmatrix}$$
$$+\sin\left[\nu_C(t) - M_C(t)\right]\begin{Bmatrix} 2\sin\left[n_C(t-t_0)\right]\sin\left[\nu_{C,0} - M_{C,0}\right] \\ +\left[4\cos\left[n_C(t-t_0)\right]-3\right]\cos\left[\nu_{C,0} - M_{C,0}\right] \end{Bmatrix}$$
$$+\left(\dot{\nu}_C(t) - n_C\right)\left\{\begin{array}{l} -\sin\left[\nu_C(t) - M_C(t)\right]\left\{\begin{array}{l} -\dfrac{\sin\left[n_C(t-t_0)\right]}{n_C}\sin\left[\nu_{C,0} - M_{C,0}\right] \\ +\left[-\dfrac{2\cos\left[n_C(t-t_0)\right]}{n_C} + \dfrac{2}{n_C}\right]\cos\left[\nu_{C,0} - M_{C,0}\right] \end{array}\right\} \\ +\cos\left[\nu_C(t) - M_C(t)\right]\left\{\begin{array}{l} -\left[\dfrac{2\cos\left[n_C(t-t_0)\right]}{n_C} - \dfrac{2}{n_C}\right]\sin\left[\nu_{C,0} - M_{C,0}\right] \\ +\left[\dfrac{4\sin\left[n_C(t-t_0)\right]}{n_C} - 3(t-t_0)\right]\cos\left[\nu_{C,0} - M_{C,0}\right] \end{array}\right\} \end{array}\right\}$$

$$\Phi_{51} = -\sin\left[\nu_C(t) - M_C(t)\right]\left[3n_C\sin\left[n_C(t-t_0)\right]\right]\cos\left[\nu_{C,0} - M_{C,0}\right]$$
$$+\cos\left[\nu_C(t) - M_C(t)\right]\left[6n_C\cos\left[n_C(t-t_0)\right] - 6n_C\right]\cos\left[\nu_{C,0} - M_{C,0}\right]$$
$$+\left(\dot{\nu}_{C,0} - n_C\right)\left\{\begin{array}{l} -\sin\left[\nu_C(t) - M_C(t)\right]\left\{\begin{array}{l} -\cos\left[n_C(t-t_0)\right]\sin\left[\nu_{C,0} - M_{C,0}\right] \\ +2\sin\left[n_C(t-t_0)\right]\cos\left[\nu_{C,0} - M_{C,0}\right] \end{array}\right\} \\ +\cos\left[\nu_C(t) - M_C(t)\right]\left\{\begin{array}{l} 2\sin\left[n_C(t-t_0)\right]\sin\left[\nu_{C,0} - M_{C,0}\right] \\ +\left[4\cos\left[n_C(t-t_0)\right]-3\right]\cos\left[\nu_{C,0} - M_{C,0}\right] \end{array}\right\} \end{array}\right\}$$
$$-\left(\dot{\nu}_C(t) - n_C\right)\left\{\begin{array}{l} \cos\left[\nu_C(t) - M_C(t)\right]\left[-3\cos\left[n_C(t-t_0)\right]+4\right]\cos\left[\nu_{C,0} - M_{C,0}\right] \\ +\sin\left[\nu_C(t) - M_C(t)\right]\left\{\begin{array}{l} \left[6\sin\left[n_C(t-t_0)\right] - 6n_C(t-t_0)\right]\cos\left[\nu_{C,0} - M_{C,0}\right] \\ +\sin\left[\nu_{C,0} - M_{C,0}\right] \end{array}\right\} \end{array}\right\}$$
$$-\left(\dot{\nu}_C(t) - n_C\right)\left(\dot{\nu}_{C,0} - n_C\right)\left\{\begin{array}{l} \cos\left[\nu_C(t) - M_C(t)\right]\left\{\begin{array}{l} -\dfrac{\sin\left[n_C(t-t_0)\right]}{n_C}\sin\left[\nu_{C,0} - M_{C,0}\right] \\ +\left[-\dfrac{2\cos\left[n_C(t-t_0)\right]}{n_C} + \dfrac{2}{n_C}\right]\cos\left[\nu_{C,0} - M_{C,0}\right] \end{array}\right\} \\ +\sin\left[\nu_C(t) - M_C(t)\right]\left\{\begin{array}{l} -\left[\dfrac{2\cos\left[n_C(t-t_0)\right]}{n_C} - \dfrac{2}{n_C}\right]\sin\left[\nu_{C,0} - M_{C,0}\right] \\ +\left[\dfrac{4\sin\left[n_C(t-t_0)\right]}{n_C}\right]\cos\left[\nu_{C,0} - M_{C,0}\right] \\ \left[-3(t-t_0)\right] \end{array}\right\} \end{array}\right\}$$

$$
\begin{aligned}
\Phi_{52} &= \sin\left[\nu_C(t) - M_C(t)\right]\left[3n_C \sin\left[n_C(t-t_0)\right]\right]\sin\left[\nu_{C,0} - M_{C,0}\right] \\
&\quad - \cos\left[\nu_C(t) - M_C(t)\right]\left[6n_C \cos\left[n_C(t-t_0)\right] - 6n_C\right]\sin\left[\nu_{C,0} - M_{C,0}\right] \\
&\quad - \left(\dot{\nu}_{C,0} - n_C\right)\left\{\begin{array}{l} -\sin\left[\nu_C(t) - M_C(t)\right]\left\{\begin{array}{l}\cos\left[n_C(t-t_0)\right]\cos\left[\nu_{C,0} - M_{C,0}\right] \\ +2\sin\left[n_C(t-t_0)\right]\sin\left[\nu_{C,0} - M_{C,0}\right]\end{array}\right\} \\ +\cos\left[\nu_C(t) - M_C(t)\right]\left\{\begin{array}{l}-2\sin\left[n_C(t-t_0)\right]\cos\left[\nu_{C,0} - M_{C,0}\right] \\ +\left[4\cos\left[n_C(t-t_0)\right] - 3\right]\sin\left[\nu_{C,0} - M_{C,0}\right]\end{array}\right\}\end{array}\right\} \\
&\quad - \left(\dot{\nu}_C(t) - n_C\right)\left\{\begin{array}{l} -\cos\left[\nu_C(t) - M_C(t)\right]\left[-3\cos\left[n_C(t-t_0)\right] + 4\right]\sin\left[\nu_{C,0} - M_{C,0}\right] \\ +\sin\left[\nu_C(t) - M_C(t)\right]\left\{\begin{array}{l}-\left[6\sin\left[n_C(t-t_0)\right] - 6n_C(t-t_0)\right]\sin\left[\nu_{C,0} - M_{C,0}\right] \\ +\cos\left[\nu_{C,0} - M_{C,0}\right]\end{array}\right\}\end{array}\right\} \\
&\quad + \left(\dot{\nu}_C(t) - n_C\right)\left(\dot{\nu}_{C,0} - n_C\right)\left\{\begin{array}{l} \cos\left[\nu_C(t) - M_C(t)\right]\left\{\begin{array}{l}\dfrac{\sin\left[n_C(t-t_0)\right]}{n_C}\cos\left[\nu_{C,0} - M_{C,0}\right] \\ +\left[-\dfrac{2\cos\left[n_C(t-t_0)\right]}{n_C} + \dfrac{2}{n_C}\right]\sin\left[\nu_{C,0} - M_{C,0}\right]\end{array}\right\} \\ +\sin\left[\nu_C(t) - M_C(t)\right]\left\{\begin{array}{l}\left[\dfrac{2\cos\left[n_C(t-t_0)\right]}{n_C} - \dfrac{2}{n_C}\right]\cos\left[\nu_{C,0} - M_{C,0}\right] \\ +\left[\begin{array}{l}\dfrac{4\sin\left[n_C(t-t_0)\right]}{n_C} \\ -3(t-t_0)\end{array}\right]\sin\left[\nu_{C,0} - M_{C,0}\right]\end{array}\right\}\end{array}\right\}
\end{aligned}
$$

$$
\begin{aligned}
\Phi_{54} &= -\sin\left[\nu_C(t) - M_C(t)\right]\left\{\begin{array}{l}\cos\left[n_C(t-t_0)\right]\cos\left[\nu_{C,0} - M_{C,0}\right] \\ +2\sin\left[n_C(t-t_0)\right]\sin\left[\nu_{C,0} - M_{C,0}\right]\end{array}\right\} \\
&\quad + \cos\left[\nu_C(t) - M_C(t)\right]\left\{\begin{array}{l}-2\sin\left[n_C(t-t_0)\right]\cos\left[\nu_{C,0} - M_{C,0}\right] \\ +\left[4\cos\left[n_C(t-t_0)\right] - 3\right]\sin\left[\nu_{C,0} - M_{C,0}\right]\end{array}\right\} \\
&\quad - \left(\dot{\nu}_C(t) - n_C\right)\left\{\begin{array}{l} \cos\left[\nu_C(t) - M_C(t)\right]\left\{\begin{array}{l}\dfrac{\sin\left[n_C(t-t_0)\right]}{n_C}\cos\left[\nu_{C,0} - M_{C,0}\right] \\ +\left[-\dfrac{2\cos\left[n_C(t-t_0)\right]}{n_C} + \dfrac{2}{n_C}\right]\sin\left[\nu_{C,0} - M_{C,0}\right]\end{array}\right\} \\ +\sin\left[\nu_C(t) - M_C(t)\right]\left\{\begin{array}{l}\left[\dfrac{2\cos\left[n_C(t-t_0)\right]}{n_C} - \dfrac{2}{n_C}\right]\cos\left[\nu_{C,0} - M_{C,0}\right] \\ +\left[\dfrac{4\sin\left[n_C(t-t_0)\right]}{n_C} - 3(t-t_0)\right]\sin\left[\nu_{C,0} - M_{C,0}\right]\end{array}\right\}\end{array}\right\}
\end{aligned}
$$

$$
\begin{aligned}
\Phi_{55} = &-\sin\left[\nu_C(t) - M_C(t)\right]\left\{\begin{array}{l} -\cos\left[n_C(t-t_0)\right]\sin\left[\nu_{C,0} - M_{C,0}\right] \\ +2\sin\left[n_C(t-t_0)\right]\cos\left[\nu_{C,0} - M_{C,0}\right] \end{array}\right\} \\
&+\cos\left[\nu_C(t) - M_C(t)\right]\left\{\begin{array}{l} 2\sin\left[n_C(t-t_0)\right]\sin\left[\nu_{C,0} - M_{C,0}\right] \\ +\left[4\cos\left[n_C(t-t_0)\right] - 3\right]\cos\left[\nu_{C,0} - M_{C,0}\right] \end{array}\right\} \\
&-\left(\dot{\nu}_C(t) - n_C\right)\left\{\begin{array}{l} +\cos\left[\nu_C(t) - M_C(t)\right]\left\{\begin{array}{l} -\dfrac{\sin\left[n_C(t-t_0)\right]}{n_C}\sin\left[\nu_{C,0} - M_{C,0}\right] \\ +\left[-\dfrac{2\cos\left[n_C(t-t_0)\right]}{n_C} + \dfrac{2}{n_C}\right]\cos\left[\nu_{C,0} - M_{C,0}\right] \end{array}\right\} \\ +\sin\left[\nu_C(t) - M_C(t)\right]\left\{\begin{array}{l} -\left[\dfrac{2\cos\left[n_C(t-t_0)\right]}{n_C} - \dfrac{2}{n_C}\right]\sin\left[\nu_{C,0} - M_{C,0}\right] \\ +\left[\dfrac{4\sin\left[n_C(t-t_0)\right]}{n_C} - 3(t-t_0)\right]\cos\left[\nu_{C,0} - M_{C,0}\right] \end{array}\right\} \end{array}\right\}
\end{aligned}
$$

Appendix F: MATLAB Code

The numerical simulations for Chapter V were conducted using several original MATLAB programs, described below.

Relative Satellite Motion Plots and Comparisons

The primary script for calculating and comparing relative satellite motion trajectories via various models is rel_sat_motion5.m. It is the core script, generating time and true anomaly arrays, calculating key constants, calling specific model functions, and plotting trajectory comparisons. The function for the two-body truth model is always called. In the input block, a different switch may be set to 1 in order to call the HCW or Virtual Chief models.

rel_sat_motion5.m passes the following inputs to each of the separate MATLAB functions described in subsequent sections: the chief satellite orbit elements, the deputy satellite's relative initial state in coordinates of the chief's LVLH frame, arrays of time and chief true anomaly, and a few constant functions pre-calculated by rel_sat_motion5.m.

Each of the functions returns three arrays, representing the deputy's relative position vector at each time step in coordinates of the chief's LVLH frame.

The Algorithm.

This function calculates, plots, and compares relative satellite trajectories from multiple models. The algorithm is as follows:

- Input. In the input section, the user must edit the script in order to select which models to call (Virtual Chief, HCW, or both), to set the chief's classical orbit

elements, to specify the deputy's initial conditions in **c**-frame coordinates, and to set other simulation details (step size, number of chief orbits, and epoch time). In the version of the code included below, the input values are designed to replicate Example II from Shulman and Scott [88].

- Calculations:

  - Known constants. Use known two-body properties (see Appendix D) to compute the chief's mean motion, time of perigee passage, period, semilatus rectum, and angular momentum.

  - Newton-Raphson iteration to find epoch conditions. Solve Kepler's equation (Eq. (D.4)) to find epoch values of chief eccentric anomaly, leading to true anomaly and angular rate (via Eqs. (D.5) and (D.8)).

  - Discrete arrays. Generate an evenly spaced array of chief true anomaly values, based on the input values for step size and number of chief orbits. In this array, true anomaly will be allowed to take on values greater than 2π, so that we can calculate and plot more than one orbit. Then use two-body properties to create arrays of chief eccentric anomaly, mean anomaly, and time, where each element corresponds to an element of the true-anomaly array. Thus, for the elliptical chief problem, the time array will not have evenly spaced values.

- Models. Organize variables into a small number of arrays for passing to functions. Call the Kepler2.m function to calculate a two-body "truth" model. Call the virtual_chief.m and HCW.m functions, if selected.

- Plots. Generate four figures. First, plot the **c**-frame coordinates vs. time for each selected model. Figure 22 shows such a plot for the example input values below. Then, plot the **c**-frame coordinates vs. chief true anomaly, as in Figure 23.

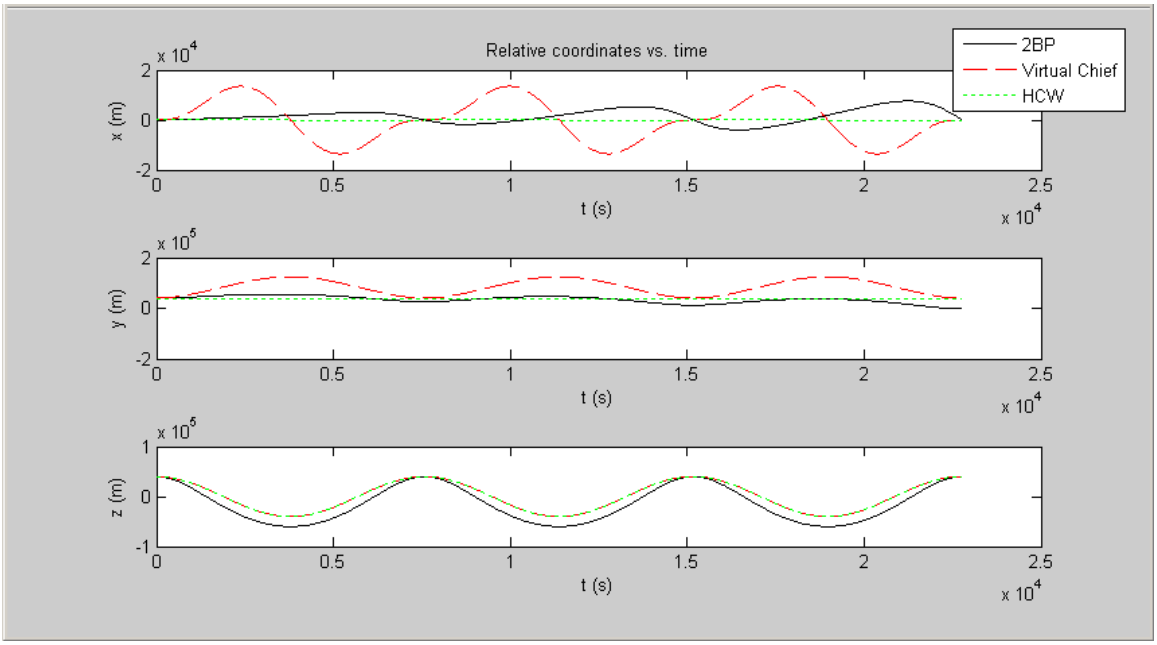

Figure 22. Coordinates vs. Time

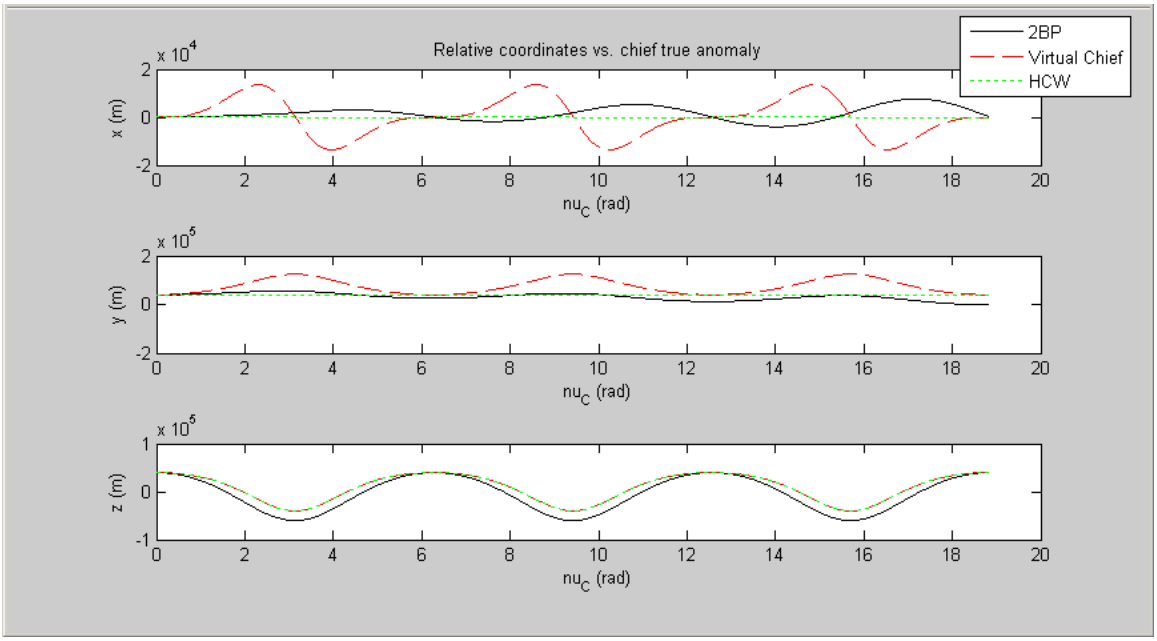

Figure 23. Coordinates vs. Chief True Anomaly

Next, plot the relative trajectory projected into each **c**-frame coordinate plane and in three dimensions, as in Figure 24.

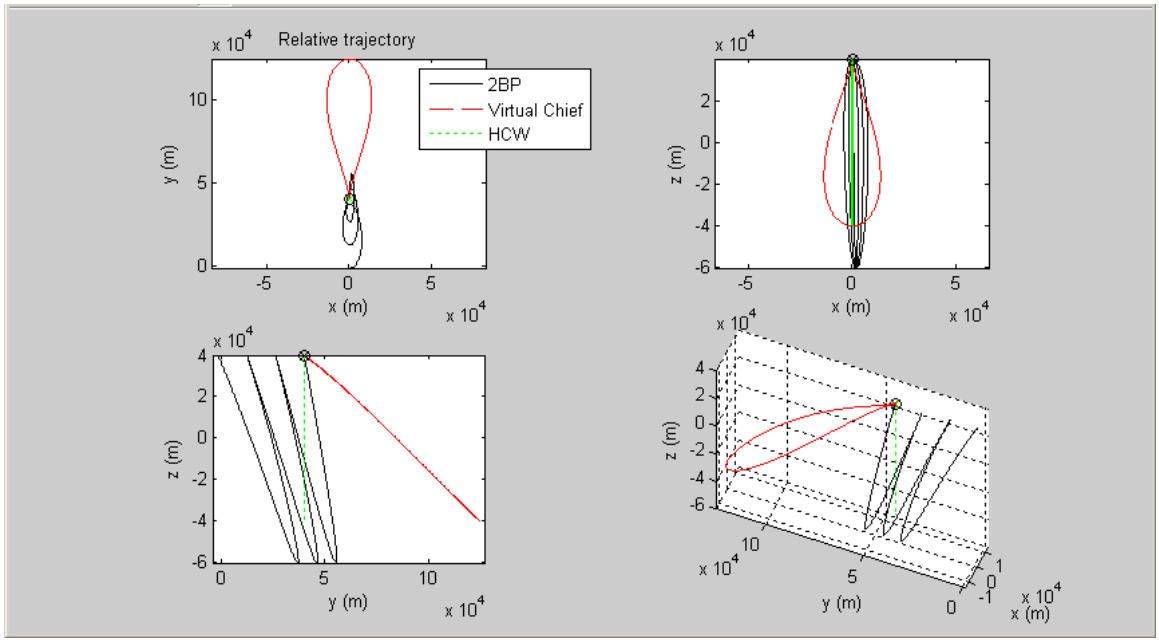

Figure 24. Relative Trajectory

Finally, plot the error (as compared with the two-body truth model) vs. time for the Virtual Chief and HCW models, as in Figure 25. Also plot the error magnitude (the root sum square of the three coordinate errors) vs. time.

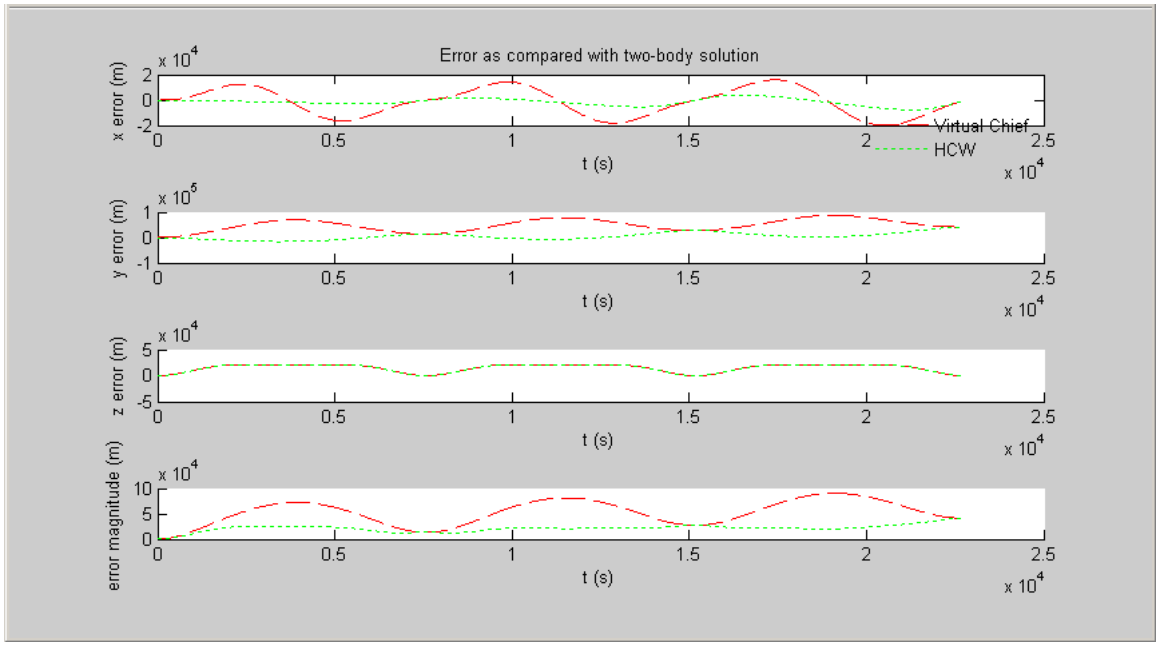

Figure 25. Error vs. Time

The Code.

This is rel_sat_motion5.m:

```
% Relative satellite motion plotter
%
% Calculates and plots the motion of a deputy satellite relative to a
% chief, according to several different relative motion models.  Each
model
% is called by a separate function, and the results are plotted together
% versus time, versus chief true anomaly, and geometrically.
%
% Input: Chief orbit elements, deputy relative initial state, desired
% number of orbits and step size, epoch time
%
% Units: SI

clc; clear all; close all; format long g


%-------------------------------------------------------------------------
---
% INPUT:
%-------------------------------------------------------------------------
---

% Desired models (set each flag to 1 if you wish to run the model):
vc=1; % the Virtual Chief method
hcw=1; % Hill's-Clohessy-Wiltshire equations

% Chief orbit elements:
a_C=8348000  ; %m (chief semi-major axis)
e_C=0.2 ; %chief orbit eccentricity
i_C=28.5*pi/180 ; %chief orbit inclination
Omega_C=0 ; %rad (chief RAAN)
omega_C=0 ; %rad (chief argument of perigee)
M_C0=0 ; %rad (chief mean anomaly at epoch)

% Deputy relative initial state (Cartesian coordinates in LVLH frame
fixed
% to chief):
x0=0 ; %m
y0=40000 ; %m
z0=40000 ; %m
xdot0=0.0111 ; %m/s
ydot0=0  ; %m/s
zdot0=0 ; %m/s

% Epoch time:
t0=0 ; %s

% Desired number of orbits:
N=3 ;

% Desired step size, in increments of chief true anomaly:
ss=pi/360 ; %rad
```

```
%-------------------------------------------------------------------------
---
% CALCULATIONS:
%-------------------------------------------------------------------------
---

% I.  Known constants and two-body properties

mu=3.98600441*10^14; %(m^3)/(s^2) (gravitational parameter)
n_C=sqrt(mu/(a_C^3)); %rad/s (chief mean motion)
t_p=t0-M_C0/n_C; %s (chief time of perigee passage)
P_C=2*pi/n_C; %s (chief period)
p_C=a_C*(1-e_C^2); %m (chief semilatus rectum)
h=sqrt(mu*p_C); %(m^2)/s (chief angular momentum)


% II.  Newton-Raphson iteration to find epoch conditions

flag=0;
E0=M_C0; % first guess
E1=10;
while flag==0,
    if abs(E1-E0)<10^(-9),
        flag=1;
    else E0=E1;
        E1=E0-(E0-e_C*sin(E0)-M_C0)/(1-e_C*cos(E0));
    end
end
E_C0=E1; %rad (chief eccentric anomaly at epoch)
if E_C0<0
    E_C0=E_C0+2*pi;
end
if M_C0==0
    E_C0=0;
end
s=sin(E_C0)*sqrt(1-e_C^2)/(1-e_C*cos(E_C0));
c=(cos(E_C0)-e_C)/(1-e_C*cos(E_C0));
nu_C0=atan2(s,c); %rad (chief true anomaly at epoch)
if nu_C0<0
    nu_C0=nu_C0+2*pi;
end
nudot_C0=n_C*(1-e_C^2)^(-3/2)*(1+e_C*cos(nu_C0))^2; %rad/s (chief
angular rate at epoch)


% III.  Discrete arrays

nu_C=nu_C0:ss:nu_C0+2*N*pi; %rad (chief true anomaly array, allowed to
take on values greater than 2*pi)
s2=sin(nu_C).*sqrt(1-e_C^2)./(1+e_C*cos(nu_C));
c2=(e_C+cos(nu_C))./(1+e_C*cos(nu_C));
E_C=atan2(s2,c2); %rad (chief eccentric anomaly array)
i=1; %atan2 is defined from -pi to pi; I need zero to 2*pi
while i<=length(E_C)
    if E_C(i)<0
```

```
        E_C(i)=2*pi+E_C(i);
    end
    i=i+1;
end
M_C=E_C-e_C*sin(E_C); %rad (chief mean anomaly array)
t=M_C./n_C+t_p; %s (time array)
i2=1; %I don't want to reset time to zero or negative after each orbit
while i2<=N
    i3=2;
    while i3<=length(t)
        if t(i3)<t(i3-1)
            t(i3)=t(i3)+P_C;
        end
        i3=i3+1;
    end
    i2=i2+1;
end


%-------------------------------------------------------------------------
---
% MODELS:
%-------------------------------------------------------------------------
---

orb_el=[a_C,t_p,i_C,omega_C,e_C,Omega_C];
rel_state=[x0,y0,z0,xdot0,ydot0,zdot0];
epoch_cond=[t0,nu_C0,M_C0,nudot_C0];
constants=[h,p_C,mu,n_C,N];
[x,y,z]=Kepler2(orb_el,rel_state,epoch_cond,t,nu_C,constants);
if vc==1

[x_vc,y_vc,z_vc]=virtual_chief(orb_el,rel_state,epoch_cond,t,nu_C,consta
nts);

[x_vcc,y_vcc,z_vcc]=vc_check(orb_el,rel_state,epoch_cond,t,nu_C,constant
s);
end
if hcw==1
    [x_hcw,y_hcw,z_hcw]=HCW(rel_state,epoch_cond,t,constants);
end


%-------------------------------------------------------------------------
---
% PLOTS:
%-------------------------------------------------------------------------
---

% Figure 1 (Coordinates versus time)

subplot(3,1,1); plot(t,x,'k')
[hand,ob,pl,text]=legend('2BP');
hold on;
if vc==1
    plot(t,x_vc,'r--')
    [hand,ob,pl,text]=legend(hand,text,'Virtual Chief');
end
```

```
if hcw==1
    plot(t,x_hcw,'g:')
    [hand,ob,pl,text]=legend(hand,text,'HCW');
end
xlabel('t (s)')
ylabel('x (m)')
title('Relative coordinates vs. time')
subplot(3,1,2); plot(t,y,'k')
hold on;
if vc==1
    plot(t,y_vc,'r--')
end
if hcw==1
    plot(t,y_hcw,'g:')
end
xlabel('t (s)')
ylabel('y (m)')
subplot(3,1,3); plot(t,z,'k')
hold on;
if vc==1
    plot(t,z_vc,'r--')
end
if hcw==1
    plot(t,z_hcw,'g:')
end
xlabel('t (s)')
ylabel('z (m)')


% Figure 2 (Coordinates versus chief true anomaly)

figure
subplot(3,1,1); plot(nu_C,x,'k')
[hand2,ob2,pl2,text2]=legend('2BP');
hold on;
if vc==1
    plot(nu_C,x_vc,'r--')
    [hand2,ob2,pl2,text2]=legend(hand2,text2,'Virtual Chief');
end
if hcw==1
    plot(nu_C,x_hcw,'g:')
    [hand2,ob2,pl2,text2]=legend(hand2,text2,'HCW');
end
title('Relative coordinates vs. chief true anomaly')
xlabel('nu_C (rad)')
ylabel('x (m)')
subplot(3,1,2); plot(nu_C,y,'k')
hold on;
if vc==1
    plot(nu_C,y_vc,'r--')
end
if hcw==1
    plot(nu_C,y_hcw,'g:')
end
xlabel('nu_C (rad)')
ylabel('y (m)')
subplot(3,1,3); plot(nu_C,z,'k')
hold on;
if vc==1
```

```
    plot(nu_C,z_vc,'r--')
end
if hcw==1
    plot(nu_C,z_hcw,'g:')
end
xlabel('nu_C (rad)')
ylabel('z (m)')


% Figure 3 (Geometric plots)

figure
subplot(2,2,1); plot(x,y,'k')
axis equal
xlabel('x (m)')
ylabel('y (m)')
[hand3,ob3,pl3,text3]=legend('2BP');
hold on;
if vc==1
    plot(x_vc,y_vc,'r--')
    [hand3,ob3,pl3,text3]=legend(hand3,text3,'Virtual Chief');
end
if hcw==1
    plot(x_hcw,y_hcw,'g:')
    [hand3,ob3,pl3,text3]=legend(hand3,text3,'HCW');
end
plot(x(1),y(1),'ko')
plot(x(15),y(15),'kx')
if vc==1
    plot(x_vc(15),y_vc(15),'rx')
end
if hcw==1
    plot(x_hcw(15),y_hcw(15),'gx')
end
title('Relative trajectory')
subplot(2,2,2); plot(x,z,'k')
axis equal
xlabel('x (m)')
ylabel('z (m)')
hold on;
if vc==1
    plot(x_vc,z_vc,'r--')
    plot(x_vc(15),z_vc(15),'rx')
end
if hcw==1
    plot(x_hcw,z_hcw,'g:')
    plot(x_hcw(15),z_hcw(15),'gx')
end
plot(x(1),z(1),'ko')
plot(x(15),z(15),'kx')
subplot(2,2,3); plot(y,z,'k')
axis equal
xlabel('y (m)')
ylabel('z (m)')
hold on;
if vc==1
    plot(y_vc,z_vc,'r--')
    plot(y_vc(15),z_vc(15),'rx')
end
```

```
if hcw==1
    plot(y_hcw,z_hcw,'g:')
    plot(y_hcw(15),z_hcw(15),'gx')
end
plot(y(1),z(1),'ko')
plot(y(15),z(15),'kx')
subplot(2,2,4); plot3(x,y,z,'k')
xlabel('x (m)')
ylabel('y (m)')
zlabel('z (m)')
hold on;
if vc==1
    plot3(x_vc,y_vc,z_vc,'r--')
    plot3(x_vc(15),y_vc(15),z_vc(15),'rx')
end
if hcw==1
    plot3(x_hcw,y_hcw,z_hcw,'g:')
    plot3(x_hcw(15),y_hcw(15),z_hcw(15),'gx')
end
plot3(x(1),y(1),z(1),'ko')
plot3(x(15),y(15),z(15),'kx')
axis equal
grid on


% Figure 4 (Error)

figure
subplot(4,1,1)
plot(0,0,'w  ')
hold on
[hand4,ob4,pl4,text4]=legend(' ');
if vc==1
    plot(t,x_vc-x,'r--')
    [hand4,ob4,pl4,text4]=legend(hand4,text4,'Virtual Chief');
end
if hcw==1
    plot(t,x_hcw-x,'g:')
    [hand4,ob4,pl4,text4]=legend(hand4,text4,'HCW');
end
legend boxoff
xlabel('t (s)')
ylabel('x error (m)')
title('Error as compared with two-body solution')
subplot(4,1,2)
hold on
if vc==1
    plot(t,y_vc-y,'r--')
end
if hcw==1
    plot(t,y_hcw-y,'g:')
end
xlabel('t (s)')
ylabel('y error (m)')
subplot(4,1,3)
hold on
if vc==1
    plot(t,z_vc-z,'r--')
end
```

```
if hcw==1
    plot(t,z_hcw-z,'g:')
end
xlabel('t (s)')
ylabel('z error (m)')
subplot(4,1,4)
hold on
if vc==1
    err_vc=sqrt((x_vc-x).^2+(y_vc-y).^2+(z_vc-z).^2);
    plot(t,err_vc,'r--')
    rms_vc=sqrt(mean(err_vc.^2))
end
if hcw==1
    err_hcw=sqrt((x_hcw-x).^2+(y_hcw-y).^2+(z_hcw-z).^2);
    plot(t,err_hcw,'g:')
    rms_hcw=sqrt(mean(err_hcw.^2))
end
xlabel('t (s)')
ylabel('error magnitude (m)')
```

The Two-body Keplerian Truth Model

The Algorithm.

This function calculates the relative satellite trajectory using the exact solution to the nonlinear two-body problem. The algorithm is as follows:

- I. Calculate the rotation matrix from the chief's LVLH frame to the **i**-frame (Earth-centered inertial), evaluated at epoch. See below for derivation of the matrix.

- II. Using the matrix just calculated, compute the chief's state vectors in **i**-frame coordinates:

$$\left[\vec{r}_{C/I}\right]_i = R_C\left[\vec{r}_{C/I}\right]_c$$
$$\left[{}^i\frac{d}{dt}\vec{r}_{C/I}\right]_i = R_C\left[{}^i\frac{d}{dt}\vec{r}_{C/I}\right]_c$$

- III. Using the same matrix, compute the deputy's relative state vectors in **i**-frame coordinates:

$$\left[\vec{r}_{D/C}\right]_i = R_C\left[\vec{r}_{D/C}\right]_c$$
$$\left[{}^i\frac{d}{dt}\vec{r}_{D/C}\right]_i = R_C\left[{}^c\frac{d}{dt}\vec{r}_{D/C} + \vec{\omega}_{C/I}\times\vec{r}_{D/C}\right]_c$$

- IV. Add these vectors to find the deputy's inertial state:

$$\left[\vec{r}_{D/I}\right]_i = \left[\vec{r}_{C/I}\right]_i + \left[\vec{r}_{D/C}\right]_i$$
$$\left[{}^i\frac{d}{dt}\vec{r}_{D/I}\right]_i = \left[{}^i\frac{d}{dt}\vec{r}_{C/I}\right]_i + \left[{}^i\frac{d}{dt}\vec{r}_{D/C}\right]_i$$

- V. Use known two-body properties (see Appendix D) to calculate the deputy's orbit elements, a_D, e_D, i_D, Ω_D, ω_D, and $\nu_{D,0}$, as well as related values $E_{D,0}$, n_D, $t_{p,D}$, and p_D.

- VI. Using the time array passed from rel_sat_motion.m, generate an array of values for the deputy's mean anomaly:

$$M_D(t) = n_D\left(t - t_{p,D}\right)$$

- VII. Using Newton-Raphson iteration, compute the deputy's eccentric and true anomalies at each step:

$$M_D(t) = E_D(t) - e_D\sin E_D(t)$$
$$\sin\nu_D(t) = \frac{\sqrt{1-e_D{}^2}\sin E_D(t)}{1-e_D\cos E_D(t)}$$
$$\cos\nu_D(t) = \frac{\cos E_D(t) - e_D}{1-e_D\cos E_D(t)}$$

- VIII. At each time step, compute the chief and deputy orbit radius:

$$r_C(t) = \frac{p_C}{1+e_C\cos\nu_C(t)}$$
$$r_D(t) = \frac{p_D}{1+e_D\cos\nu_D(t)}$$

- IX. At each time step, calculate a rotation matrix from LVLH to **i**-frame coordinates, evaluated at the current time, for both the chief and the deputy. This matrix follows the same formula as that in Step I.

- X. At each time step, rotate the chief and deputy position vectors into **i**-frame coordinates, as was done for the chief initial position in Step II.

- XI. At each time step, difference the chief and deputy positions to create a relative position vector in **i**-frame coordinates:

$$\left[\vec{r}_{D/C}\right]_i = \left[\vec{r}_{D/I}\right]_i - \left[\vec{r}_{C/I}\right]_i$$

- XII. At each time step, use the transpose of the chief's rotation matrix from Step IX to rotate the relative position vector into coordinates of the chief's LVLH frame:

$$\left[\vec{r}_{D/C}\right]_c = R_C{}^T \left[\vec{r}_{D/C}\right]_i = \begin{bmatrix} x(t) \\ y(t) \\ z(t) \end{bmatrix}$$

The Rotation Matrices.

The rotation-matrix formula used in Steps I and IX of the algorithm will now be derived.

An arbitrary vector $\vec{r}$ defined in **i**-frame (ECI) coordinates can be expressed in coordinates of a particular satellite's nodal-equatorial (**q**) reference frame as follows:

$$\left[\vec{r}\right]_q = R^{i\to q}\left[\vec{r}\right]_i$$

where $R^{i\to q}$ is simply a three-rotation of magnitude Ω, the satellite's right ascension of the ascending node:

$$R^{i\to q} = R_3(\Omega) = \begin{bmatrix} \cos\Omega & \sin\Omega & 0 \\ -\sin\Omega & \cos\Omega & 0 \\ 0 & 0 & 1 \end{bmatrix} \tag{F.1}$$

This rotation is illustrated in Figure 26, which depicts the **i**-frame unit basis vector $\hat{i}_1$ rotated to the **q**-frame.

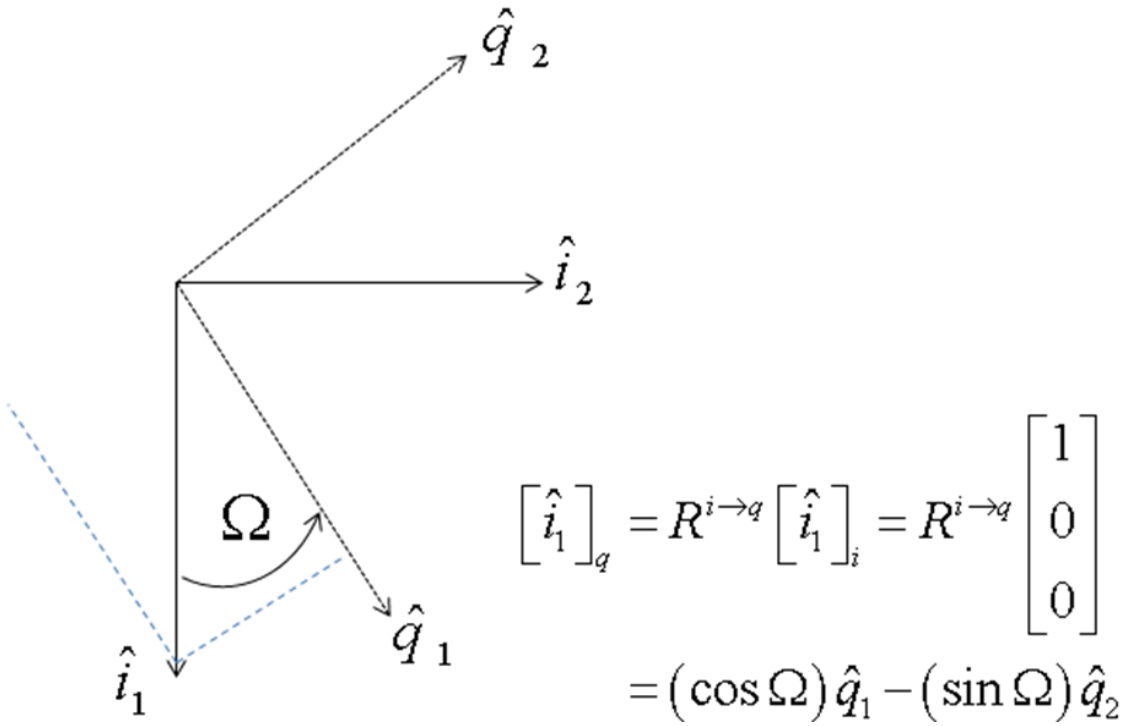

Figure 26. Rotation from i to q

Likewise, a vector defined in **q**-frame coordinates can be expressed in the satellite's nodal (**n**) frame via a 1-rotation of magnitude i, the satellite's inclination:

$$R^{q\to n} = R_1(i) = \begin{bmatrix} 1 & 0 & 0 \\ 0 & \cos i & \sin i \\ 0 & -\sin i & \cos i \end{bmatrix} \tag{F.2}$$

This rotation is illustrated in Figure 27, which depicts the **q**-frame unit basis vector $\hat{q}_2$ rotated to the **n**-frame.

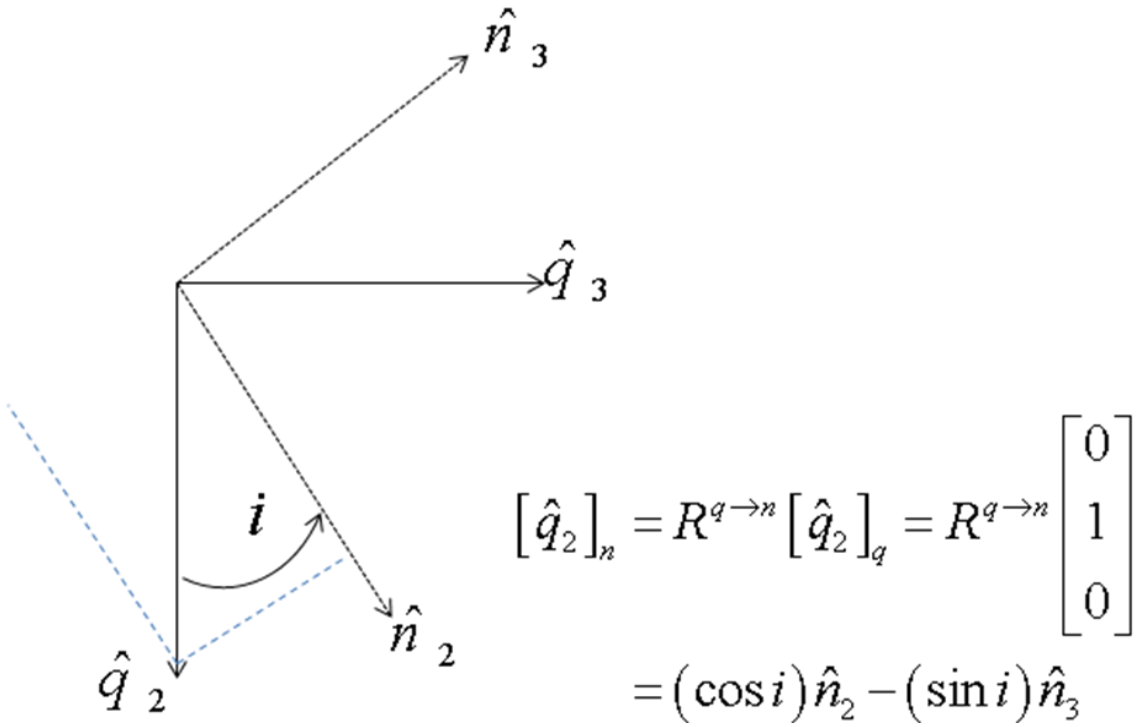

Figure 27. Rotation from q to n

It is worth noting that for satellites in equatorial orbits, Ω and i should each be set to zero. The rotations in Eqs. (F.1) and (F.2) will then produce the identity matrix.

Finally, a vector defined in **n**-frame coordinates can be expressed in the satellite's orbit (**o**) frame via a 3-rotation of magnitude u, the satellite's argument of latitude. If the

satellite is in a non-circular orbit, u may be replaced by its equivalent, $\omega+\nu$, or argument of perigee plus true anomaly:

$$R^{n\to o} = R_3(\omega+\nu) = \begin{bmatrix} \cos(\omega+\nu) & \sin(\omega+\nu) & 0 \\ -\sin(\omega+\nu) & \cos(\omega+\nu) & 0 \\ 0 & 0 & 1 \end{bmatrix} \tag{F.3}$$

Thus, we can use **o**-frame coordinates to express a vector defined in **i**-frame coordinates as follows:

$$\left[\mathrm{v}_r\right]_o = R^{i\to o}\left[\mathrm{v}_r\right]_i = R^{n\to o}R^{q\to n}R^{i\to q}\left[\mathrm{v}_r\right]_i$$

Multiplying the matrices from Eqs. (F.1), (F.2), and (F.3) yields

$$R^{i\to o} = \begin{bmatrix} \mathrm{c}\Omega\mathrm{c}(\omega+\nu)-\mathrm{s}\Omega\mathrm{c}i\mathrm{s}(\omega+\nu) & \mathrm{s}\Omega\mathrm{c}(\omega+\nu)+\mathrm{c}\Omega\mathrm{c}i\mathrm{s}(\omega+\nu) & \mathrm{s}i\mathrm{s}(\omega+\nu) \\ -\mathrm{c}\Omega\mathrm{s}(\omega+\nu)-\mathrm{s}\Omega\mathrm{c}i\mathrm{c}(\omega+\nu) & -\mathrm{s}\Omega\mathrm{s}(\omega+\nu)+\mathrm{c}\Omega\mathrm{c}i\mathrm{c}(\omega+\nu) & \mathrm{s}i\mathrm{c}(\omega+\nu) \\ \mathrm{s}\Omega\mathrm{s}i & -\mathrm{c}\Omega\mathrm{s}i & \mathrm{c}i \end{bmatrix}$$

where cosine and sine are signified by c and s, respectively. This is the rotation needed for the chief satellite in Step XII of the algorithm.

However, we need the inverse transformation, $R^{o\to i}$. Since the inverse of a rotation matrix is its transpose,

$$R^{o\to i} = \begin{bmatrix} \mathrm{c}\Omega\mathrm{c}(\omega+\nu)-\mathrm{s}\Omega\mathrm{c}i\mathrm{s}(\omega+\nu) & -\mathrm{c}\Omega\mathrm{s}(\omega+\nu)-\mathrm{s}\Omega\mathrm{c}i\mathrm{c}(\omega+\nu) & \mathrm{s}\Omega\mathrm{s}i \\ \mathrm{s}\Omega\mathrm{c}(\omega+\nu)+\mathrm{c}\Omega\mathrm{c}i\mathrm{s}(\omega+\nu) & -\mathrm{s}\Omega\mathrm{s}(\omega+\nu)+\mathrm{c}\Omega\mathrm{c}i\mathrm{c}(\omega+\nu) & -\mathrm{c}\Omega\mathrm{s}i \\ \mathrm{s}i\mathrm{s}(\omega+\nu) & \mathrm{s}i\mathrm{c}(\omega+\nu) & \mathrm{c}i \end{bmatrix} \tag{F.4}$$

Eq. (F.4) gives the formula needed in Steps I and IX of the algorithm.

The Code.

This is Kepler2.m, the MATLAB function which calculates the relative satellite trajectory using fully nonlinear two-body Keplerian motion:

```
% Two-body Exact Relative Orbit Plotter (rev 2)
%
% Provides the exact relative trajectory of a deputy satellite in the
% local-vertical/local-horizontal (LVLH) reference frame of a chief
% satellite, assuming simple two-body Keplerian motion.
%
% This function should work for all chief orbits (circular or elliptical,
% equatorial or inclined).
%
% Required inputs are the chief's orbit elements, the deputy's relative
% initial state in LVLH coordinates, and matched arrays of time and
chief
% true anomaly.

function [x,y,z]=Kepler2(orb_el,rel_state,epoch_cond,t,nu_C,constants)

% Assign variables

a_C=orb_el(1);
i_C=orb_el(3);
omega_C=orb_el(4);
e_C=orb_el(5);
Omega_C=orb_el(6);
x0=rel_state(1);
y0=rel_state(2);
z0=rel_state(3);
xdot0=rel_state(4);
ydot0=rel_state(5);
zdot0=rel_state(6);
t0=epoch_cond(1);
nu_C0=epoch_cond(2);
nudot_C0=epoch_cond(4);
p_C=constants(2);
mu=constants(3);


% I.  Rotation matrix from chief LVLH frame (o) to ECI frame (i), evaluated
% at epoch.  Uses R_C=R(o to i)=R'(i to o),
% where R(i to o)=R3(omega+nu)R1(i)R3(Omega).

R_C0(1,1)=cos(Omega_C)*cos(omega_C+nu_C0)-
sin(Omega_C)*cos(i_C)*sin(omega_C+nu_C0);
R_C0(1,2)=-cos(Omega_C)*sin(omega_C+nu_C0)-
sin(Omega_C)*cos(i_C)*cos(omega_C+nu_C0);
R_C0(1,3)=sin(Omega_C)*sin(i_C);
R_C0(2,1)=sin(Omega_C)*cos(omega_C+nu_C0)+cos(Omega_C)*cos(i_C)*sin(omega_C+nu_C
0);
R_C0(2,2)=-
sin(Omega_C)*sin(omega_C+nu_C0)+cos(Omega_C)*cos(i_C)*cos(omega_C+nu_C0);
R_C0(2,3)=-cos(Omega_C)*sin(i_C);
R_C0(3,1)=sin(i_C)*sin(omega_C+nu_C0);
R_C0(3,2)=sin(i_C)*cos(omega_C+nu_C0);
R_C0(3,3)=cos(i_C);
```

```
% II.  Calculate chief epoch state in Earth-centered inertial (ECI)
% coordinates

r_C0=p_C/(1+e_C*cos(nu_C0)); %m (chief orbit radius at epoch)
pos_C0_o=[r_C0;0;0]; % chief position vector at epoch, LVLH coordinates
rdot_C0=sqrt(mu/p_C)*e_C*sin(nu_C0); %m/s (chief radial rate at epoch)
vel_C0_o=[rdot_C0;r_C0*nudot_C0;0]; % chief velocity vector at epoch, LVLH
coordinates
pos_C0_i=R_C0*pos_C0_o; % chief position vector at epoch, ECI coordinates
vel_C0_i=R_C0*vel_C0_o; % chief velocity vector at epoch, ECI coordinates


% III.  Rotate deputy relative state to ECI coordinates

pos_rel0_i=R_C0*[x0;y0;z0]; % relative position vector at epoch, ECI coordinates
vel_rel0_i=R_C0*([xdot0;ydot0;zdot0]+cross([0;0;nudot_C0],[x0;y0;z0])); %
relative velocity vector at epoch, ECI coordinates


% IV.  Add vectors to find deputy inertial state

pos_D0_i=pos_C0_i+pos_rel0_i; % deputy position vector at epoch, ECI coordinates
vel_D0_i=vel_C0_i+vel_rel0_i; % deputy velocity vector at epoch, ECI coordinates


% V.  Calculate deputy orbit elements

r_D0=norm(pos_D0_i); %m (deputy radius at epoch)
v_D0=norm(vel_D0_i); %m/s (deputy speed at epoch)
epsilon_D=v_D0^2/2-mu/r_D0; %m^2/s^2 (deputy specific energy)
a_D=-mu/(2*epsilon_D) %m (deputy semi-major axis)
H_D_vec=cross(pos_D0_i,vel_D0_i); %deputy angular momentum vector
H_D=norm(H_D_vec); %m^2/s (deputy angular momentum)
e_D_vec=cross(vel_D0_i,H_D_vec)/mu-pos_D0_i/r_D0; % deputy eccentricity vector
e_D=norm(e_D_vec) %deputy eccentricity
i_D=acos([0 0 1]*H_D_vec)/H_D) %rad (deputy inclination)
nhat=cross([0;0;1],H_D_vec)/norm(cross([0;0;1],H_D_vec)); %deputy unit nodal
vector
Omega_D=atan2(nhat(2),nhat(1)) %rad (deputy RAAN)
omega_D=acos((e_D_vec/e_D)'*nhat) %rad (deputy argument of perigee)
if [0 0 1]*e_D_vec<0
    omega_D=2*pi-omega_D
end
nu_D0=acos((e_D_vec/e_D)'*(pos_D0_i/r_D0)) %rad (deputy true anomaly at epoch)
if pos_D0_i'*vel_D0_i<0
    nu_D0=2*pi-nu_D0 % correcting for cases when the deputy is past apogee
end
E_D0=2*atan2(sqrt((1-e_D)/(1+e_D))*sin(nu_D0/2),cos(nu_D0/2)); %rad (deputy
eccentric anomaly at epoch)
n_D=sqrt(mu/a_D^3); %rad/s (deputy mean motion)
t_pD=t0-(E_D0-e_D*sin(E_D0))/n_D; %s (deputy time of perigee passage)
p_D=a_D*(1-e_D^2); %m (deputy semilatus rectum)


% VI.  Create deputy mean anomaly array

M_D=n_D.*(t-t_pD); % rad (deputy mean anomaly array)
for i=1:length(M_D) %I want to reset M_D to zero after each orbit
    f=fix(M_D(i)/(2*pi));
    M_D(i)=M_D(i)-2*f*pi;
end

% VII.  Create deputy true anomaly array
```

```
for i2=1:length(t)
    flag=0;
    E0=M_D(i2); % first guess
    E1=8;
    while flag==0,
        if abs(E1-E0)<10^(-9),
            flag=1;
        else E0=E1;
            E1=E0-(E0-e_D*sin(E0)-M_D(i2))/(1-e_D*cos(E0));
        end
    end
    E_D(i2)=E1; %rad (deputy eccentric anomaly)
    s2=sin(E_D(i2))*sqrt(1-e_D^2)/(1-e_D*cos(E_D(i2)));
    c2=(cos(E_D(i2))-e_D)/(1-e_D*cos(E_D(i2)));
    nu_D(i2)=atan2(s2,c2); %rad (deputy true anomaly)
end


% Propagate chief and deputy inertial states, then rotate to LVLH
for i3=1:length(t)

  % VIII.  Chief and deputy trajectory and velocity equations
    r_C=p_C/(1+e_C*cos(nu_C(i3))); %m (chief orbit radius)
    r_D=p_D/(1+e_D*cos(nu_D(i3))); %m (deputy orbit radius)
    v_C=sqrt(2*mu/r_C-mu/a_C); %m/s (chief velocity)
    v_D=sqrt(2*mu/r_D-mu/a_D); %m/s (deputy velocity)

  % IX.  Chief and deputy rotation matrices
    % rotation matrix from chief LVLH frame to ECI frame, using R(i to
o)=R3(omega+nu)R1(i)R3(Omega) and R(o to i)=R'(i to o)
    R_C(1,1)=cos(Omega_C)*cos(omega_C+nu_C(i3))-
sin(Omega_C)*cos(i_C)*sin(omega_C+nu_C(i3));
    R_C(1,2)=-cos(Omega_C)*sin(omega_C+nu_C(i3))-
sin(Omega_C)*cos(i_C)*cos(omega_C+nu_C(i3));
    R_C(1,3)=sin(Omega_C)*sin(i_C);

R_C(2,1)=sin(Omega_C)*cos(omega_C+nu_C(i3))+cos(Omega_C)*cos(i_C)*sin(omega_C+nu
_C(i3));
    R_C(2,2)=-
sin(Omega_C)*sin(omega_C+nu_C(i3))+cos(Omega_C)*cos(i_C)*cos(omega_C+nu_C(i3));
    R_C(2,3)=-cos(Omega_C)*sin(i_C);
    R_C(3,1)=sin(i_C)*sin(omega_C+nu_C(i3));
    R_C(3,2)=sin(i_C)*cos(omega_C+nu_C(i3));
    R_C(3,3)=cos(i_C);
    % rotation matrix from deputy orbit frame to ECI frame
    R_D(1,1)=cos(Omega_D)*cos(omega_D+nu_D(i3))-
sin(Omega_D)*cos(i_D)*sin(omega_D+nu_D(i3));
    R_D(1,2)=-cos(Omega_D)*sin(omega_D+nu_D(i3))-
sin(Omega_D)*cos(i_D)*cos(omega_D+nu_D(i3));
    R_D(1,3)=sin(Omega_D)*sin(i_D);

R_D(2,1)=sin(Omega_D)*cos(omega_D+nu_D(i3))+cos(Omega_D)*cos(i_D)*sin(omega_D+nu
_D(i3));
    R_D(2,2)=-
sin(Omega_D)*sin(omega_D+nu_D(i3))+cos(Omega_D)*cos(i_D)*cos(omega_D+nu_D(i3));
    R_D(2,3)=-cos(Omega_D)*sin(i_D);
    R_D(3,1)=sin(i_D)*sin(omega_D+nu_D(i3));
    R_D(3,2)=sin(i_D)*cos(omega_D+nu_D(i3));
    R_D(3,3)=cos(i_D);

  % X.  Chief and deputy conditions rotated to ECI frame
    r_C_vec=R_C*[r_C;0;0]; % chief ECI position vector
    r_D_vec=R_D*[r_D;0;0]; % deputy ECI position vector

  % XI.  ECI relative position vector
```

```
    r_ECI_vec=r_D_vec-r_C_vec;

  % XII.  Relative coordinates rotated back to chief LVLH frame
    r_LVLH_vec=R_C'*r_ECI_vec; % relative position vector in chief orbit frame
coordinates
    x(i3)=r_LVLH_vec(1); %m
    y(i3)=r_LVLH_vec(2); %m
    z(i3)=r_LVLH_vec(3); %m
end
```

Examples Compared against Satellite Toolkit.

In order to demonstrate the accuracy of the two-body relative satellite motion predicted by Kepler2.m, I will compare its output against output from the Two Body propagator in Satellite Toolkit (STK). I will perform this comparison for three examples.

The first example is a typical relative satellite motion case, with small distances and small but non-negligible eccentricities. For this example, the orbit elements of the chief satellite and the deputy satellite's relative state in coordinates of the chief LVLH frame are given in Table 7, along with the resulting deputy orbit elements.

Table 7. Input for the First Example

Chief orbit	Relative initial state	Deputy orbit
$a_C = 26778137$ m	$x_0 = -2357.02260395516$ m	$a_D = 26778090.7194924$ m
$e_C = 0.01$	$y_0 = 5714.04520791032$ m	$e_D = 0.0100867011056697$
$i_C = 28.5°$	$z_0 = 0$	$i_D = 0.49756671315498$ rad
$\Omega_C = 0$	$\dot{x}_0 = 0.35626933756075 \frac{\text{m}}{\text{s}}$	$\Omega_D = 6.67858183316407\text{e-}008$ rad
$\omega_C = 0$	$\dot{y}_0 = 0.686069106910399 \frac{\text{m}}{\text{s}}$	$\omega_D = 6.27424251721299$ rad
$M_{C,0} = 0$	$\dot{z}_0 = 0.576312899024239 \frac{\text{m}}{\text{s}}$	$\nu_{D,0} = 0.0091582905573582$ rad

Results for the first example are compared over four chief orbits and shown in Figure 28. For this simulation, the epoch time was set to zero, and the chief true anomaly step size was set to half a degree.

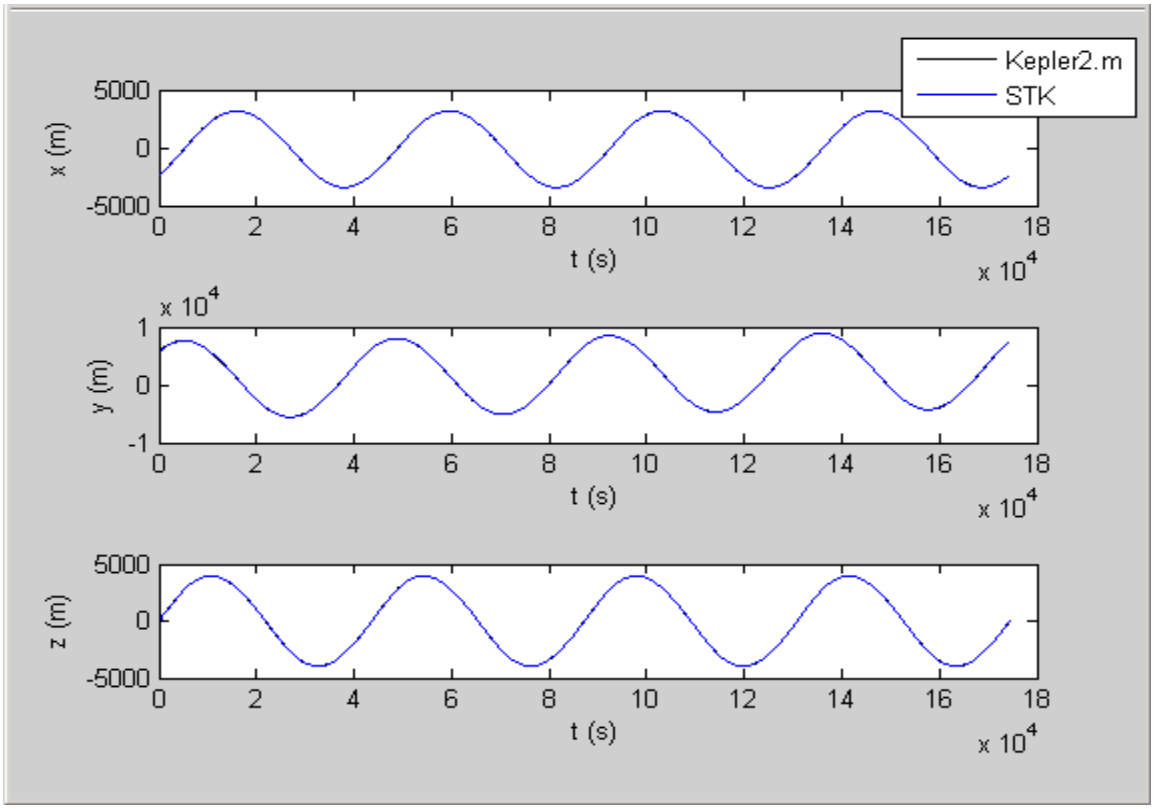

Figure 28. First Example Results

The second example illustrates a case with large separation distances and a chief in a circular, equatorial orbit. For this example, Table 8 gives the orbit elements and initial relative coordinates.

Results for the second example are compared over four chief orbits and shown in Figure 29. Epoch time is zero, and chief true anomaly step size is half a degree.

Table 8. Input for the Second Example

Chief orbit	Relative initial state	Deputy orbit
$a_C = 6778137$ m	$x_0 = 2000$ m	$a_D = 6790311.93490504$ m
$e_C = 0$	$y_0 = 100000$ m	$e_D = 0.00139062906315371$
$i_C = 0$	$z_0 = 2000$	$i_D = 0.000304358514095287$ rad
$\Omega_C = 0$	$\dot{x}_0 = 0.35626933756075 \frac{\text{m}}{\text{s}}$	$\Omega_D = -1.30671940634345$ rad
$\omega_C = 0$	$\dot{y}_0 = 0.686069106910399 \frac{\text{m}}{\text{s}}$	$\omega_D = 1.28706041049096$ rad
$M_{C,0} = 0$	$\dot{z}_0 = 0.576312899024239 \frac{\text{m}}{\text{s}}$	$\nu_{D,0} = 0.0344069021226111$ rad

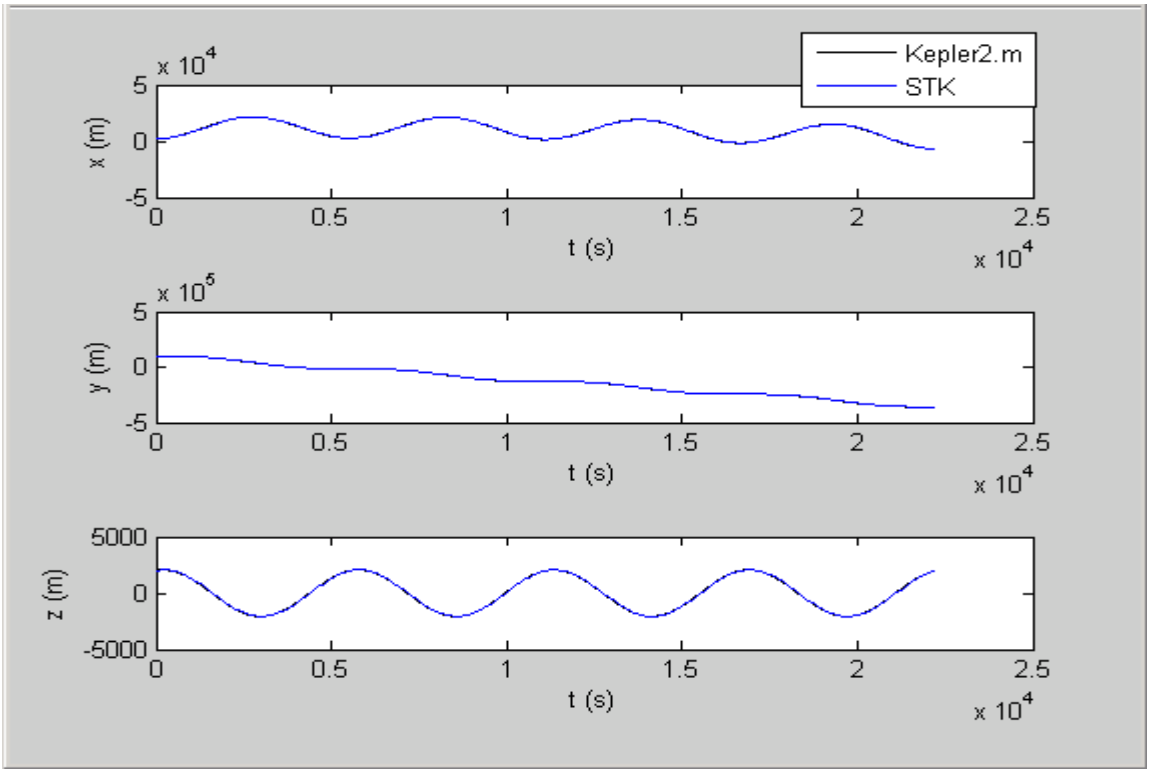

Figure 29. Second Example Results

The third example illustrates satellites in highly eccentric orbits. Table 9 gives the orbit elements and initial relative coordinates.

Table 9. Input for Third Example

Chief orbit	Relative initial state	Deputy orbit
$a_C = 30778137$ m	$x_0 = 0$ m	$a_D = 30777601.1837545$ m
$e_C = 0.75$	$y_0 = 150$ m	$e_D = 0.749999394965603$
$i_C = 28.5°$	$z_0 = 2000$ m	$i_D = 0.497453372017292$ rad
$\Omega_C = 0$	$\dot{x}_0 = 0$	$\Omega_D = 0.00039059160523208 9$ rad
$\omega_C = 0$	$\dot{y}_0 = 0$	$\omega_D = 6.28283388440474$ rad
$M_{C,0} = \frac{\pi}{8}$ rad	$\dot{z}_0 = 1 \ \frac{\text{m}}{\text{s}}$	$\nu_{D,0} = 1.97382718065585$ rad

Results for the third example are compared over three chief orbits and shown in Figure 30. Again, epoch time is zero, and chief true anomaly step size is half a degree.

As demonstrated by these three widely varying examples, the relative trajectories calculated by Kepler2.m provide an accurate representation of the nonlinear two-body solution.

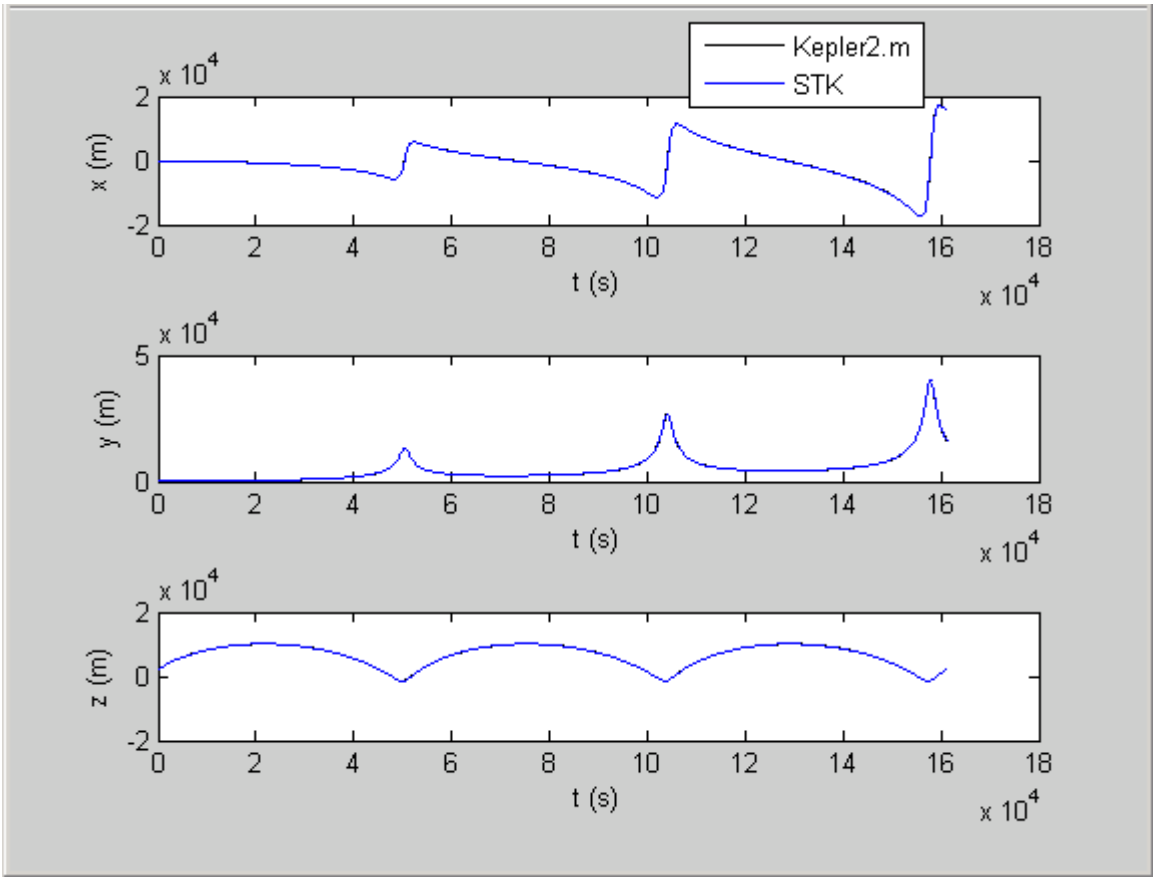

Figure 30. Third Example Results

The Virtual Chief Method

The Algorithm.

This function calculates the relative satellite trajectory using the Virtual Chief model. The algorithm is as follows:

- I. Calculate the intermediate parameters A, B, C, and D. Then print a boundedness check: if motion is bounded, then the index $6A+3C$ should equal zero. Next, calculate and print the virtual chief parameters A_1, ϕ_1, A_2, ϕ_2, z_{max}, and ψ_0.

- II. Compute the solution, the deputy's **c**-frame position coordinates, for each time step.

The Code.

This is virtual_chief.m:

```
% Virtual chief model relative satellite motion plotter
%
% Assumptions: Both satellites remain close to virtual chief in a
circular
% orbit (i.e., small separation and small eccentricity).
%
% Model initial time is t=t0.
%
% Reference frame: The c-frame, a Cartesian LVLH frame attached to
actual
% chief.  Realization is the six new parameters.
%

function
[x,y,z]=virtual_chief(orb_el,rel_state,epoch_cond,t,nu_C,constants)

% Assign Variables

t_p=orb_el(2);
e_C=orb_el(5);
x0=rel_state(1);
y0=rel_state(2);
z0=rel_state(3);
xdot0=rel_state(4);
ydot0=rel_state(5);
zdot0=rel_state(6);
t0=epoch_cond(1);
nu_C0=epoch_cond(2);
M_C0=epoch_cond(3);
nudot_C0=epoch_cond(4);
n_C=constants(4);


% I.  Parameters:

A=cos(nu_C0-M_C0)*x0-sin(nu_C0-M_C0)*y0;
B=sin(nu_C0-M_C0)*x0+cos(nu_C0-M_C0)*y0;
C=(1/n_C)*(sin(nu_C0-M_C0)*(xdot0-(nudot_C0-n_C)*y0)+cos(nu_C0-
M_C0)*(ydot0+(nudot_C0-n_C)*x0));
D=(1/n_C)*(cos(nu_C0-M_C0)*(xdot0-(nudot_C0-n_C)*y0)-sin(nu_C0-
M_C0)*(ydot0+(nudot_C0-n_C)*x0));

6*A+3*C %boundedness check

A1=sqrt((9/4)*D^2+(81/4)*A^2+27*A*C+9*C^2)
phi1=n_C*t0+atan2(3*A+2*C,D)
A2=sqrt(B^2-4*B*D+4*D^2+16*A^2+16*A*C+4*C^2)
phi2=atan2(4*A+2*C,B-2*D)
z_max=sqrt(z0^2+(zdot0/n_C)^2)
psi0=atan2(z0,zdot0/n_C)
```

```
% II.  Solution:

x=A1*sin(nu_C+n_C*t_p-phi1)+A2*sin(nu_C-
n_C*t+n_C*t_p+phi2)+(A1/3)*sin(nu_C-2*n_C*t+n_C*t_p+phi1)-
(3/2)*A2*sin(phi2)*n_C*(t-t0).*sin(nu_C-n_C*t+n_C*t_p);
y=A1*cos(nu_C+n_C*t_p-phi1)+A2*cos(nu_C-
n_C*t+n_C*t_p+phi2)+(A1/3)*cos(nu_C-2*n_C*t+n_C*t_p+phi1)-
(3/2)*A2*sin(phi2)*n_C*(t-t0).*cos(nu_C-n_C*t+n_C*t_p);
z=z_max*sin(n_C*(t-t0)+psi0);
```

Hill-Clohessy-Wiltshire equations

The Algorithm.

This function calculates the relative satellite trajectory using the HCW model.

The algorithm is as follows:

- I. Calculate the submatrices of the state transition matrix, defined in Eqs. (3.4) and (3.6).

- II. Using the submatrices, compute the solution for each element in the discrete time array. The result will be the deputy's relative state vectors in **c**-frame coordinates for each time step.

- III. Calculate and print the values of the Relative Orbit Elements described in Chapter III.

The Code.

This is HCW.m:

```
% Clohessy-Wiltshire Relative Satellite Motion Plotter
%
% Based on Equations 3.34 - 3.39 from Wiesel, _Spaceflight Dynamics_,
2nd
% Ed.
%
% Assumptions: Chief satellite in circular orbit; distance from chief to
% deputy satellite is small compared to distance to center of the Earth.
%
% Reference frame: converted to Cartesian coordinates fixed to the chief
(radial,
% along-track, and normal to the orbit plane).
%
% Units: converted to SI.  After conversions, these results should match
% Algorithm 47 from Vallado, _Fundamentals of Astrodynamics and
% Applications_, 2nd Ed.
```

```
function [x,y,z]=HCW(rel_state,epoch_cond,t,constants)

% Assign variables

x0=rel_state(1);
y0=rel_state(2);
z0=rel_state(3);
xdot0=rel_state(4);
ydot0=rel_state(5);
zdot0=rel_state(6);
t0=epoch_cond(1);
n=constants(4); % chief mean motion
%Deputy initial relative position:
delta_r0=[x0;y0;z0]; %m
%Deputy initial relative velocity:
delta_v0=[xdot0;ydot0;zdot0]; %m/s
% Other variables:
t=t';
psi=n*t; % normalized time


% I.  State transition matrices:

zer=zeros(size(t));
one=zer;
one(:)=1;

Phi_rr=[4-3*cos(psi) zer zer;6*(sin(psi)-psi) one zer;zer zer cos(psi)];
%Eq. 3.36

Phi_rv=[(1/n)*sin(psi) (2/n)*(1-cos(psi)) zer;(2/n)*(cos(psi)-1)
(4/n)*sin(psi)-(3/n)*psi zer;zer zer (1/n)*sin(psi)]; %Eq. 3.37

Phi_vr=[3*n*sin(psi) zer zer;6*n*(cos(psi)-one) zer zer;zer zer -
n*sin(psi)]; %Eq. 3.38

Phi_vv=[cos(psi) 2*sin(psi) zer;-2*sin(psi) -3*one+4*cos(psi) zer;zer
zer cos(psi)]; %Eq. 3.39


% II.  Solution:

%Position vector:
delta_r_vector=Phi_rr*delta_r0+Phi_rv*delta_v0; %Eq. 3.34

%Velocity vector:
delta_v_vector=Phi_vr*delta_r0+Phi_vv*delta_v0; %Eq. 3.35

%Scalar state variables:
x=delta_r_vector(1:length(t));
y=delta_r_vector(length(t)+1:2*length(t));
z=delta_r_vector(2*length(t)+1:3*length(t));
x_dot=delta_v_vector(1:length(t));
y_dot=delta_v_vector(length(t)+1:2*length(t));
z_dot=delta_v_vector(2*length(t)+1:3*length(t));
x=x';
```

```
y=y';
z=z';


% III.  ROE printouts:
a_e=2*sqrt((3*x0+2*ydot0/n)^2+(xdot0/n)^2)
x_d=4*x0+2*ydot0/n
y_d0=y0-2*xdot0/n-(3/2)*n*x_d*t0
beta0=atan2(xdot0,3*n*x0+2*ydot0)
z_max=sqrt(z0^2+(zdot0/n)^2)
psi0=atan2(z0,zdot0/n)
```

Transforming Virtual Chief Parameters to Cartesian Initial Conditions

If the Virtual Chief Parameters are the input for a particular case, then the script VCM_parameter_tool.m plots the Virtual Chief trajectory and prints the equivalent Cartesian initial conditions as outputs. These Cartesian initial conditions can then be used as inputs to rel_sat_motion5.m.

The Algorithm.

The algorithm is as follows:

- I. Calculations. Using two-body properties from Appendix D, calculate known constants, epoch conditions, and arrays of chief true anomaly and time.

- II. Parameterized motion model. Calculate the solution, **c**-frame coordinates for each time step, using the results of Chapter IV.

- III. Plots. Generate figures similar to those of rel_sat_motion5.m showing the relative coordinates and the trajectory.

- IV. Equivalent Cartesian initial conditions. Compute and print Cartesian initial conditions equivalent to the input Virtual Chief parameters.

The Code.

This is VCM_parameter_tool.m:

```
% Relative orbit plotter
%
% This is a stand-alone script that plots relative satellite motion
using
```

```
% the six new virtual-chief method parameters as inputs.  The script
prints
% the equivalent Cartesian initial conditions, which can then be used as
% inputs to rel_sat_motion.m.

clc; clear all; close all; format long g

%-------------------------------------------------------------------------
---
% INPUT:
%-------------------------------------------------------------------------
---

A1= ; %m  (gives the order of magnitude of the y-motion)

phi1= ; %rad  (if phi2=0, gives the approximate starting angle in the
%x-y plane, measured clockwise from the y-axis; affects "skewness" and
%"pointiness" of the x-y projection; for trajectories with out-of-plane
%motion, affects the orientation of the 3D (near-planar)trajectory)

A2= ; %m  (A2*e_C gives the order of magnitude of the x-motion; A2
%also scales the x- and y-drift when phi2 is not zero or pi; when phi2
%equals zero or pi, the coordinates of the "center" of the near-ellipse
are
%(0,A2,0).)

phi2= ; %rad  (if A2=0, this has no effect; otherwise, gives an
%indication of drift rate; dominant drift is along the y-direction, and
is
%negative for 0<phi2<pi, and positive for pi<phi2<2*pi; maximum drift
for
%phi2=pi/2 and 3*pi/2; that includes the t*sin(t)-type drift in the
%x-direction)

z_max= ; %m  (gives the amplitude of the z-motion)

psi0= ; %rad  (for nonzero z_max and phi1=0, gives the orientation about
the
%z-axis of the (near-planar) 3D trajectory, measured clockwise from the
%negative x-axis)

e_C=0.001 ; %chief orbit eccentricity
a_C=7778137 ; %m (chief semi-major axis)
M_C0=0 ; %rad (chief mean anomaly at epoch)
N=4 ; %(Desired number of orbits)
ss=pi/360 ; %rad (Desired step size, in increments of chief true
anomaly)
mu=3.98600441*10^14; %(m^3)/(s^2) (gravitational parameter)
t0=0 ; %s (epoch time)


%-------------------------------------------------------------------------
---
% I.  CALCULATIONS:
%-------------------------------------------------------------------------
---
```

```
n_C=sqrt(mu/(a_C^3)); %rad/s (chief mean motion)
t_p=t0-M_C0/n_C; %s (chief time of perigee passage)
P_C=2*pi/n_C; %s (chief period)
flag=0; %Newton-Raphson iteration to find epoch conditions
E0=M_C0; % first guess
E1=10;
while flag==0,
    if abs(E1-E0)<10^(-9),
        flag=1;
    else E0=E1;
        E1=E0-(E0-e_C*sin(E0)-M_C0)/(1-e_C*cos(E0));
    end
end
E_C0=E1; %rad (chief eccentric anomaly at epoch)
if E_C0<0
    E_C0=E_C0+2*pi;
end
if M_C0==0
    E_C0=0;
end
s=sin(E_C0)*sqrt(1-e_C^2)/(1-e_C*cos(E_C0));
c=(cos(E_C0)-e_C)/(1-e_C*cos(E_C0));
nu_C0=atan2(s,c); %rad (chief true anomaly at epoch)
if nu_C0<0
    nu_C0=nu_C0+2*pi;
end
nudot_C0=n_C*(1-e_C^2)^(-3/2)*(1+e_C*cos(nu_C0))^2; %rad/s (chief
angular rate at epoch)

nu_C=nu_C0:ss:nu_C0+2*N*pi; %rad (chief true anomaly array, allowed to
take on values greater than 2*pi)
s2=sin(nu_C).*sqrt(1-e_C^2)./(1+e_C*cos(nu_C));
c2=(e_C+cos(nu_C))./(1+e_C*cos(nu_C));
E_C=atan2(s2,c2); %rad (chief eccentric anomaly array)
i=1; %atan2 is defined from -pi to pi; I need zero to 2*pi
while i<=length(E_C)
    if E_C(i)<0
        E_C(i)=2*pi+E_C(i);
    end
    i=i+1;
end
M_C=E_C-e_C*sin(E_C); %rad (chief mean anomaly array)
t=M_C./n_C+t_p; %s (time array)
i2=1; %I don't want to reset time to zero or negative after each orbit
while i2<=N
    i3=2;
    while i3<=length(t)
        if t(i3)<t(i3-1)
            t(i3)=t(i3)+P_C;
        end
        i3=i3+1;
    end
    i2=i2+1;
end


%-------------------------------------------------------------------------
---
% PARAMETERIZED MOTION MODEL:
```

```
%-------------------------------------------------------------------------
---

x=A1*sin(nu_C+n_C*t_p-phi1)+A2*sin(nu_C-
n_C*t+n_C*t_p+phi2)+(A1/3)*sin(nu_C-2*n_C*t+n_C*t_p+phi1)-
(3/2)*A2*sin(phi2)*n_C*(t-t0).*sin(nu_C-n_C*t+n_C*t_p);
y=A1*cos(nu_C+n_C*t_p-phi1)+A2*cos(nu_C-
n_C*t+n_C*t_p+phi2)+(A1/3)*cos(nu_C-2*n_C*t+n_C*t_p+phi1)-
(3/2)*A2*sin(phi2)*n_C*(t-t0).*cos(nu_C-n_C*t+n_C*t_p);
z=z_max*sin(n_C*(t-t0)+psi0);


%-------------------------------------------------------------------------
---
% PLOTS:
%-------------------------------------------------------------------------
---

subplot(3,1,1); plot(t,x,'b')
xlabel('t')
ylabel('x')
title('Relative coordinates vs. time')
subplot(3,1,2); plot(t,y,'b')
xlabel('t')
ylabel('y')
ylabel('z')
subplot(3,1,3); plot(t,z,'b')
xlabel('t')

figure
subplot(3,1,1); plot(nu_C,x,'b')
xlabel('nu_C')
ylabel('x')
title('Relative coordinates vs. chief true anomaly')
subplot(3,1,2); plot(nu_C,y)
xlabel('nu_C')
ylabel('y')
subplot(3,1,3); plot(nu_C,z)
xlabel('nu_C')
ylabel('z')

figure
subplot(2,2,1); plot(x,y,'b')
axis equal
xlabel('x')
ylabel('y')
hold on; plot(x(1),y(1),'ro')
plot(x(15),y(15),'rx')
title('Relative trajectory')
subplot(2,2,2); plot(x,z)
axis equal
xlabel('x')
ylabel('z')
hold on; plot(x(1),z(1),'ro')
plot(x(15),z(15),'rx')
subplot(2,2,3); plot(y,z)
axis equal
xlabel('y')
```

```
ylabel('z')
hold on; plot(y(1),z(1),'ro')
plot(y(15),z(15),'rx')
subplot(2,2,4); plot3(x,y,z)
axis equal
grid on
xlabel('x')
ylabel('y')
zlabel('z')
hold on; plot3(x(1),y(1),z(1),'ro')
plot3(x(15),y(15),z(15),'rx')


%-------------------------------------------------------------------------
---
% EQUIVALENT CARTESIAN INITIAL CONDITIONS:
%-------------------------------------------------------------------------
---

x0=A1*sin(nu_C0+n_C*t_p-phi1)+A2*sin(nu_C0-
n_C*t0+n_C*t_p+phi2)+(1/3)*A1*sin(nu_C0-2*n_C*t0+n_C*t_p+phi1)
y0=A1*cos(nu_C0+n_C*t_p-phi1)+A2*cos(nu_C0-
n_C*t0+n_C*t_p+phi2)+(1/3)*A1*cos(nu_C0-2*n_C*t0+n_C*t_p+phi1)
z0=z_max*sin(psi0)
xdot0=-A2*n_C*sqrt(1-(3/4)*(sin(phi2))^2)*cos(nu_C0-
n_C*t0+n_C*t_p+atan2(-sin(phi2),2*cos(phi2)))-(2/3)*A1*n_C*cos(nu_C0-
2*n_C*t0+n_C*t_p+phi1)+nudot_C0*A1*cos(nu_C0+n_C*t_p-
phi1)+nudot_C0*A2*cos(nu_C0-
n_C*t0+n_C*t_p+phi2)+(1/3)*nudot_C0*A1*cos(nu_C0-2*n_C*t0+n_C*t_p+phi1)
ydot0=A2*n_C*sqrt(1-(3/4)*(sin(phi2))^2)*sin(nu_C0-
n_C*t0+n_C*t_p+atan2(-sin(phi2),2*cos(phi2)))+(2/3)*A1*n_C*sin(nu_C0-
2*n_C*t0+n_C*t_p+phi1)-nudot_C0*A1*sin(nu_C0+n_C*t_p-phi1)-
nudot_C0*A2*sin(nu_C0-n_C*t0+n_C*t_p+phi2)-(1/3)*nudot_C0*A1*sin(nu_C0-
2*n_C*t0+n_C*t_p+phi1)
zdot0=z_max*n_C*cos(psi0)
```

Appendix G: A Decreasing Function of Time

This section will prove that $\Delta u(t) - n_C t$ is always a decreasing function of time for values of e_C less than about 0.3106016499352.

From Eq. (4.44),

$$\Delta u(t) - n_C t = \nu_C(t) - 2n_C t + n_C t_p$$

Thus, our goal is to find when $\nu(t) - 2n_C t + n_C t_p$ is a decreasing function of time. In other words, to find when

$$\frac{d}{dt}\left(\nu(t) - 2n_C t + n_C t_p\right) < 0 \tag{G.1}$$

Evaluating,

$$\dot{\nu}(t) - 2n_C < 0$$

Applying the property of two-body orbits contained in Eq. (D.8) and rearranging,

$$2n_C > n_C\left(1 - e_C{}^2\right)^{-3/2}\left(1 + e_C \cos\left[\nu_C(t)\right]\right)^2$$

Assuming an elliptical orbit (i.e., e_C less than unity),

$$2\left(1-{e_C}^2\right)^{3/2} > \left(1+e_C \cos\left[\nu_C\left(t\right)\right]\right)^2 \tag{G.2}$$

If Inequality (G.2) is true when the right-hand side is a maximum, then it is always true. The right-hand side is a maximum at chief perigee, when $\cos\left[\nu_C\left(t\right)\right]$ equals unity. Thus, we must determine for what values of e_C the following is true:

$$2\left(1-{e_C}^2\right)^{3/2} > \left(1+e_C\right)^2 \tag{G.3}$$

Of course, e_C is already confined to the domain $0 \le e_C < 1$. As e_C increases, the left-hand side of Inequality (G.3) decreases, and the right-hand side increases. Thus, the maximum value of e_C for which Inequality (G.1) is always true can be found from

$$2\left(1-{e_C}^2\right)^{3/2} = \left(1+e_C\right)^2$$

After squaring, expanding, and collecting terms, we have

$$-4{e_C}^3 + 12{e_C}^2 - 13e_C + 3 = 0$$

The above polynomial has only one real root, 0.310601649935225. (The complex roots are $1.34469917503239 \pm 0.778750642891565i$.)

Thus, for e_C less than or equal to 0.310601649935225, $\Delta u\left(t\right) - n_C t$ is a decreasing function of time.

Bibliography

[1] AFRL/RV, "Linear Mapping between Hill Frame Coordinates and Orbital Element Differences," internal message.

[2] Alfriend, K. T., and Yan, H., “Evaluation and Comparison of Relative Motion Theories,” *Journal of Guidance, Control, and Dynamics*; Vol. 28, No. 2, 2005, pp. 254-261.

[3] Alfriend, K. T., Yan, H., and Vadali, S. R., “Nonlinear Considerations in Satellite Formation Flying,” AIAA Paper 2002-4741, Aug. 2002.

[4] Anthony, M. L., and Sasaki, F. T., “Rendezvous Problem for Nearly Circular Orbits,” *AIAA Journal*; Vol. 3, No. 9, 1965, pp. 1666-1673.

[5] Balaji, S. K., and Tatnall, A. R., “Relative Trajectory Analysis of Dissimilar Formation Flying Spacecraft,” American Astronautical Society Paper 03-134, Feb. 2003.

[6] Battin, R. H., *An Introduction to the Mathematics and Methods of Astrodynamics*, AIAA, New York, 1987.

[7] Breger, L., and How, J. P., “Safe Trajectories for Autonomous Rendezvous of Spacecraft,” *Journal of Guidance, Control, and Dynamics*; Vol. 31, No. 5, 2008, pp. 1478-1489.

[8] Broucke, R. A., “Solution of the Elliptic Rendezvous Problem with the Time as Independent Variable,” *Journal of Guidance, Control, and Dynamics*; Vol. 26, No. 4, 2003, pp. 615-621.

[9] Carpenter, J. R., Leitner, J., Folta, D., and Burns, R., “Benchmark Problems for Spacecraft Formation Flying Missions,” AIAA Paper 2003-5364, Aug. 2003.

[10] Carter, T. E., "Closed-form Solution of an Idealized, Optimal, Highly Eccentric Hyperbolic Rendezvous Problem," *Dynamics and Control*; Vol. 6, No. 3, 1996, pp. 293-307.

[11] Carter, T. E., "New Form for the Optimal Rendezvous Equations near a Keplerian Orbit," *Journal of Guidance, Control, and Dynamics*; Vol. 13, No. 1: Engineering Notes, 1990, pp. 183-186.

[12] Carter, T. E., "State Transition Matrices for Terminal Rendezvous Studies: Brief Survey and New Examples," *Journal of Guidance, Control, and Dynamics*; Vol. 21, No. 1, 1998, pp. 148-155.

[13] Carter, T., and Humi, M., "Clohessy-Wiltshire Equations can be Modified to Include Quadratic Drag," American Astronautical Society Paper 03-240, Feb. 2003.

[14] Carter, T., and Humi, M., "Fuel-optimal Rendezvous near a Point in General Keplerian Orbit," *Journal of Guidance, Control, and Dynamics*; Vol. 10, No. 6, 1987, pp. 567-573.

[15] Chobotov, V. A., *Orbital Mechanics*, 3rd Ed., AIAA, Reston, 2002.

[16] Clohessy, W. H., and Wiltshire, R. S., "Terminal Guidance System for Satellite Rendezvous," *Journal of the Aerospace Sciences*; Vol. 27, Sept. 1960, pp. 653-658, 674.

[17] Condurache, D., and Martinuşi, V., "A Quaternionic Exact Solution to the Relative Orbital Motion," AIAA Paper 2008-6764, Aug. 2008.

[18] Condurache, D., and Martinuşi, V., "Kepler's Problem in Rotating Reference Frames Part 1: Prime Integrals, Vectorial Regularization," *Journal of Guidance, Control, and Dynamics*; Vol. 30, No. 1, 2007, pp. 192-200.

[19] Condurache, D., and Martinuşi, V., "Kepler's Problem in Rotating Reference Frames Part 2: Relative Orbital Motion," *Journal of Guidance, Control, and Dynamics*; Vol. 30, No. 1, 2007, pp. 201-213.

[20] Condurache, D., and Martinuşi, V., "Relative Spacecraft Motion in a Central Force Field," *Journal of Guidance, Control, and Dynamics*; Vol. 30, No. 3: Engineering Notes, 2007, pp. 873-876.

[21] Curtis, S., "The Magnetosphere Multiscale Mission…Resolving Fundamental Processes in Space Plasmas," NASA Technical Memorandum TM-2000-209883, NASA Science and Technology Definition Team for the Magnetosphere Multiscale (MMS) Mission, 1999.

[22] D'Amico, S., Gill, E., and Montenbruck, O., "Relative Orbit Control Design for the PRISMA Formation Flying Mission," AIAA Paper 2006-6067, Aug. 2006.

[23] D'Amico, S., and Montenbruck, O., "Proximity Operations of Formation-Flying Spacecraft Using an Eccentricity/Inclination Vector Separation," *Journal of Guidance, Control, and Dynamics*; Vol. 29, No. 3, 2006, pp. 554-563.

[24] D'Angelo, H., *Linear Time-Varying Systems: Analysis and Synthesis*, Allyn and Bacon, Boston, 1970.

[25] Der, G. J., and Danchick, R., "An Analytic Approach to Optimal Rendezvous Using the Der-Danchick Equations," American Astronautical Society Paper 97-647, Aug. 1997.

[26] De Vries, J. P., "Elliptic Elements in Terms of Small Increments of Position and Velocity Components," *AIAA Journal*; Vol. 1, No. 11, 1963, pp. 2626-2629.

[27] Doolittle, C. M., Chavez, F. R., and Lovell, T. A., "Relative Orbit Element Estimation for Satellite Navigation," AIAA Paper 2005-6462, Aug. 2005.

[28] Euler, E. A., and Shulman, Y., "Second-order Solution to the Elliptical Rendezvous Problem," *AIAA Journal*; Vol. 5, No. 5, 1967, pp. 1033-1035.

[29] Evans, J. W., Piñon, E., and Mulder, T. A., "Autonomous Rendezvous Guidance and Navigation for Orbital Express and Beyond," American Astronautical Society Paper 06-194, Jan. 2006.

[30] Fasano, G., and D'Errico, M., "Design of Satellite Formations for Interferometric and Bistatic SAR," Institute of Electrical and Electronics Engineers Aerospace Conference Paper No. 1064, Mar. 2007.

[31] Fehse, Wigbert, *Automated Rendezvous and Docking of Spacecraft*, Cambridge University Press, Cambridge, 2003.

[32] Garrison, J. L., Gardner, T. G., and Axelrad, P., "Relative Motion in Highly Elliptical Orbits," American Astronautical Society Paper 95-194, Feb. 1995.

[33] Gim, D., and Alfriend, K. T., "State Transition Matrix of Relative Motion for the Perturbed Noncircular Reference Orbit," *Journal of Guidance, Control, and Dynamics*; Vol. 26, No. 6, 2003, pp. 956-971.

[34] Gramling, C., Carpenter, R., Lee, T., and Long, A., "Relative Navigation Strategies for the Magnetospheric Multiscale Mission," 18th International Symposium on Space Flight Dynamics, Munich, Germany, 2004.

[35] Gurfil, P., "Relative Motion Between Elliptic Orbits: Generalized Boundedness Conditions and Optimal Formationkeeping," *Journal of Guidance, Control, and Dynamics*; Vol. 28, No. 4, 2005, pp. 761-767.

[36] Gurfil, P., and Kasdin, N. J., "Nonlinear Modeling and Control of Spacecraft Relative Motion in the Configuration Space," American Astronautical Society Paper 03-108, Feb. 2003.

[37] Gurfil, P., and Kasdin, N. J., "Nonlinear Modeling of Spacecraft Relative Motion in the Configuration Space," *Journal of Guidance, Control, and Dynamics*; Vol. 27, No. 1: Engineering Notes, 2004, pp. 154-157.

[38] Hamel, J., and de Lafontaine, J., "Autonomous Guidance and Control of Earth-orbiting Formation Flying Spacecraft: Closing the Loop," *Acta Astronautica*; Vol. 63, No. 11-12, 2008, pp. 1246-1258.

[39] Hamel, J., and de Lafontaine, J., "Linearized Dynamics of Formation Flying Spacecraft on a J2-Perturbed Elliptical Orbit," *Journal of Guidance, Control, and Dynamics*; Vol. 30, No. 6, 2007, pp. 1649-1658.

[40] Hill, G. W., "Researches in the Lunar Theory," *American Journal of Mathematics*; Vol. 1, No. 1, 1878, pp. 5-26, 129-147, 245-260.

[41] Inalhan, G., Tillerson, M., and How, J. P., "Relative Dynamics and Control of Spacecraft Formations in Eccentric Orbits," *Journal of Guidance, Control, and Dynamics*; Vol. 25, No. 1, 2002, pp. 48-59.

[42] Irvin, D. J., "Optimal Control Strategies for Constrained Relative Orbits," AFIT Dissertation, 2007.

[43] Irvin, D., Cobb, R., and Lovell, T., "Fuel-Optimal Maneuvers for Constrained Relative Satellite Orbits," *Journal of Guidance, Control, and Dynamics*; Vol. 32, No. 3, 2009, pp. 960-973.

[44] Jezewski, D. J., Brazzell, J. P., Prust, E. E., Brown, B. G., Mulder, T. A., and Wissinger, D. B., "A Survey of Rendezvous Trajectory Planning," American Astronautical Society Paper 91-505, Aug. 1991.

[45] Jiang, F., Li, J., Baoyin, H., and Gao, Y., "Study on Relative Orbit Geometry of Spacecraft Formations in Elliptical Reference Orbits," *Journal of Guidance, Control, and Dynamics*; Vol. 31, No. 1, 2008, pp. 123-134.

[46] Jones, J. B., "A Solution of the Variational Equations for Elliptic Orbits in Rotating Coordinates," AIAA Paper 1980-1690, Aug. 1980.

[47] Karlgaard, C. D., "Robust Rendezvous Navigation in Elliptical Orbit," *Journal of Guidance, Control, and Dynamics*; Vol. 29, No. 2: Engineering Notes, 2006, pp. 495-499.

[48] Karlgaard, C. D., and Lutze, F. H., "Second-Order Relative Motion Equations," *Journal of Guidance, Control, and Dynamics*; Vol. 26, No. 1, 2003, pp. 41-49.

[49] Kelley, H. J., Cliff, E. M., and Lutze, F. H., "Pursuit/Evasion in Orbit," *Journal of the Astronautical Sciences*; Vol. 29, No. 3, 1981, pp. 277-288.

[50] Kelly, T. J., "An Analytical Approach to the Two-Impulse Optimal Rendezvous Problem," AAS Paper 94-156, Feb. 1994.

[51] Ketema, Y., "An Analytical Solution for Relative Motion with an Elliptic Reference Orbit," *Journal of the Astronautical Sciences*; Vol. 53, No. 4, 2006, pp. 373-389.

[52] Kong, E. M. C., Miller, D. W., and Sedwick, R. J., "Exploiting Orbital Dynamics for Aperture Synthesis Using Distributed Satellite Systems: Applications to a Visible Earth Imager System," *Journal of the Astronautical Sciences*; Vol. 47, No. 1 and 2, 1999, pp. 53-75.

[53] Lancaster, E. R., "Relative Motion of Two Particles in Elliptic Orbits," *AIAA Journal*; Vol. 8, No. 10, 1970, pp. 1878-1879.

[54] Lane, C., and Axelrad, P., "Formation Design in Eccentric Orbits Using Linearized Equations of Relative Motion," *Journal of Guidance, Control, and Dynamics*; Vol. 29, No. 1, 2006, pp. 146-160.

[55] Lawden, D. F., "Fundamentals of Space Navigation," *Journal of the British Interplanetary Society*; Vol. 13, No. 2, 1954, pp. 87-101.

[56] Lawden, D. F., *Optimal Trajectories for Space Navigation*, Butterworths, London, 1963.

[57] London, H. S., "Second Approximation to the Solution of the Rendezvous Equations," *AIAA Journal*; Vol. 1, No. 7, 1963, pp. 1691-1693.

[58] Lovell, T. A., Chavez, F. R., and Johnson, R. L., "A Comparison of Relative Motion Models for Close Proximity Satellite Missions", AFRL-VS-PS-PR-2005-1007, Jan. 2005.

[59] Lovell, T. A., Horneman, K. R., Tragesser, S. G., and Tollefson, M. V., "A Guidance Algorithm for Formation Reconfiguration and Maintenance Based on the Perturbed Clohessy-Wiltshire Equations," American Astronautical Society Paper 03-649, Aug. 2003.

[60] Lovell, T. A., and Tragesser, S. G., "Guidance for Relative Motion of Low Earth Orbit Spacecraft Based on Relative Orbit Elements," AIAA Paper 2004-4988, Aug. 2004.

[61] Lovell, T. A., Tragesser, S. G., and Tollefson, M. V., "A Practical Guidance Methodology for Relative Motion of LEO Spacecraft Based on the Clohessy-Wiltshire Equations," American Astronautical Society Paper 04-252, Feb. 2004.

[62] Mailhe, L., Schiff, C., and Hughes, S., "Formation Flying in Highly Elliptical Orbits: Initializing the Formation," 15th International Symposium on Space Flight Dynamics, Biarritz, France, 2000.

[63] Marcos, A., Penin, L. F., Di Sotto, E., and Drai, R., "Formation Flying Control in Highly Elliptical Orbits," AIAA Paper 2007-6542, Aug. 2007.

[64] McSpadden, J., Chang, K., Little, F., and Duke, M., "Study of ISS Free-Flyer Power Beaming," Proceedings of SPS 97 Conference Digest, Montreal, Aug. 1997, pp. 169-174.

[65] Melton, R. G., "Comparison of Relative-Motion Models for Elliptical Orbits," *Proceedings of the 3rd International Workshop on Satellite Constellations and Formation Flying*; International Astronautical Federation, Paris, 2003, pp. 181-189.

[66] Melton, R. G., "Time-Explicit Representation of Relative Motion Between Elliptical Orbits," *Journal of Guidance, Control, and Dynamics*; Vol. 23, No. 4, 2000, pp. 604-610.

[67] Naasz, B. J., "Safety Ellipse Motion with Coarse Sun Angle Optimization," NASA Document 20050241964, 2005.

[68] Ohkami, Y., and Kawano, I., "Autonomous Rendezvous and Docking by Engineering Test Satellite VII: A Challenge of Japan in Guidance, Navigation and Control—Breakwell Memorial Lecture," *Acta Astronautica*; Vol. 53, No. 1, 2003, pp. 1-8.

[69] Olsen, C., and Fowler, W., "Characterization of the Relative Motion of Rendezvous between Vehicles in Proximate, Highly Elliptic Orbits," American Astronautical Society Paper 04-159, Feb. 2004.

[70] Park, C., Guibout, V., and Scheeres, D. J., "Solving Optimal Continuous Thrust Rendezvous Problems with Generating Functions," *Journal of Guidance, Control, and Dynamics*; Vol. 29, No. 2, 2006, pp. 321-331.

[71] Press, M. J., "Geometric Approach to Orbital Formation Mission Design," AFIT Thesis, 2004.

[72] Rathke, A., and Izzo, D., "Keplerian Consequences of an Impact on an Asteroid and Their Relevance for a Deflection Demonstration Mission," *Near Earth Objects, our Celestial Neighbors: Opportunity and Risk*, International Astronomical Union, Prague, Aug. 2006, pp. 417-426.

[73] Reid, J. G., *Linear System Fundamentals: Continuous and Discrete, Classic and Modern*, McGraw-Hill Book Company, New York, 1983.

[74] Roger, A. B., and McInnes, C. R., "Safety Constrained Free-Flyer Path Planning at the international Space Station," *Journal of Guidance, Control, and Dynamics*; Vol. 23, No. 6, 2000, pp. 971-979.

[75] Sabol, C., Burns, R., and McLaughlin, C. A., "Satellite Formation Flying Design and Evolution," *Journal of Spacecraft and Rockets*; Vol. 38, No. 2, 2001, pp. 270-278.

[76] Sabol, C., McLaughlin, C. A., and Luu, K. K., "Meet the Cluster Orbits with Perturbations of Keplerian Elements (COWPOKE) Equations," American Astronautical Society Paper 03-138, Feb. 2003.

[77] Schaub, H., “Incorporating Secular Drifts into the Orbit Element Difference Description of Relative Orbits,” American Astronautical Society Paper 03-115, Feb. 2003.

[78] Schaub, H., "Relative Orbit Geometry through Classical Orbital Element Differences," *Journal of Guidance, Control, and Dynamics*; Vol. 27, No. 5, 2004, pp. 839-848.

[79] Schaub, H., and Junkins, J. L., *Analytical Mechanics of Space Systems*, AIAA, Reston, 2003.

[80] Schiff, C., Rohrbaugh, D., and Bristow, J., “Formation Flying in Elliptical Orbits,” *Aerospace Conference Proceedings, 2000 IEEE*, Institute of Electrical and Electronics Engineers, Vol. 7, Mar. 2000, pp. 37-47.

[81] Sedwick, R. J., Miller, D. W., and Kong, E. M. C., “Mitigation of Differential Perturbations in Formation Flying Satellite Clusters,” *Journal of the Astronautical Sciences*; Vol. 47, No. 3 and 4, 1999, pp. 309-331.

[82] Segal, S., and Gurfil, P., “Effect of Kinematic Rotation-Translation Coupling on Relative Spacecraft Translation Dynamics,” *Journal of Guidance, Control, and Dynamics*; Vol. 32, No. 3: Engineering Notes, 2009, pp. 1045-1050.

[83] Sengupta, P., “Dynamics and Control of Satellite Relative Motion in a Central Gravitational Field,” Texas A&M University Dissertation, 2006.

[84] Sengupta, P., Sharma, R., and Vadali, S., “Periodic Relative Motion near a Keplerian Elliptic Orbit with Nonlinear Differential Gravity,” *Journal of Guidance, Control, and Dynamics*; Vol. 29, No. 5, 2006, pp. 1110-1121.

[85] Sengupta, P., and Vadali, S. R., “Formation Design and Geometry for Keplerian Elliptic Orbits with Arbitrary Eccentricity,” AAS Paper 06-161, Jan. 2006.

[86] Sengupta, P., and Vadali, S. R., “Relative Motion and the Geometry of Formations in Keplerian Elliptic Orbits,” *Journal of Guidance, Control, and Dynamics*; Vol. 30, No. 4, 2007, pp. 953-964.

[87] Sharma, R., Sengupta, P., and Vadali, S., “Near-Optimal Feedback Rendezvous in Elliptic Orbits Accounting for Nonlinear Differential Gravity,” *Journal of Guidance, Control, and Dynamics*; Vol. 30, No. 6, 2007, pp. 1803-1813.

[88] Shulman, Y., and Scott, J. J., “Terminal Rendezvous for Elliptical Orbits,” AIAA Paper 66-533, Jun. 1966.

[89] Silva, N., Ganet, M., Gogibus, E., Delpy, P., and Augros, P., “Autonomous Rendezvous: Guidance and Control in Elliptical Orbit,” AIAA Paper 2007-6355, Aug. 2007.

[90] Stern, R. G., “Interplanetary Midcourse Guidance Analysis,” Report TE-5, Experimental Astronomy Laboratory, MIT, 1963.

[91] Tollefson, M. V., "Converting between Alan's and Clark's Formation Elements," AFRL/RV internal message, Dec. 2003.

[92] Trask, A. J., and Hope, A. S., “Primer Vector Theory for Optimal Relative Waypoint Flying,” American Astronautical Society Paper 04-207, Feb. 2004.

[93] Tschauner, J., “Elliptic Orbit Rendezvous,” *AIAA Journal*; Vol. 5, No. 6, 1967, pp. 1110-1113.

[94] Tschauner, J. F. A., and Hempel, P. R., “Rendezvous zu einemin Elliptischer Bahn umlaufenden Ziel,” *Astronautica Acta*; Vol. 11, No. 2, 1965, pp. 104-109.

[95] Vaddi, S. S., Alfriend, K. T., Vadali, S. R., and Sengupta, P., “Formation Establishment and Reconfiguration Using Impulsive Control,” *Journal of Guidance, Control, and Dynamics*; Vol. 28, No. 2, 2005, pp. 262-268.

[96] Vaddi, S. S., and Vadali, S. R., "Linear and Nonlinear Control Laws for Formation Flying," American Astronautical Society Paper 03-109, Feb. 2003.

[97] Vaddi, S. S., Vadali, S. R., and Alfriend, K. T., "Formation Flying: Accommodating Nonlinearity and Eccentricity Perturbations," ," *Journal of Guidance, Control, and Dynamics*; Vol. 26, No. 2, 2003, pp. 214-223.

[98] Vallado, D. A., *Fundamentals of Astrodynamics and Applications*, 2nd ed., Microcosm Press, El Segundo, 2004.

[99] Wartenberg, H., and Amadieu, P., "ATV: Rendezvous with ISS," *On Station*; No. 11, 2002, pp. 17-19.

[100] Weismuller, T., and Leinz, M., "GN&C Technology Demonstrated by the Orbital Express Autonomous Rendezvous and Capture Sensor System," American Astronautical Society Paper 06-616, Feb. 2006.

[101] Weisstein, Eric W., "Harmonic Addition Theorem," from *MathWorld*—A Wolfram Web Resource, http://mathworld.wolfram.com/HarmonicAdditionTheorem.html.

[102] Wiesel, W. E., *Spaceflight Dynamics*, 2nd ed., Irwin McGraw-Hill, Boston, 1997.

[103] Wiesel, W. E., "Optimal Impulsive Control of Relative Satellite Motion," *Journal of Guidance, Control, and Dynamics*; Vol. 26, No. 1, 2003, pp. 74-78.

[104] Woffinden, D. C., and Geller, D. K., "Navigating the Road to Autonomous Orbital Rendezvous," *Journal of Spacecraft and Rockets*; Vol. 44, No. 4, 2007, pp. 898-909.

[105] Wolfsberger, W., Weiß, J., and Rangnitt, D., "Strategies and Schemes for Rendezvous on Geostationary Transfer Orbit," *Acta Astronautica*; Vol. 10, No. 8, 1983, pp. 527-538.

[106] Yamanaka, K., and Ankersen, F., "New State Transition Matrix for Relative Motion on an Arbitrary Elliptical Orbit," *Journal of Guidance, Control, and Dynamics*; Vol. 25, No. 1, 2002, pp. 60-66.

[107] Yan, H., Alfriend, K. T., Vadali, S. R., and Sengupta, P., "Optimal Design of Satellite Formation Relative Motion Orbits Using Least-Squares Methods," *Journal of Guidance, Control, and Dynamics*; Vol. 32, No. 2, 2009, pp. 599-604.

[108] Yan, H., Sengupta, P., Vadali, S. R., and Alfriend, K. T., "Development of a State Transition Matrix for Relative Motion Using the Unit Sphere Approach," American Astronautical Society Paper 04-163, Feb. 2004.

[109] Zanon, D., and Campbell, M., "Optimal Planner for Spacecraft Formations in Elliptical Orbits," *Journal of Guidance, Control, and Dynamics*; Vol. 29, No. 1, 2006, pp. 161-171.

[110] Zanon, D. J., and Campbell, M. E., "Fuel Optimal Maneuvers with Spacecraft Attitude Constraints," AIAA Paper 2006-6588, Aug. 2006.

[111] Zhang, H., and Sun, L., "Spacecraft Formation-Flying in Eccentric Orbits," AIAA Paper 2003-5589, Aug. 2003.

Vita

Captain Kirk W. Johnson received a Bachelor of Science in Mechanical Engineering with Aerospace from Worcester Polytechnic Institute in Worcester, Massachusetts, in 2000. At the same time, he received a commission from Air Force ROTC Detachment 340.

After completing a year of training at Vandenberg AFB, he was stationed at Malmstrom AFB, where he served as an ICBM combat crewmember and instructor. In 2005, he was assigned to the National Air and Space Intelligence Center at Wright-Patterson AFB. While there, he managed a combat identification signatures program, supervised a branch in the Engineering Division, and served as Operations Officer in the Aircraft Analysis Squadron. In August 2008, he entered the Graduate School of Engineering and Management, Air Force Institute of Technology. Upon graduation, he will be assigned to Kirtland AFB.

REPORT DOCUMENTATION PAGE

Form Approved
OMB No. 074-0188

1. REPORT DATE *(DD-MM-YYYY)*	**2. REPORT TYPE**	**3. DATES COVERED** *(From – To)*
25-03-2010	Master's Thesis	Aug 2008 - Mar 2010

4. TITLE AND SUBTITLE

Relative Orbit Elements for Satellites in Elliptical Orbits

5a. CONTRACT NUMBER

5b. GRANT NUMBER

5c. PROGRAM ELEMENT NUMBER

6. AUTHOR(S)

Johnson, Kirk W., Capt, USAF

5d. PROJECT NUMBER

5e. TASK NUMBER

5f. WORK UNIT NUMBER

7. PERFORMING ORGANIZATION NAMES(S) AND ADDRESS(S)
Air Force Institute of Technology
Graduate School of Engineering and Management (AFIT/EN)
2950 Hobson Way
WPAFB OH 45433-7765

8. PERFORMING ORGANIZATION REPORT NUMBER

AFIT/GA/ENY/10-M04

9. SPONSORING/MONITORING AGENCY NAME(S) AND ADDRESS(ES)
Air Force Research Laboratory, Space Vehicles Directorate
Attn: Dr. T. Alan Lovell
3550 Aberdeen Ave SE
Kirtland AFB, NM 87117-5776
(505) 853-4132 (DSN: 263-4132)

10. SPONSOR/MONITOR'S ACRONYM(S)
AFRL/RV

11. SPONSOR/MONITOR'S REPORT NUMBER(S)

12. DISTRIBUTION/AVAILABILITY STATEMENT
APPROVED FOR PUBLIC RELEASE; DISTRIBUTION UNLIMITED.

13. SUPPLEMENTARY NOTES

14. ABSTRACT
The purpose of this research was to describe the unperturbed relative motion of Earth satellites in elliptical orbits using a simple dynamics model whose parameters allow significant geometrical insight and operational efficacy. The goal was to retain the advantages of the Relative Orbit Elements (ROE) realization of the Hill-Clohessy-Wiltshire (HCW) equations, a linearized dynamics model for circular reference orbits. Specifically, this thesis analyzed the geometry of satellite rendezvous and proximity operations using the ROE parameters to characterize the model's utility. Next, through a comprehensive literature review, this thesis sought possible approaches for developing a similarly useful parameterization for chief orbits with nonzero eccentricity. The approach selected was a novel linear time-varying system which requires both chief and deputy satellites to remain close to a virtual chief on a known circular orbit. The research derived and solved the equations of motion, expressing the solution in terms of simple geometric parameters. Numerical simulations compared the new model against both HCW and Keplerian two-body motion, revealing less accurate performance than HCW for some cases. Error analysis explained this behavior and found restricted regions where the new model performed accurately. Finally, this study identified new approaches for researching relative satellite motion on elliptical orbits.

15. SUBJECT TERMS
Relative Satellite Motion, Elliptical Rendezvous, Autonomous Rendezvous, Rendezvous and Proximity Operations, Relative Orbit Elements

16. SECURITY CLASSIFICATION OF:			**17. LIMITATION OF ABSTRACT**	**18. NUMBER OF PAGES**	**19a. NAME OF RESPONSIBLE PERSON**
REPORT	**ABSTRACT**	**c. THIS PAGE**			Douglas D. Decker, Lt Col, USAF (ENY)
U	**U**	**U**	**UU**	193	**19b. TELEPHONE NUMBER** *(Include area code)* (937) 255-3636, x7465 douglas.decker@afit.edu

Standard Form 298 (Rev: 8-98)
Prescribed by ANSI Std. Z39-18